UNIVERSITY OF SOUTHERN CALIFORNIA
DEPARTMENT OF CIVIL ENGINEERING

ANALYTICAL MODEL FOR IN PLANE BUILDING-FOUNDATION-SOIL INTERACTION: INCIDENT P-, SV- AND RAYLEIGH WAVES

by

Maria I. Todorovska and Mihailo D. Trifunac

Report No. 90-01

Los Angeles, California
March, 1990

ABSTRACT

Foundation-soil and building-foundation-soil interaction has been studied using a two-dimensional analytical model, including both the dynamic and the kinematic interaction effects. The building has been represented by an infinitely long shear wall resting on a rigid circular foundation, embedded into an elastic homogeneous half-space. Deep and shallow foundations have been considered (with depth-to-half-width ratio of 1 and 0.5) and excitation consisting of plane P- and SV- and surface Rayleigh waves. The wave function expansion method has been used to represent the motion in the half-space and a substructure approach to solve the interaction problem. Special attention has been paid to the wave passage effects, and to the influence of the depth of the embedment.

TABLE OF CONTENTS

CHAPTER I

INTRODUCTION

I.1 General Introduction

Since the 1960's, the soil-structure interaction has been recognized as an important factor that may significantly affect the relative building response, the motion of its base, and the motion of the surrounding soil. Some of the important manifestations of the interaction are the following: (1) it generally reduces the strains and the forces in the building at the resonant frequencies, (2) it may cause significant rotation of the base, and (3) it changes the frequencies of the peaks in the relative response transfer function. The degree of the modification of the transfer function of the building on flexible foundation medium, relative to the one on a fixed-base, is larger when the stiffness of the building relative to the soil is larger. Solving the complete problem is complicated for routine calculations and requires detailed knowledge of the soil properties in the vicinity of the foundation (Luco and Wong, 1990), such as the material damping and the values and the variations of the shear-wave velocity and of the Poison's ratio. Also, the large deformations of the soil, caused by the large rotations of the base, may require nonlinear analyses. Another problem, which arises in densely populated urban areas, is measuring the free-field motion in the close vicinity of the building site, so that it could be used as realistic input for the interaction models. So, the engineers have looked for some simplified and easy approach to use models for dynamic analyses of buildings, that would account for the interaction. A common means to model the dynamic interaction effects is by associating linear springs and dashpots to the degrees of freedom of the foundation, the former accounting for the change in the stiffness, and consequently the changes in the natural frequencies, and the latter for the dissipation of the building vibrational energy via radiation damping. This hysteretic model makes it possible to combine the radiation damping with the material damping (which is also assumed to be of hysteretic nature).

I.2 Literature Review

In general, the building-soil interaction consists of two parts: a kinematic and a dynamic interaction. The former is a result of the wave nature of the excitation, and is manifested through scattering of the incident waves from the building foundation and through the filtering effect of the foundation, that may be stiffer than the soil and, therefore, may not follow the higher frequency deformations of the soil. This interaction depends on the frequency, angle of incidence and type of incident waves, as well as on the shape of the foundation and on the depth of the embedment. The latter is due to the inertia forces of the building and of the foundation which act onto the soil through the contact area, and it depends on the mass and height of the building and the mass and depth of the foundation, on the relative stiffness of the soil compared with the building and on the shape of the foundation. The kinematic interaction is usually described by the foundation input motion (response of the massless foundation without the action of the forces of the building), and the dynamic interaction by the foundation impedance functions. A common

approach is that those are first calculated for different types of foundations, and are readily available (e.g., in tabular form) for the next stage which is calculation of the structural response. This approach is known as a substructure approach, and is used only when both the soil and the building are linear. When this is not the case, the structural response is calculated by step by step solution of the equations of motion for the complete soil-foundation-structure system, using finite element models or combination of finite element and integral equation methods.

Pioneering work in the area of building-soil interaction was done by Luco (1969), on a two-dimensional (2D) building model on a circular rigid foundation and for incident plane SH-waves. Trifunac (1971) generalized the solution to arbitrary incident angle of the SH-waves. Both authors arrived at analytical closed form solutions. Later, Wong and Trifunac (1974) solved analytically the same problem, but for a building on a semi-elliptical foundation, which enabled them to study the effect of the depth of the embedment for incident SH-waves. Wong and Trifunac (1975) generalized their solution to interaction of two or more buildings, again for incident plane SH-waves.

The foundation-soil interaction has been studied by many authors for foundations of different shapes, embedded into homogeneous or layered half-space, and excited by different types of waves. Some of those are: Luco and Westmann (1971), Veletsos and Verbič (1973), Thau and Umec (1974), Luco et al. (1975), Thau (1976), Apsel and Luco (1976), Day and Frazier (1979), Iguchi (1984), and Pais and Kausel (1989). Some of the conclusions of these studies are the following. (1) The kinematic interaction can change significantly the foundation input motion relative to the free-field motion. At higher frequencies the translation is reduced but the rotation increases (Day and Frazier, 1979). Iguchi (1984) concluded that (2) the usual assumption for vertically arriving incident waves does not always lead to the most conservative estimates, both for flat and for embedded foundations. Yet, in numerous analyses the kinematic interaction and often the frequency dependant nature of the foundation stiffness are neglected, as well as the coupling of the rotational and the translational stiffnesses.

A typical model to study dynamic building-soil interaction consists of an N degree-of-freedom lumped mass building model, attached by springs and dashpots (one pair for the horizontal and another pair for the rocking foundation motion) to a rigid base. This is solved for the dynamic response of the N+2 degree-of freedom fixed base system excited by horizontal translation only, equal to the free-field motion. Using such a model, Bielak (1971) arrived at analytical expressions for the modal damping, "natural" frequencies and the peak response of a SDOF and a MDOF building model on a flexible surface foundation. He assumed frequency independent and uncoupled stiffnesses and damping coefficients for the foundation, calculated from the diagonal terms of the foundation impedance function, evaluated at the first peak frequency of the interacting system. He included the material damping in the soil, which he superimposed linearly to the foundation damping. Assuming small values for the radiation, soil material and building damping coefficients, he neglected the higher order terms of their contribution. In his later work (Bielak, 1976) he arrived at the same analytical expressions assuming orthogonal modes of the flexible base structure. He concluded that (1) the assumption of orthogonal modes is equivalent to neglecting the

higher order terms in the damping coefficients. (2) The fundamental natural frequency, as well as the amplitude of the equivalent input acceleration, always decrease, but the effective damping can increase or decrease relative to the damping in fixed base models, depending on the value of the other parameters. (3) The average undamped response is always decreased as a result of the interaction, while for a damped structure either an increase or a decrease can take place, i.e. the effects of the interaction are not always conservative. (4) The effect of the base mass is small. (5) The effect of the interaction may be negligible for the higher modes of the structure. (6) Although all the resonant frequencies decrease, only the fundamental frequency decreases significantly. Except for short structures this reduction is essentially due to rocking rather than to translation of the base.

Using the same model and the assumption of small damping coefficients, Luco (1980a) studied the effects of the interaction on the modal quantities obtained by typical identification techniques in which the interaction is neglected. Neglecting the contribution of the higher modes, he also arrived at analytical expressions for the apparent system frequency and the apparent system damping. Those are the modal characteristics calculated from the transfer function between the total translation of the base and the relative translation of the top of the building (equal to the total translation of the top minus the total translation of the base). His study showed that the apparent system frequency is slightly higher than the true system frequency, and that they both can be significantly lower than the fixed base building frequency. When the relative stiffness of the building relative to the soil is larger, the contribution of the building damping to the true and apparent system damping decreases and, then, those are mainly governed by the radiation and material soil damping.

Recently Dangla (1988) used a numerical method (finite element and boundary element method) to study two-dimensional soil-structure interaction of a building (modeled by a two-dimensional finite element model) for incident plane P- and SV- and surface Rayleigh waves. In his paper, he focused only on the interpretation of the foundation response transfer function amplitudes for his example system. He concluded that, in general, the horizontal and the vertical displacement amplitudes have local minima at he bending and compressional natural frequencies of the fixed-base building model, and that rotational amplitudes of the foundation have local maxima at the bending natural frequencies of the fixed-base building model. The shortest wave lengths of the shear wave in the soil in his results were equal to $4/\pi$ times the width of the foundation.

Other studies of building-soil interaction are by Wong (1975), Lee (1979), Luco (1980b) and many others.

I.3 Subject of Study and Organization of this Report

Analyses of two-dimensional models have not been detailed enough in the study of building-soil interaction. There remain many physical phenomena that need to be explained before moving to more complex three-dimensional models. Even though the real

world is three-dimensional, because of the possibility of separation of the in-plane from the anti-plane motion, the two-dimensional models may allow better understanding and explanation of many physical phenomena. In this work, and analytical two-dimensional model will be employed to study a building-soil interaction for general in-plane wave excitation. The purpose of the study is to understand the influence of various parameters, such as the relative building-soil stiffness, the depth of the embedment, the type of incident waves, and the building mass and slenderness ratio on the foundation and relative building response transfer function, with special attention to the effects of the wave passage.

In Chapter II, the problem and the boundary conditions are defined, as well as the superstructure model, the representation of the scattered waves in the soil, and the series expansion of the free-field motion and the closed form solution for incident plane P-waves. This is followed by presentation of some results and a discussion. The first part of Chapter III focuses on the series expansion of the motion of the inhomogeneous P-wave of the free-field motion, generated by the mode conversion for incident plane SV-waves beyond critical angle. Then, the closed form solution of the interaction equations and results and analysis are presented for incident plane SV-waves. In Chapter IV the same is repeated for incident Rayleigh waves. Chapter V contains the summary and the conclusions. Appendix A contains the list of symbols used in this report, and Appendix B an example of evaluation of the dimensionless stiffness parameter for the building.

CHAPTER II

DEFINITION OF THE PROBLEM AND SOLUTION FOR INCIDENT PLANE P-WAVES

II.1 The Model

II.1.1 Description of the Model and Definition of the Problem

The interaction model is shown in Fig. II.1. The building, of width W and height H, is represented by a homogeneous shear beam with mass m_b per unit length, shear wave velocity β_b, longitudinal wave velocity α_b and shear modulus μ_b. The shear beam is also allowed to deform in its longitudinal direction z. These two types of deformation are assumed not to couple with each other. The building is supported by a rigid circular foundation of width $2a$ and depth h, having center of curvature at O_1 and radius of curvature b. The depth of the foundation, h, can vary in the range $0 < h \leq a$. Its mass will be denoted by m_f. The foundation is embedded into a homogeneous half-space with shear modulus μ, density ρ and Poissons ratio ν. The shear and the longitudinal wave velocities, β and α, are

$$\beta = \sqrt{\frac{\mu}{\rho}}$$

and

$$\alpha = \sqrt{\frac{2(1-\nu)}{(1-2\nu)}}\beta.$$

It is assumed that the foundation and the half-space are perfectly bonded to each other at the contact surface $r_1 = b$, where $r_1 - \theta_1$ is a fixed polar coordinate system with origin at O_1. The $x-0-z$ coordinate system and the $0-\xi$ coordinate axis are also fixed. (Fig. II. 2) the former is attached to the half space and the latter coincides with the vertical axis of symmetry of the building at rest. A linear stress-stain relationship is assumed both in the building and in the half-space. No damping is assumed in either of the two media. The undisturbed configuration is taken as a reference system.

The excitation can be a plane monochromatic P- or SV-wave, with frequency ω and incident angle γ, or a Rayleigh wave. An incident P-wave, can be represented by its P-potential

$$\phi^i = \exp[ik_\alpha(x\sin\gamma - z\cos\gamma) - i\omega t] \qquad (II.1)$$

where $k_\alpha = \omega/\alpha$ is its wave number. This incident wave is reflected by the stress-free half-space surface and is scattered by the foundation. In this process additional P- and SV-waves are generated. The displacements in the half-space, in the positive x- and z-directions, are denoted by u and v. The excited foundation moves with three degrees of freedom: translations Δ and V, in the positive x and z directions, and a clockwise rotation φ about an axis perpendicular to the $x-z$ plane and passing through O. The moving foundation excites the building to vibrate with displacements u_b and v_b, in the positive x and ξ-directions, relative to its position at rest (Fig. II. 2).

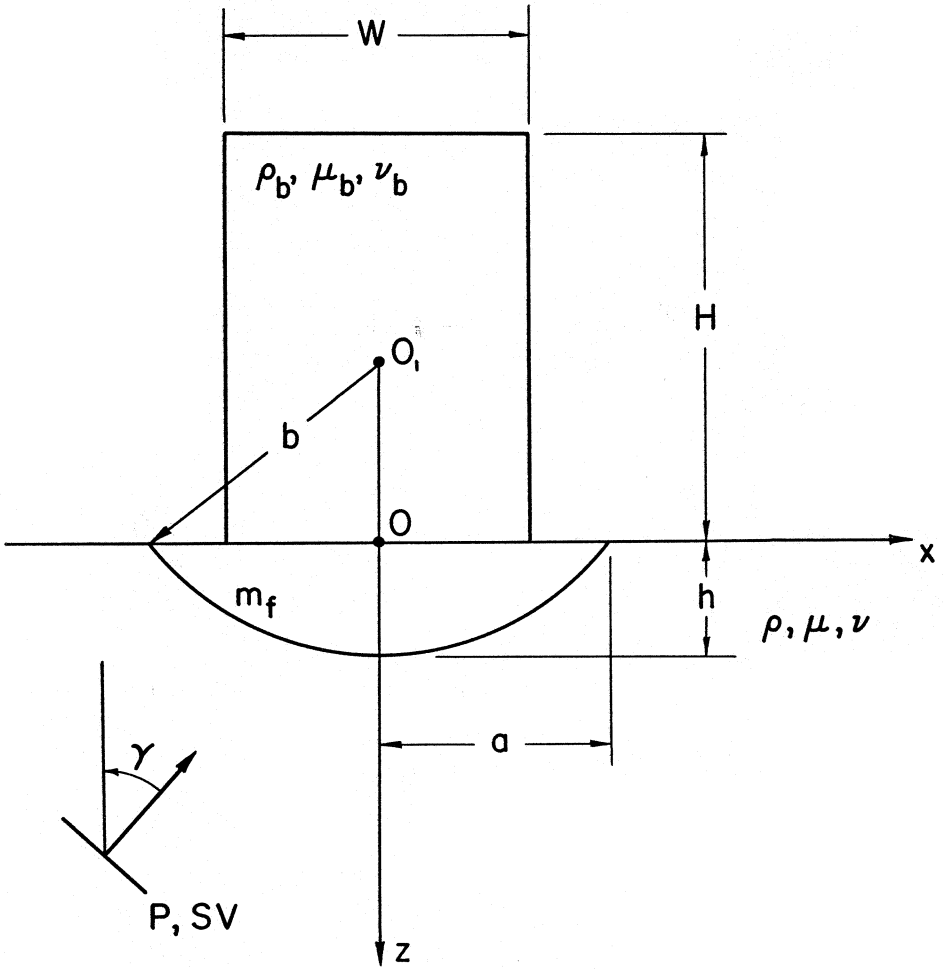

Figure II.1 The model

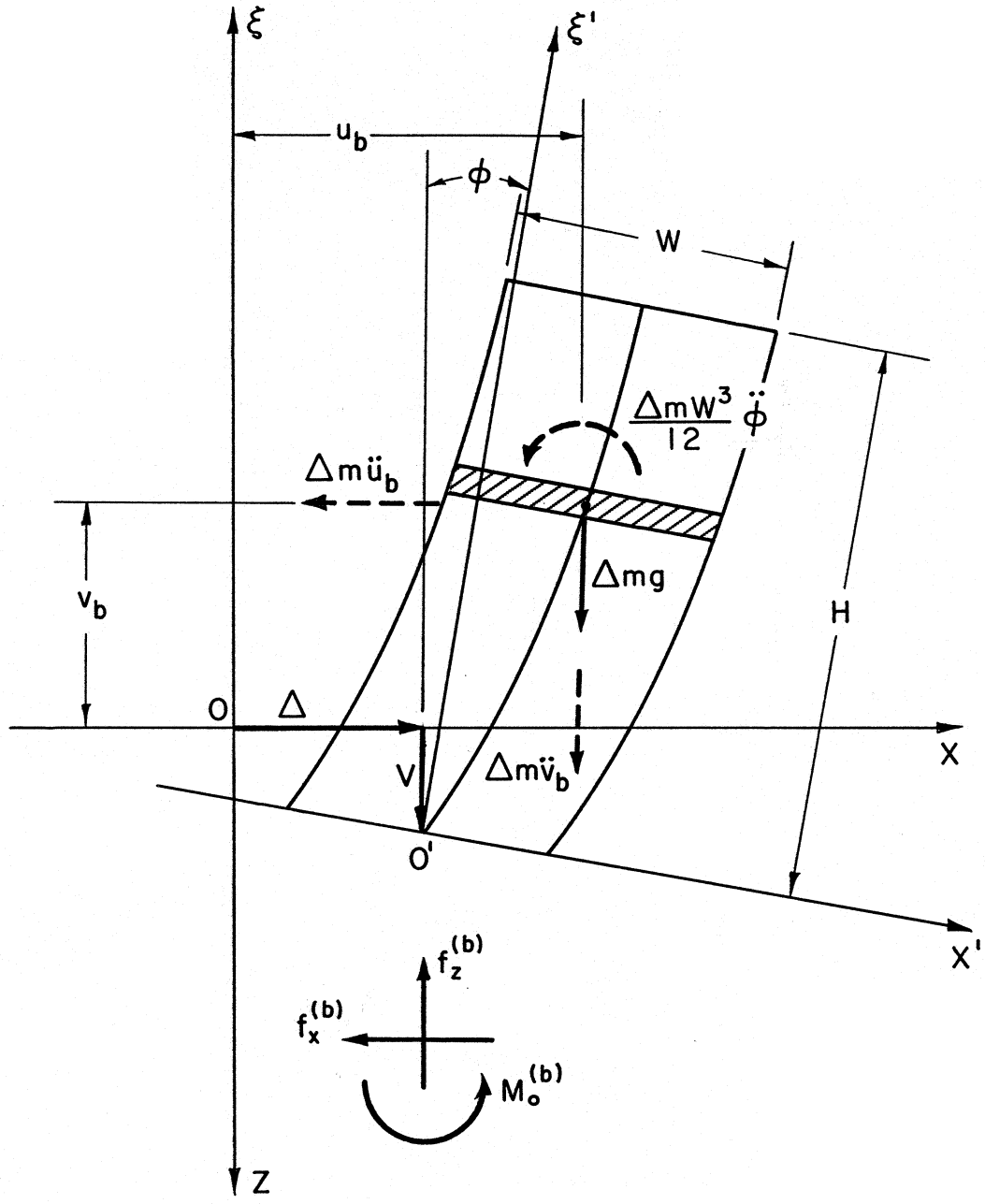

Figure II.2 Motion of the building

The steady-state motions of the building, of the foundation and of the half-space have to satisfy the following conditions:

(a) the motions of the half-space, u and v, and the motions of the building u_b and v_b have to satisfy the corresponding differential equations of motions;

(b) on the surface of the half-space, at $z = 0$ and left and right of the foundation, and on the top of the building, at $\xi = H$, all stresses have to be zero;

(c) continuity of displacements must exist between the motions of the foundation and of the half-space at the contact surface, $r_1 = b$ and $-\theta_0 \leq \theta_1 \leq \theta_0$, $\theta_0 = \sin^{-1} \frac{a}{b}$;

(d) the displacements of the building and of the foundation must be continuous at their contact surface, at $\xi = 0$;

(e) the motion of the foundation must be such that all the dynamic forces acting onto it are in dynamic equilibrium, and

(f) the influence of foundation and the superstructure on the motion of the half-space has to vanish at sufficiently large distances.

The aim of this work is to derive analytical expressions for the motions in the building, in the half-space and of the foundation. This will be carried out in several steps. In the subsequent sections, first, expressions for the displacements of the building and the forces acting onto it will be derived in terms of a given general displacement of the foundation. Next, the displacements of the half-space and the forces with which it acts onto the foundation will be derived in terms of the incident motion and given imposed displacement of the foundation. Finally, implementing the previous results into the equilibrium equations of the foundation, the motion of the foundation will be expressed in terms of the excitation. This approach of decomposition of the original problem into two separate problems and then implementing the results of those into the equilibrium equations is called a substructure approach. It can be applied only in linear problems. In this chapter the problem will be defined and solved only for incident plane monochromatic P-waves. In the next chapters the solution will be generalized for incident monochromatic plane SV-waves and for Rayleigh waves. In the time domain, the problem can be solved by the Fourier synthesis, with the response to monochromatic excitation as a transfer function.

II.1.2 Displacements and Forces in the Building

The free-body diagram of the building is shown in Fig. II.2. The undisturbed, as well as the exaggerated disturbed configuration at time t are shown. The absolute displacements u_b and v_b of the building, in the positive x- and negative z- (positive ξ) directions, respectively, will be measured with respect to the $0 - \xi$ axis. The $0' - \xi'$ axis in Fig. II.2 is a coordinate axis attached to and moving with the base of the building. The relative displacements of the building will be measured with respect to this axis.

The displacement of the base of the building, which is the same as the displacement of the foundation, is described by the horizontal translation Δ, the vertical translation V and the clockwise rotation φ about the center of the base. For a harmonic excitation, Δ, V and φ will be also harmonic, and can be written as

$$\Delta = \Delta_0 e^{-i\omega t} \tag{II.2a}$$

$$V = V_0 e^{-i\omega t} \tag{II.2b}$$

$$\varphi = \varphi_0 e^{-i\omega t} \tag{II.2c}$$

where Δ_0, V_0 and φ_0 are complex amplitudes. The finial displacement response of the building is a linear superposition of the responses to each of the components in equation (II.2) separately. The displacements Δ, V and φ are assumed to be small and thus the analysis is linear. With these assumptions, only the horizontal motions and the rotations will be coupled. Therefore,

$$u_b(\xi,t) = u_{b,\Delta}(\xi,t) + u_{b,\varphi}(\xi,t) \tag{II.3a}$$

$$v_b(\xi,t) = v_{b,V}(\xi,t) \tag{II.3b}$$

where $u_{b,\Delta}(\xi,t)$ and $u_{b,\varphi}(\xi,t)$ are the absolute horizontal displacements (in the positive x-direction) due to motions of the base Δ and φ, respectively, and $u_{b,V}$, is the absolute vertical displacement (in the positive ξ-direction) due to vertical motion of the base, V.

The horizontal and vertical displacements of the building, u_b and v_b, satisfy the following one-dimensional wave equations

$$\frac{\partial^2 u_b}{\partial \xi^2} = \frac{1}{\beta_b^2}\frac{\partial^2 u_b}{\partial t^2} \tag{II.4a}$$

$$\frac{\partial^2 v_b}{\partial \xi^2} = \frac{1}{\alpha_b^2}\frac{\partial^2 v_b}{\partial t^2}. \tag{II.4b}$$

The displacement $u_{b,\Delta}$ is a solution of equation (II.4a) that satisfies the boundary conditions

$$u_b(0,t) = \Delta_0 e^{-i\omega t} \tag{II.5a}$$

$$\frac{\partial u_b}{\partial \xi}(H,t) = 0 \tag{II.5b}$$

and it is equal to

$$u_{b,\Delta}(\xi,t) = \Delta_0 \left(\cos\frac{\omega\xi}{\beta_b} + \tan\frac{\omega H}{\beta_b}\sin\frac{\omega\xi}{\beta_b}\right) e^{-i\omega t}. \tag{II.5c}$$

Similarly, $u_{b,\varphi}$ is a solution of equation (II.4a) that satisfies the boundary conditions (see Fig. II.2)

$$u_b(0,t) = 0 \tag{II6a}$$

$$\frac{\partial u_b}{\partial \xi}(H,t) = \varphi_0 e^{-i\omega t} \tag{II.6b}$$

and it is equal to

$$u_{b,\varphi}(\xi,t) = \frac{\varphi_0}{\frac{\omega}{\beta_b}\cos\frac{\omega H}{\beta_b}} \sin\frac{\omega\xi}{\beta_b} e^{-i\omega t}. \qquad (II.6c)$$

Both $u_{b,\Delta}$ and $u_{b,\varphi}$ are positive in the positive x-direction. The vertical displacement $v_{b,V}$ is a solution of equation (II.4b) with the boundary conditions

$$v_b(0,t) = -V_0 e^{-i\omega t} \qquad (II.7a)$$

$$\frac{\partial v_b}{\partial \xi}(H,t) = 0 \qquad (II.7b)$$

and it is equal to

$$v_b(\xi,t) = V_0\left(\cos\frac{\omega\xi}{\alpha_b} + \tan\frac{\omega H}{\alpha_b}\sin\frac{\omega\xi}{\beta_b}\right) e^{-i\omega t}. \qquad (II.7c)$$

The minus sign arises (in equation II.7a) because V is measured downwards, while positive v_b is up. The boundary conditions, stated by equations (II.5b), (II.6b) and (II.7b), follow from the zero-stress condition at the top of the building.

The dynamic forces acting on the building are the inertia forces, the moments of the gravity forces, and the external forces $f_x^{(b)}$, $f_z^{(b)}$ and the external moment $M_0^{(b)}$ exerted onto the building by the foundation. The inertia forces are illustrated for accelerations of small elements of the beam with mass Δm, as shown in Fig. II.2.

Imposing dynamic equilibrium conditions of all the horizontal forces acting on the building, with the $x-0-z$ coordinate system as reference, it follows that

$$f_x^{(b)} = -\int_0^H W\rho_b \ddot{u}_b(\xi,t)d\xi \qquad (II.8a)$$

where the two dots over u_b denote second derivative with respect to time. Recalling equations (II.3a) , (II.5c) and (II.6c)

$$f_x^{(b)} = m_b\omega^2\left[\Delta_0\frac{\tan\frac{\omega H}{\beta_b}}{\frac{\omega H}{\beta_b}} - \frac{\varphi_0 H}{\left(\frac{\omega H}{\beta_b}\right)^2}\left(1-\frac{1}{\cos\frac{\omega H}{\beta_b}}\right)\right] e^{-i\omega t}. \qquad (II.8b)$$

From the dynamic equilibrium of vertical forces it follows that

$$f_z^{(b)} = \int_0^H W\rho_b \ddot{v}_b(\xi,t)d\xi \qquad (II.9a)$$

and recalling equation (II.7c)

$$f_z^{(b)} = m_b\omega^2 V_0 \frac{\tan\frac{\omega H}{\alpha_b}}{\frac{\omega H}{\alpha_b}} e^{-i\omega t}. \qquad (II.9b)$$

From the dynamic equilibrium of moments about O it follows that

$$\begin{aligned} M_0^{(b)} = &- \int_0^H W\rho_b \ddot{u}_b(\xi,t)\xi d\xi + \int_0^H W\rho_b g(u_{b,\varphi} + u_{b,\Delta}^{\text{rel}})d\xi \\ &- \int_0^H W\rho_b \frac{W^2}{12}\ddot{\varphi}(\xi,t)d\xi \end{aligned} \qquad (II.10a)$$

where

$$u_{b,\Delta}^{\text{rel}} = u_{b,\Delta} - \Delta$$

is the elastic deformation of the building due to the imposed horizontal motion Δ at the base. In equation (II.10a), the first integral includes the moments about O of the horizontal inertia forces due to rigid body translation Δ and rigid body rotation φ, as well as the overturning moment about O' of the inertia forces due to the elastic deformation of the building. The second integral represents the overturning moment of the gravity forces about O'. The third integral is a sum of the moments of the inertia forces due to clockwise rotation φ of each of the horizontal slices of thickness $\Delta\xi$ and mass Δm (see Fig. II.2) about a horizontal axis through their center. The last term is negligible for slender buildings, but must be considered for wide and short buildings. The moment of the vertical inertia forces has been dropped in (equation II.10a) because it involves terms that are of order $O(V_0 \cdot \Delta_0)$ and $O(V_0 \cdot \varphi_0)$ which are higher order terms in our analysis. Recalling the expression for u_b, $u_{b,\varphi}$ and $u_{v,\Delta}$, equations (II.3a), (II.5c) and (II.6c),

$$\begin{aligned} M_0^{(b)} = &\frac{m_b\omega^2}{H}\left\{\Delta_0\left[\frac{1}{\left(\frac{\omega}{\beta_b}\right)^2}\left(\frac{1}{\cos\frac{\omega H}{\beta_b}} - 1\right) + \frac{1}{\left(\frac{\omega}{\beta_b}\right)^2}\tan\frac{\omega H}{\beta_b}\sin\frac{\omega H}{\beta_b}\right]\right. \\ &\left. + \varphi_0\left[\frac{\tan\frac{\omega H}{\beta_b}}{\left(\frac{\omega}{\beta_b}\right)^3} - \frac{H}{\left(\frac{\omega}{\beta_b}\right)^2}\right]\right\} e^{-i\omega t} \\ &+ \frac{m_b g}{H}\left[\Delta_0\left(\frac{\tan\frac{\omega H}{\beta_b}}{\frac{\omega}{\beta_b}} - H\right) + \frac{\varphi_0}{\left(\frac{\omega}{\beta_b}\right)^2}\left(\frac{1}{\cos\frac{\omega H}{\beta_b}} - 1\right)\right] e^{-i\omega t} \\ &+ m_b\omega^2\frac{W^2}{12}\varphi_0 e^{-i\omega t} \end{aligned} \qquad (II.10b)$$

Equations (II.8b), (II.9b) and (II.10b) can be written in matrix form as follows

$$\begin{Bmatrix} f_z^{(b)} \\ f_x^{(b)} \\ M_0^{(b)}/H \end{Bmatrix} = m_b\omega^2\left[[K^{(b)}] + [C_g^{(b)}]\right]\begin{Bmatrix} V_0 \\ \Delta_0 \\ \varphi_0 H \end{Bmatrix} e^{-i\omega t} \qquad (II.11)$$

where [K] is a 3×3 block diagonal matrix

$$[K^{(b)}] = \begin{bmatrix} k_{11} & 0 & 0 \\ 0 & k_{22} & k_{23} \\ 0 & k_{32} & k_{33} \end{bmatrix} \qquad (II.12)$$

with real entries

$$k_{11} = \frac{\tan \frac{\omega H}{\alpha_b}}{\frac{\omega H}{\alpha_b}} \qquad (II.12a)$$

$$k_{22} = \frac{\tan \frac{\omega H}{\beta_b}}{\frac{\omega H}{\beta_b}} \qquad (II.12b)$$

$$k_{23} = \frac{-1}{\left(\frac{\omega H}{\beta_b}\right)^2}\left(1 - \frac{1}{\cos \frac{\omega H}{\beta_b}}\right) \qquad (II.12c)$$

$$k_{32} = \frac{-1}{\left(\frac{\omega H}{\beta_b}\right)^2}\left(1 - \frac{1}{\cos \frac{\omega H}{\beta_b}}\right) \qquad (II.12d)$$

$$k_{33} = \frac{-1}{\left(\frac{\omega H}{\beta_b}\right)^2}\left(\frac{\tan \frac{\omega H}{\beta_b}}{\frac{\omega H}{\beta_b}} - 1\right) + \frac{1}{12}\left(\frac{W}{H}\right)^2. \qquad (II.12e)$$

and $[C_g^{(b)}]$ is

$$[C_g^{(b)}] = \frac{g}{\omega^2 H}\begin{bmatrix} 0 & 0 & 0 \\ 0 & 0 & 0 \\ 0 & c_{32} & c_{33} \end{bmatrix} \qquad (II.13)$$

where

$$c_{32} = \frac{\tan \frac{\omega H}{\beta_b}}{\frac{\omega H}{\beta_b}} - 1 \qquad (II.13a)$$

$$c_{33} = \frac{1}{\cos \frac{\omega H}{\beta_b}} - 1 \qquad (II.13b)$$

and g is the acceleration due to gravity. The matrix $m_b\omega^2[K^{(b)}]$ is the stiffness matrix for the building. Because of the absence of damping, all of its terms are real. The matrix $m_b\omega^2[C_g^{(b)}]$ is a stiffness matrix associated with the force vector $\{F_g^{(b)}\} = \{0 \quad 0 \quad M_{0,g}^{(b)}/H\}^T$, where $M_{0,g}^{(b)}$ is the dynamic moment of the gravity forces of the building about the center of its base.

II.1.3 Motion of the Half-space

II.1.3.1 The Free-field Motion

It is convenient to represent the motion in the half-space as a superposition of the "free-field" motion and the waves scattered from the foundation. The "free-field" motion

consists of the plane incident P-wave and the reflected plane P- and SV-waves from the half-space surface in the absence of the foundation and the building. The reflected P and SV-waves have potentials ϕ^r and ψ^r as follows

$$\phi^r = K_1 \exp[ik_\alpha(x\sin\theta_\alpha + z\cos\theta_\alpha) - i\omega t] \qquad (II.14a)$$

$$\psi^r = K_2 \exp[ik_\beta(x\sin\theta_\beta + z\cos\theta_\beta) - i\omega t] \qquad (II.14b)$$

where the angle of the reflected P-wave θ_α ($= \gamma$, the incident angle of the P-wave) and the angle of the reflected S-wave, θ_β, are related by

$$\frac{\sin\theta_\alpha}{\alpha} = \frac{\sin\theta_\beta}{\beta}$$

and where $k_\beta = \omega/\beta$ is the wave number of the S-waves. The reflection coefficients K_1 and K_2 are both real and are equal to

$$K_1 = \frac{\sin 2\theta_\alpha \sin 2\theta_\beta - (\alpha/\beta)^2 \cos^2 2\theta_\beta}{\sin 2\theta_\alpha \sin 2\theta_\beta + (\alpha/\beta)^2 \cos^2 2\theta_\beta} \qquad (II.15a)$$

$$K_2 = \frac{-2\sin 2\theta_\beta \cos 2\theta_\beta}{\sin 2\theta_\alpha \sin 2\theta_\beta + (\alpha/\beta)^2 \cos^2 2\theta_\beta} \qquad (II.15b)$$

(e.g. see Cao and Lee, 1988).

II.1.3.2 Representation of the Scattered Waves

The essential part of this analysis, is to represent the waves scattered from the foundation. We have used here the method developed by Cao and Lee (1990) and Lee and Cao (1989) for scattering of plane P- and SV-waves by shallow cylindrical canyons. The geometry of their canyon is the same as the geometry of the canyons in Fig. II.1 and Fig. II.3, where the foundation is imbedded. They represented each of the potentials of the scattered P- and SV-waves, by a combination of two series of cylindrical wave functions with origin at O_1: a series of Hankel $\mathcal{H}_n^{(1)}$ functions and a series of Bessel J_n functions, i.e.

$$\phi^R = \phi_1^R + \phi_2^R \qquad (II.16a)$$

and

$$\psi^R = \psi_1^R + \psi_2^R \qquad (II.16b)$$

where

$$\phi_1^R = \sum_{n=0}^{\infty}\left(A_{1,n}\cos n\theta_1 + B_{1,n}\sin n\theta_1\right)\mathcal{H}_n^{(1)}(k_\alpha r_1)e^{-i\omega t} \qquad (II.17a)$$

$$\phi_2^R = \sum_{n=0}^{\infty}\left(A^*_{2,n}\cos n\theta_1 + B^*_{2,n}\sin n\theta_1\right)J_n(k_\alpha r_1)e^{-i\omega t} \qquad (II.17b)$$

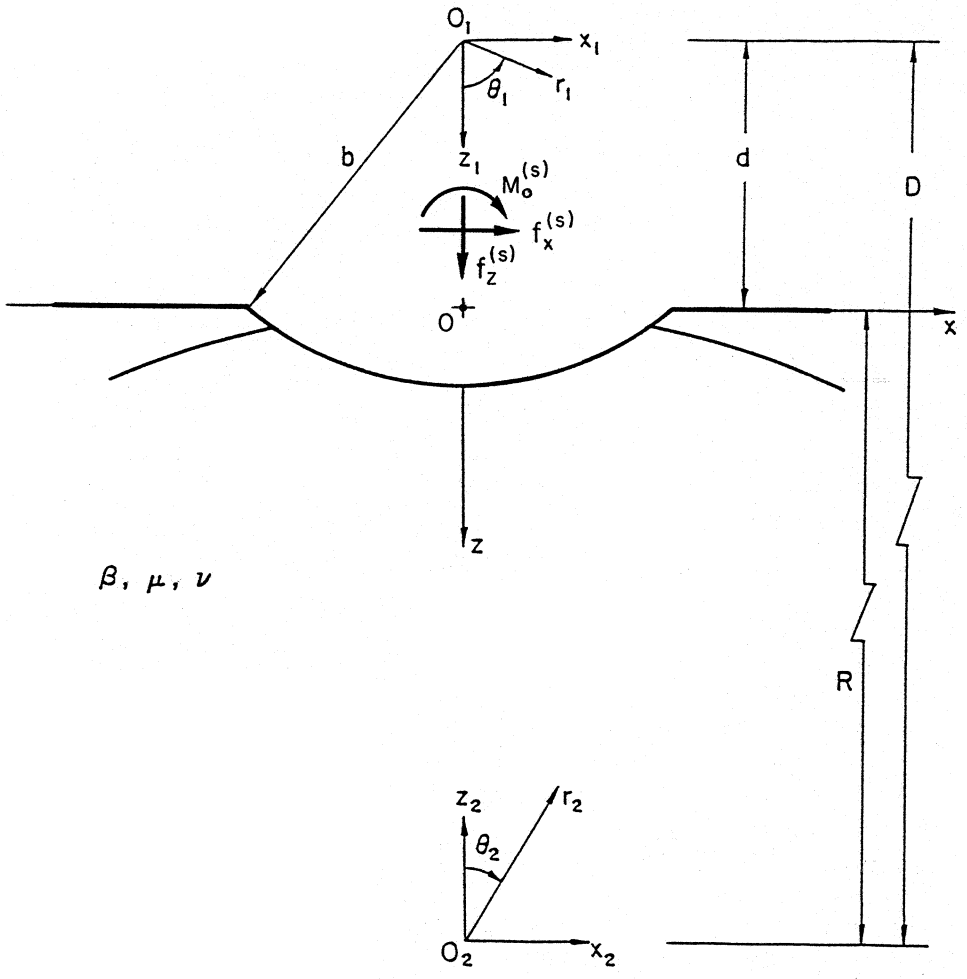

Figure II.3 Motion of the half-space

$$\psi_1^R = \sum_{n=0}^{\infty}\Big(C_{1,n}\sin n\theta_1 + D_{1,n}\cos n\theta_1\Big)\mathcal{H}_n^{(1)}(k_\beta r_1)e^{-i\omega t} \qquad (II.17c)$$

$$\psi_2^R = \sum_{n=0}^{\infty}\Big(C_{2,n}^*\sin n\theta_1 + D_{2,n}^*\cos n\theta_1\Big)J_n^{(1)}(k_\beta r_1)e^{-i\omega t} \qquad (II.17d)$$

(The function $\mathcal{H}_n^{(1)}(kr_1)e^{-i\omega t}$ represents a cylindrical wave propagating away from O_1 with wave number k, while $J_n(kr_1)$ represents a standing cylindrical wave with the same wave number and with origin at O_1.) Such a representation of the scattered waves is complete. Those waves were required to satisfy the condition at $r_1 = b$ (zero-stress) exactly, but the zero-stress condition on the half-space surface only approximately. Lee and Cao approximated the half-space surface in the vicinity of the canyon by a concave cylindrical surface of very large radius R ($R \sim 100a$) that is tangent to the plane $z = 0$ at O, and required that the scattered waves satisfy the zero-stress condition on this surface. Using the Addition theorem for cylindrical Bessel functions, they transformed ϕ_1^R, ψ_1^R, and ϕ_2^R and ψ_2^R into Fourier-Bessel series of r_2 and θ_2, where $r_2 - \theta_2$ is a polar coordinate system with origin at O_2, the center of the big cylinder approximating free half-space surface (see Fig. II.3). The series of $J_n(kr_1)$ were transformed into series of $J_n(kr_2)$. But the series of $\mathcal{H}_n^{(1)}(kr_1)$ were also transformed into series of $J_n(kr_2)$. This implied that only the trivial solution could satisfy the zero-stress condition on $r_2 = R$. If we denote the coefficients of ϕ_1^R and ϕ_2^R in the series in $r_2 - \theta_2$ coordinate system by $A_{1,n}^*$ and $B_{1,n}^*$, and $A_{2,n}$ and $B_{2,n}$, respectively, the trivial solution implied that

$$A_{1,n}^* = -A_{2,n} \qquad (II.18a)$$

$$B_{1,n}^* = -B_{2,n}. \qquad (II.18b)$$

Similarly, the coefficients of the series representing ψ_1^R and ψ_2^R in the $r_2 - \theta_2$ coordinate system, $C_{1,n}^*$ and $D_{1,n}^*$, and $C_{2,n}$ and $D_{2,n}$, respectively had to satisfy

$$C_{1,n}^* = -C_{2,n} \qquad (II.18c)$$

$$D_{1,n}^* = -D_{2,n}. \qquad (II.18d)$$

Still, Cao and Lee did not reject their idea of transforming ϕ_1^R, ϕ_2^R, ψ_1^R and ψ_2^R in the $(r_2 - \theta_2)$ coordinate system. First, they truncated the infinite series representing the potentials of the scattered waves in $r_1 - \theta_1$ coordinate system at some $n = N$, and then they transformed those potentials into series in the $r_2 - \theta_2$ coordinate system. Then, they truncated these series at some $n = M$, applied the conditions in equations (II.18), and transformed the potentials back into the $r_1 - \theta_1$ coordinate system, using again the Addition theorem. Consequently, relationships were established between the sets $\{A_{1,n}\}_{n=0}^N$ and $\{A_{2,n}^*\}_{n=0}^N$, $\{B_{1,n}\}_{n=0}^N$ and $\{B_{2,n}^*\}_{n=0}^N$, $\{C_{1,n}\}_{n=0}^N$ and $\{C_{2,n}^*\}_{n=0}^N$, and $\{D_{1,n}\}_{n=0}^N$ and $\{D_{2,n}^*\}_{n=0}^N$. In their calculations Cao and Lee took $M = N$. Using a similar approach for incident SH waves, Cao and Lee (1989) got excellent agreement with the exact solution by Trifunac (1971).

There are, so far, no exact analytical solutions for scattering of in-plane incident waves by cylindrical canyons. For incident P- and SV-waves, our study showed that the results by this method are in good agreement with published approximate results by Wong (1979)) (using the Ohsaki's method with point sources), with the results of Sanchez-Sesma et al. (1985) (using the method of Hankel function expansion of the scattered waves and application of the zero-stress condition in the least squares sense), and with the results of Kawase (1988) (who used the discrete wave numbers and the boundary element method). Moreover, our study showed that if we take $M = 0$, i.e. if we relax the zero-stress condition on the half-space surface, the surface displacements change little for the cases we considered, and the results by the method of Cao and Lee are again in good agreement with the results by the previously mentioned approximate methods. The fact that the zero-stress condition at $z = 0$ appears to affect only little the motion of the scattered waves, relative to the conditions at the canyon wall (i.e. $r_1 = b$), and the fact that the method of Cao and Lee satisfies the second condition exactly, influenced our decision to use this approximate method in our interaction problem.

II.1.3.3 Displacements and Stresses in the Half-space

The radial and tangential components of the displacements, u_r and u_θ, and the stresses τ_{r_1,r_1} and τ_{r_1,θ_1}, at a point (r_1, θ_1) in the half-space, can be calculated from the potentials as follows:

$$
\begin{aligned}
\left\{ \begin{matrix} u_{r_1} \\ u_{\theta_1} \end{matrix} \right\} = \frac{1}{r_1} \Bigg\{ & \sum_{n=0}^{N} \left[\begin{matrix} D_{11}^{(3)} \cos n\theta_1 & D_{12}^{(3)+} \cos n\theta_1 \\ D_{21}^{(3)+} \sin n\theta_1 & D_{22}^{(3)} \sin n\theta_1 \end{matrix} \right] \left\{ \begin{matrix} A_{1,n} \\ C_{1,n} \end{matrix} \right\} \\
& + \left[\begin{matrix} D_{11}^{(3)} \sin n\theta_1 & D_{12}^{(3)-} \sin n\theta_1 \\ D_{21}^{(3)-} \cos n\theta_1 & D_{22}^{(3)} \cos n\theta_1 \end{matrix} \right] \left\{ \begin{matrix} B_{1,n} \\ D_{1,n} \end{matrix} \right\} \\
& + \left[\begin{matrix} D_{11}^{(1)} \cos n\theta_1 & D_{12}^{(1)+} \cos n\theta_1 \\ D_{21}^{(1)+} \sin n\theta_1 & D_{22}^{(1)} \sin n\theta_1 \end{matrix} \right] \left\{ \begin{matrix} A_{0,n} + A_{2,n}^{*} \\ C_{0,n} + C_{2,n}^{*} \end{matrix} \right\} \\
& + \left[\begin{matrix} D_{11}^{(1)} \sin n\theta_1 & D_{12}^{(1)-} \sin n\theta_1 \\ D_{21}^{(1)+} \cos n\theta_1 & D_{22}^{(1)} \cos n\theta_1 \end{matrix} \right] \left\{ \begin{matrix} B_{0,n} + B_{2,n}^{*} \\ D_{0,n} + D_{2,n}^{*} \end{matrix} \right\} \Bigg\} e^{-i\omega t}
\end{aligned}
\qquad (II.19)
$$

$$
\begin{aligned}
\left\{ \begin{matrix} \tau_{r_1 r_1} \\ \tau_{r_1 \theta_1} \end{matrix} \right\} = \frac{2\mu}{r_1^2} \Bigg\{ & \sum_{n=0}^{N} \left[\begin{matrix} \mathcal{E}_{11}^{(3)} \cos n\theta_1 & \mathcal{E}_{12}^{(3)+} \cos n\theta_1 \\ \mathcal{E}_{21}^{(3)+} \sin n\theta_1 & \mathcal{E}_{22}^{(3)} \sin n\theta_1 \end{matrix} \right] \left\{ \begin{matrix} A_{1,n} \\ C_{1,n} \end{matrix} \right\} \\
& + \left[\begin{matrix} \mathcal{E}_{11}^{(3)} \sin n\theta_1 & \mathcal{E}_{12}^{(3)-} \sin n\theta_1 \\ \mathcal{E}_{21}^{(3)-} \cos n\theta_1 & \mathcal{E}_{22}^{(3)} \cos n\theta_1 \end{matrix} \right] \left\{ \begin{matrix} B_{1,n} \\ D_{1,n} \end{matrix} \right\} \\
& + \left[\begin{matrix} \mathcal{E}_{11}^{(1)} \cos n\theta_1 & \mathcal{E}_{12}^{(1)+} \cos n\theta_1 \\ \mathcal{E}_{21}^{(1)+} \sin n\theta_1 & \mathcal{E}_{22}^{(1)} \sin n\theta_1 \end{matrix} \right] \left\{ \begin{matrix} A_{0,n} + A_{2,n}^{*} \\ C_{0,n} + C_{2,n}^{*} \end{matrix} \right\} \\
& + \left[\begin{matrix} \mathcal{E}_{11}^{(1)} \sin n\theta_1 & \mathcal{E}_{12}^{(1)-} \sin n\theta_1 \\ \mathcal{E}_{21}^{(1)+} \cos n\theta_1 & \mathcal{E}_{22}^{(1)} \cos n\theta_1 \end{matrix} \right] \left\{ \begin{matrix} B_{0,n} + B_{2,n}^{*} \\ D_{0,n} + D_{2,n}^{*} \end{matrix} \right\} \Bigg\} e^{-i\omega t}
\end{aligned}
\qquad (II.20)
$$

where (see Paw and Mow, 1971)

$$\mathcal{D}_{11}^{(\ell)} = -nC_n(k_\alpha r) + k_\alpha r C_{n-1}(k_\alpha r) \tag{II.21a}$$

$$\mathcal{D}_{12}^{(\ell)\pm} = \pm nC_n(k_\beta r) \tag{II.21b}$$

$$\mathcal{D}_{21}^{(\ell)\pm} = \mp nC_n(k_\alpha r) \tag{II.21c}$$

$$\mathcal{D}_{22}^{(\ell)} = nC_n(k_\beta r) - k_\beta r C_{n-1}(k_\beta r) \tag{II.21d}$$

and

$$\mathcal{E}_{11}^{(\ell)} = (n^2 + n - \frac{1}{2}k_\alpha r^2)C_n(k_\alpha r) - k_\alpha r C_{n-1}(k_\alpha r) \tag{II.22a}$$

$$\mathcal{E}_{12}^{(\ell)\pm} = \pm n\left[-(n+1)C_n(k_\beta r) + k_\beta r C_{n-1}(k_\beta r)\right] \tag{II.22b}$$

$$\mathcal{E}_{21}^{(\ell)\pm} = \mp n\left[-(n+1)C_n(k_\alpha r) + k_\alpha r C_{n-1}(k_\alpha r)\right] \tag{II.22c}$$

$$\mathcal{E}_{22}^{(\ell)} = -(n^2 + n - \frac{1}{2}k_\beta r^2)C_n(k_\beta r) + k_\beta r C_{n-1}(k_\beta r)\ . \tag{II.22d}$$

In equation (II.21) and (II.22), $C_n^{(\ell)}(\cdot) = J_n(\cdot)$ when $\ell = 1$, and $C_n^{(\ell)}(\cdot) = \mathcal{H}_n^{(1)}(\cdot)$ when $\ell = 3$. The coefficients $A_{0,n}$, $B_{0,n}$, $C_{0,n}$ and $D_{0,n}$ $n = 0, 1, \ldots$ are the coefficients of the expansion of the potentials of the free-field motion in Fourier-Bessel series in the $r_1 - \theta_1$ coordinate system,

$$\phi^{i+r}(r_1, \theta_1) = \sum_{n=0}^{\infty} J_n(k_\alpha r_1)\left(A_{0,n}\cos n\theta_1 + B_{0,n}\sin n\theta_1\right)\exp\left(-i\omega t\right) \tag{II.23a}$$

$$\psi^{r}(r_1, \theta_1) = \sum_{n=0}^{\infty} J_n(k_\beta r_1)\left(C_{0,n}\sin n\theta_1 + D_{0,n}\cos n\theta_1\right)\exp\left(-i\omega t\right), \tag{II.23b}$$

where

$$A_{0,n} = \epsilon_n i^n \cos n\theta_\alpha \left((-1)^n e^{ik_\alpha d\cos\theta_\alpha} + K_1 e^{-ik_\alpha d\cos\theta_\alpha}\right) \tag{II.24a}$$

$$B_{0,n} = \epsilon_n i^n \sin n\theta_\alpha \left(-(-1)^n e^{ik_\alpha d\cos\theta_\alpha} + K_1 e^{-ik_\alpha d\cos\theta_\alpha}\right) \tag{II.24b}$$

$$C_{0,n} = \epsilon_n K_2 e^{-ik_\beta d\cos\theta_\beta} i^n \sin n\theta_\beta \tag{II.24c}$$

$$D_{0,n} = \epsilon_n K_2 e^{-ik_\beta d\cos\theta_\beta} i^n \cos n\theta_\beta. \tag{II.24d}$$

In equations (II.19) and (II.20) N is the index where the infinite sums have been truncated. The coefficients of ϕ_1^R, ϕ_2^R, ψ_1^R, ψ_2^R in equations (II.17) are related as follows:

$$\begin{Bmatrix} A_{2,n}^* \\ C_{2,n}^* \end{Bmatrix} = -\sum_{m=0}^{M} \begin{bmatrix} R_{nm}^+(k_\alpha D) & 0 \\ 0 & R_{nm}^-(k_\beta D) \end{bmatrix} \begin{Bmatrix} A_{1,m} \\ C_{1,m} \end{Bmatrix} \tag{II.25a}$$

$$\begin{Bmatrix} B_{2,n}^* \\ D_{2,n}^* \end{Bmatrix} = -\sum_{m=0}^{M} \begin{bmatrix} R_{nm}^+(k_\alpha D) & 0 \\ 0 & R_{nm}^-(k_\beta D) \end{bmatrix} \begin{Bmatrix} B_{1,m} \\ D_{1,m} \end{Bmatrix} \tag{II.25b}$$

where

$$R^{\pm}_{nm}(kr) = \frac{\epsilon_n}{2}\sum_{l=0}^{M}\frac{\epsilon_l}{2}\Big[J_{n+l}(kr)\pm(-1)^l J_{n-l}(kr)\Big]\cdot\Big[\mathcal{H}^{(1)}_{l+m}(kr)\pm(-1)^m H^{(1)}_{l-m}(kr)\Big] \quad (II.26)$$

and where $\epsilon_0 = 2$ and $\epsilon_n = 1$ for $n \geq 1$.

II.1.3.4 Imposing Continuity of Displacements at $r_1 = b$

The foundation moves as a rigid body, and its motion is defined by the translations Δ and V and the rotation φ. At $r_1 = b$, the r_1 and θ_1 components of the displacements are

$$\begin{Bmatrix} u_{r_1}(b,\theta_1) \\ u_{\theta_1}(b,\theta_1) \end{Bmatrix} = \begin{bmatrix} \cos\theta_1 & \sin\theta_1 & (d/H)\sin\theta_1 \\ -\sin\theta_1 & \cos\theta_1 & -b/H + (d/H)\cos\theta_1 \end{bmatrix} \begin{Bmatrix} V_0 \\ \Delta_0 \\ \varphi_0 H \end{Bmatrix} e^{-i\omega t}. \quad (II.27)$$

The 2×3 matrix on the right-hand-side (RHS) of equation (II.27) is a foundation motion influence matrix. For a rigid foundation it depends on its shape. Since those displacements must be continuous with the displacements of the half-space at $r_1 = b$, for all angles θ_1 the RHS of equation (II.27) must be equal to the RHS of equation (II.19), evaluated at $r_1 = b$. This implies the following relationships between the coefficients of the scattered waves and the displacements of the foundation:

$$\begin{Bmatrix} \vdots \\ \begin{Bmatrix} A_{1,n} \\ C_{1,n} \end{Bmatrix} \\ \vdots \end{Bmatrix} = [W^+]^{-1} \begin{bmatrix} \ddots & & \\ & \Big[\mathcal{D}^{(1)+}(n,b)\Big]_{2\times 2} & \\ & & \ddots \end{bmatrix} \begin{Bmatrix} \vdots \\ \begin{Bmatrix} A_{0,n} \\ C_{0,n} \end{Bmatrix} \\ \vdots \end{Bmatrix} - b[X^+] \begin{Bmatrix} V_0 \\ \Delta_0 \\ \varphi_0 H \end{Bmatrix} \quad (II.28a)$$

$$\begin{Bmatrix} \vdots \\ \begin{Bmatrix} B_{1,n} \\ D_{1,n} \end{Bmatrix} \\ \vdots \end{Bmatrix} = [W^-]^{-1} \begin{bmatrix} \ddots & & \\ & \Big[\mathcal{D}^{(1)-}(n,b)\Big]_{2\times 2} & \\ & & \ddots \end{bmatrix} \begin{Bmatrix} \vdots \\ \begin{Bmatrix} B_{0,n} \\ D_{0,n} \end{Bmatrix} \\ \vdots \end{Bmatrix} - b[X^-] \begin{Bmatrix} V_0 \\ \Delta_0 \\ \varphi_0 H \end{Bmatrix} \quad (II.28b)$$

where the matrices $[W^{\pm}]_{(N+1)\times(N+1)}$ consist of 2×2 blocks $[WW^{\pm}]_{2\times 2}$, such that the blocks occupying the n-th row and m-th column are

$$[WW^{\pm}(n,m)] = [\mathcal{D}^{(1)\pm}(n,b)][RR^{\pm}(n,m)] - \delta_{nm}[\mathcal{D}^{(3)\pm}(n,b)]. \quad (II.29)$$

In the above equations

$$\Big[\mathcal{D}(n,b)^{(\ell)\pm}\Big]_{2\times 2} = \begin{bmatrix} \mathcal{D}^{(\ell)}_{11}(n,b) & \mathcal{D}^{(\ell)\pm}_{12}(n,b) \\ \mathcal{D}^{(\ell)\pm}_{21}(n,b) & \mathcal{D}^{(\ell)}_{22}(n,b) \end{bmatrix} \quad (II.30a)$$

$$[RR^{\pm}(n,m)]_{2\times 2} = \begin{bmatrix} R^{\pm}_{nm}(k_\alpha D) & 0 \\ 0 & R^{\mp}_{nm}(k_\beta D) \end{bmatrix} \qquad (II.30b)$$

$$[X^{+}]_{2(N+1)\times 3} = \begin{bmatrix} 0 & 0 & 0 \\ 0 & 0 & 0 \\ 1 & 0 & 0 \\ -1 & 0 & 0 \\ 0 & 0 & 0 \\ \vdots & \vdots & \vdots \\ 0 & 0 & 0 \end{bmatrix} \qquad (II.30c)$$

$$[X^{-}]_{2(N+1)\times 3} = \begin{bmatrix} 0 & 0 & 0 \\ 0 & 0 & -b/H \\ 0 & 1 & d/H \\ 0 & 1 & d/H \\ 0 & 0 & 0 \\ \vdots & \vdots & \vdots \\ 0 & 0 & 0 \end{bmatrix}. \qquad (II.30d)$$

II.1.4 Forces Acting on the Half-space

Integrating the stresses in the half-space along $r_1 = b$ and $-\theta_0 \leq \theta_1 \leq \theta_0$, where $\theta_0 = \sin^{-1}(a/b)$, the resultant forces with which the foundation acts on the half-space can be calculated, as

$$\begin{Bmatrix} f_z^{(s)} \\ f_x^{(s)} \\ M_0^{(s)}/H \end{Bmatrix} = -\int_{-\theta_0}^{\theta_0} b \begin{bmatrix} \cos\theta_1 & -\sin\theta_1 \\ \sin\theta_1 & \cos\theta_1 \\ \frac{d}{H}\sin\theta_1 & -\frac{b}{H}+\frac{d}{H}\cos\theta_1 \end{bmatrix} \begin{Bmatrix} \tau_{r_1 r_1}(b,\theta_1) \\ \tau_{r_1\theta_1}(b,\theta_1) \end{Bmatrix} d\theta_1 \qquad (II.31a)$$

where $f_z^{(s)}$ and $f_x^{(s)}$ are the resultant forces in the positive z- and x-directions, and $M_0^{(s)}$ is the resultant clockwise moment about O. Recalling the expression for the stresses, equation (II.20), for the coefficients $\left\{ \begin{matrix} A_{1,n} \\ C_{1,n} \end{matrix} \right\}_{n=0}^{N}$ and $\left\{ \begin{matrix} B_{1,n} \\ D_{1,n} \end{matrix} \right\}_{n=0}^{N}$, equations (II.28), and for the coefficients $\left\{ \begin{matrix} A^*_{1,n} \\ C^*_{1,n} \end{matrix} \right\}_{n=0}^{N}$ and $\left\{ \begin{matrix} B^*_{1,n} \\ D^*_{1,n} \end{matrix} \right\}_{n=0}^{N}$, equation (II.25), and performing the integration in equation (II.31a), the resultant forces acting onto the half-space at $r_1 = b$ and $-\theta_0 \leq \theta_1 \leq \theta_0$ are as follows:

$$\begin{Bmatrix} f_z^{(s)} \\ f_x^{(s)} \\ M_0^{(s)}/H \end{Bmatrix} = \Big[\frac{-2\mu}{b}[P^+] \begin{Bmatrix} \vdots \\ \left\{ \begin{matrix} A_{0,n} \\ C_{0,n} \end{matrix} \right\} \\ \vdots \end{Bmatrix} + \frac{-2\mu}{b}[P^-] \begin{Bmatrix} \vdots \\ \left\{ \begin{matrix} B_{0,n} \\ D_{0,n} \end{matrix} \right\} \\ \vdots \end{Bmatrix} - 2\mu[Q] \begin{Bmatrix} V_0 \\ \Delta_0 \\ \varphi_0 H \end{Bmatrix} \Big] e^{-i\omega t} \qquad (II.31b)$$

$$[P^{\pm}]_{3\times 2(N+1)} = \left[\cdots \left[L^{(1)\pm}\right]_{3\times 2} \cdots\right] - [T^{\pm}][W^{\pm}]^{-1} \begin{bmatrix} \ddots & & \\ & \left[(\mathcal{D}^{(1)\pm}_{n,b})\right] & \\ & & \ddots \end{bmatrix} \qquad (II.32a)$$

$$[Q] = [T^{+}][W^{+}]^{-1}[X^{+}] + [T^{-}][W^{-}]^{-1}[X^{-}] \qquad (II.32b)$$

and

$$[T^{\pm}]_{3\times 2(N+1)} = \left[\cdots \left[\sum_{n} [L(n)^{(1)\pm}]\,[RR(n,l)^{\pm}] - [L(l)^{(3)\pm}]\right]_{3\times 2} \cdots\right]. \qquad (II.32c)$$

The 3×2 matrices $[L(n)^{(\ell)\pm}]$ are as follows:

$$[L(n)^{(\ell)+}] = \int_{-\theta_0}^{\theta_0} \begin{bmatrix} \cos\theta_1 & -\sin\theta_1 \\ \sin\theta_1 & \cos\theta_1 \\ \frac{d}{H}\sin\theta_1 & -\frac{b}{H} + \frac{d}{H}\cos\theta_1 \end{bmatrix} \begin{bmatrix} \mathcal{E}^{(\ell)}_{11}(n,b)\cos n\theta_1 & \mathcal{E}^{(\ell)+}_{12}(n,b)\cos n\theta_1 \\ \mathcal{E}^{(\ell)+}_{21}(n,b)\sin\theta_1 & \mathcal{E}^{(\ell)}_{22}(n,b)\sin n\theta_1 \end{bmatrix} d\theta_1 \qquad (II.33a)$$

$$[L(n)^{(\ell)-}] = \int_{-\theta_0}^{\theta_0} \begin{bmatrix} \cos\theta_1 & -\sin\theta_1 \\ \sin\theta_1 & \cos\theta_1 \\ \frac{d}{H}\sin\theta_1 & -\frac{b}{H} + \frac{d}{H}\cos\theta_1 \end{bmatrix} \begin{bmatrix} \mathcal{E}^{(\ell)}_{11}(n,b)\sin n\theta_1 & \mathcal{E}^{(\ell)-}_{12}(n,b)\sin n\theta_1 \\ \mathcal{E}^{(\ell)-}_{21}(n,b)\cos\theta_1 & \mathcal{E}^{(\ell)}_{22}(n,b)\cos n\theta_1 \end{bmatrix} d\theta_1. \qquad (II.33b)$$

Because of the symmetry in the limits of integration and of the trigonometric functions, the second and third rows of $[L(n)^{(\ell)+}]$ and the first row of $[L(n)^{(\ell)-}]$ have zero entries, i.e.

$$[L(n)^{(\ell)+}] = \begin{bmatrix} \mathcal{E}^{(\ell)}_{11} I_1 - \mathcal{E}^{(\ell)+}_{21} I_4 & \mathcal{E}^{(\ell)+}_{12} I_1 - \mathcal{E}^{(\ell)}_{22} I_4 \\ 0 & 0 \\ 0 & 0 \end{bmatrix} \qquad (II.33c)$$

and

$$[L(n)^{(\ell)-}] = \begin{bmatrix} 0 & 0 \\ \mathcal{E}^{(\ell)}_{11} I_4 + \mathcal{E}^{(\ell)-}_{21} I_1 & \mathcal{E}^{(\ell)-}_{12} I_4 + \mathcal{E}^{(\ell)}_{22} I_1 \\ \mathcal{E}^{(\ell)}_{11}\frac{d}{H} I_4 + \mathcal{E}^{(\ell)-}_{21}\left(-\frac{b}{H} I_5 + \frac{d}{H} I_1\right) & \mathcal{E}^{(\ell)-}_{12}\frac{d}{H} I_4 + \mathcal{E}_{22}\left(-\frac{b}{H} I_5 + \frac{d}{H} I_1\right) \end{bmatrix} \qquad (II.33d)$$

where $\mathcal{E}^{(\ell)}_{ij} = \mathcal{E}^{(\ell)}_{ij}(n,b)$, i = 1,2 and j = 1, 2. The terms I_i, i = 1, 4 and 5, are functions of n and are the following integrals:

$$I_1(n) = \int_{-\theta_0}^{\theta_0} \cos\theta_1 \cos n\theta_1 d\theta_1 \qquad (II.34a)$$

$$I_4(n) = \int_{-\theta_0}^{\theta_1} \sin\theta_1 \sin n\theta_1 d\theta_1 \qquad (II.34b)$$

and

$$I_5(n) = \int_{-\theta_0}^{\theta_0} \cos\theta_1 d\theta_1, \qquad (II.34c)$$

equal to

$$I_1(n) = \begin{cases} \frac{\sin(n+1)\theta_0}{n+1} + \frac{\sin(n-1)\theta_0}{n-1}, & n \neq 1 \\ \frac{\sin 2\theta_0}{2} + \theta_0, & n = 1 \end{cases} \qquad (II.35a)$$

$$I_4(n) = \begin{cases} -\frac{\sin(n+1)\theta_0}{n+1} + \frac{\sin(n-1)\theta_0}{n-1}, & n \neq 1 \\ -\frac{\sin 2\theta_0}{2} + \theta_0, & n = 1 \end{cases} \qquad (II.35b)$$

and

$$I_5(n) = \begin{cases} 2\frac{\sin n\theta_0}{n} & , n \neq 1 \\ 2\theta_0 & , n = 0. \end{cases} \qquad (II.35c)$$

The generalized force vector $F^{(s)} = \{f_z^{(s)}, f_x^{(s)}, M_0^{(s)}/H\}^T$ in equation (II.31) can be broken into two parts

$$\{F^{(s)}\} = \{F_0^{(s)}\} + \{F_\Delta^{(s)}\}. \qquad (II.36)$$

The generalized force vector $\{F_0^{(s)}\} = \{f_{z,0}^{(s)},\ f_{x,0}^{(s)},\ M_{0,0}/H\}^T$ represents the resultant forces that act onto the half-space, and are caused by the free-field waves and by scattered waves from a fixed foundation. It is equal to

$$\left\{F_0^{(s)}\right\} = -\frac{2\mu}{b}[P^+] \left\{ \begin{Bmatrix} \vdots \\ A_{0,n} \\ C_{0,n} \\ \vdots \end{Bmatrix} \right\} e^{-i\omega t} - \frac{2\mu}{b}[P^-] \left\{ \begin{Bmatrix} \vdots \\ B_{0,n} \\ D_{0,n} \\ \vdots \end{Bmatrix} \right\} e^{-i\omega t}. \qquad (II.37)$$

It's components are the forces that must be applied to the foundation in order to keep it at rest, in the absence of forces from the superstructure. The opposite of those forces are called "foundation driving forces." The generalized force vector $\{F_\Delta^{(s)}\} = \{f_{z,\Delta}^{(s)},\ f_{x,\Delta}^{(s)},\ M_{0,\Delta}^{(s)}/H\}^T$, where

$$\left\{F_\Delta^{(s)}\right\} = -2\mu[Q] \begin{Bmatrix} V_0 \\ \Delta_0 \\ \varphi_0 H \end{Bmatrix} e^{-i\omega t} \qquad (II.38)$$

represents the forces acting onto the half-space when there is no free-field motion, but only waves generated by the foundation moving as $\{V_0, \Delta_0, \varphi_0 H\}^T e^{-i\omega t}$. The matrix $2\mu[Q]$ can be thought of as a stiffness matrix of the half-space. It is usually called the "foundation impedance matrix."

II.1.5 Equilibrium of Forces Acting on the Foundation

The free-body diagram of the foundation is shown in Fig. II.4. The forces $f_x^{(b)}$ $f_z^{(b)}$, and the moment $M_0^{(b)}$ are those exerted onto the foundation by the building and by the Third Newton's law they are equal in magnitude, but with opposite direction, with the forces that the foundation exerts onto the building in Fig. II.2. Similarly, $f_x^{(s)}$, $f_z^{(s)}$ and $M_0^{(s)}$ in Fig. II.4 are the forces with which the half-space acts onto the foundation. Those forces are equal in magnitude but have opposite sign from the forces in Fig. II.3 with which the foundation acts onto the soil. Next, $m_f\ddot{\Delta}$ and $m_f\ddot{V}$ are the horizontal and vertical d'Alambert forces and $I_0^{(f)}\ddot{\varphi}$ is the d'Alamberts moment about O. Here $I_0^{(f)}$ is the moment of inertia of the foundation about O and is calculated as follows

$$\begin{aligned} I_0^{(f)} &= \int_{-\theta_0}^{\theta_0}\int_{d/\cos\theta_1}^{b} \rho_f r dr d\theta (r^2 + d^2 - 2dr\cos\theta) \\ &= b^4\left[\left(\frac{1}{2}+\cos^2\theta_0\right)\theta_0 - \frac{3}{2}\sin\theta_0\cos\theta_0\right]\rho_f \end{aligned}$$

where ρ_f is the density of the foundation material. The area of the cross-section of the foundation, A_f, is

$$\begin{aligned} A_f &= b^2\theta_0 - ad \\ &= b^2(\theta_0 - \sin\theta_0\cos\theta_0) \end{aligned}$$

and in terms of the total mass of the foundation, m_f,

$$I_0^{(f)} = \frac{b^2 m_f}{\theta_0 - \sin\theta_0\cos\theta_0}\left[\left(\frac{1}{2}+\cos^2\theta_0\right)\theta_0 - \frac{3}{2}\sin\theta_0\cos\theta_0\right].$$

The center of mass of the foundation, C, is at depth c from the top surface, where

$$\begin{aligned} c &= \frac{1}{A_f}\int_0^{\theta_0} b^3\sin^2\theta\cos\theta d\theta - d \\ &= \frac{b}{3}\frac{\sin^3\theta_0}{\theta_0 - \sin\theta_0\cos\theta_0} - d. \end{aligned}$$

For positive rotation φ about O, the gravity force $m_f g$ will produce a counter clockwise dynamic moment about O which for small φ is equal to $m_f g c\varphi$.

The dynamic equilibrium of the forces acting onto the foundation implies

$$\begin{bmatrix} m_f & & 0 \\ & m_f & \\ 0 & & \frac{I_0^{(f)}}{H^2} \end{bmatrix}\begin{Bmatrix} \ddot{V} \\ \ddot{\Delta} \\ \ddot{\varphi}H \end{Bmatrix} = \begin{Bmatrix} f_z^{(b)} \\ f_x^{(b)} \\ M_0^{(b)}/H \end{Bmatrix} - \begin{Bmatrix} f_z^{(s)} \\ f_x^{(s)} \\ M_0^{(s)}/H \end{Bmatrix} - \begin{Bmatrix} 0 \\ 0 \\ m_f g c\varphi \end{Bmatrix}. \quad (II.39a)$$

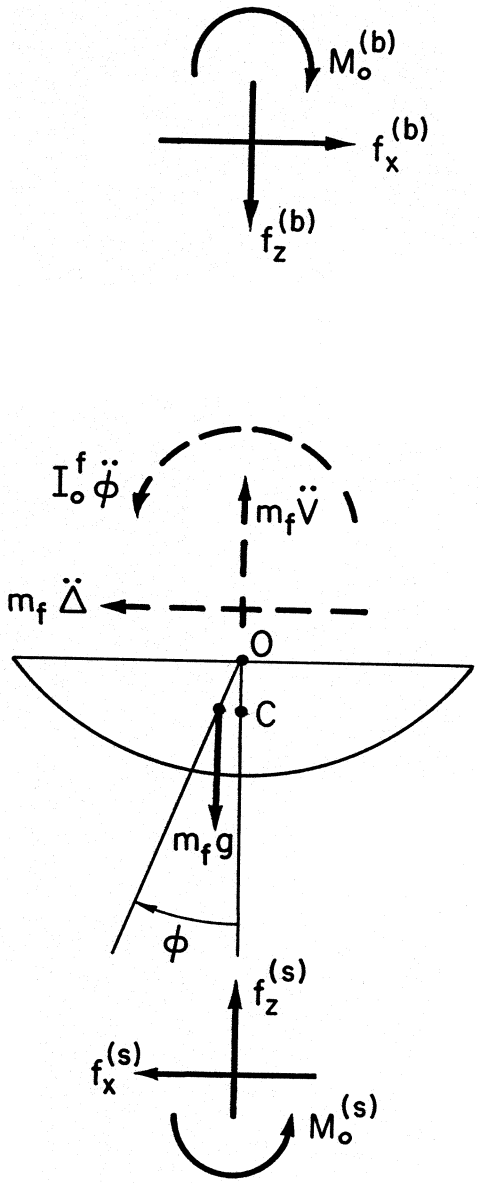

Figure II.4 Equilibrium of forces acting on the foundation

From this equation, and recalling equations (II.2), (II.11) and (II.31), the displacements of the foundation can be expressed as

$$\left\{ \begin{array}{c} V \\ \Delta \\ \varphi H \end{array} \right\} = \frac{1}{b}\left[[Q]+\frac{m_f\omega^2}{2\mu}([M_f]+[C_g^{(f)}])+\frac{m_b\omega^2}{2\mu}([K^{(b)}]+[C_g^{(b)}])\right]^{-1}\frac{b}{2\mu}\left\{F_0^{(s)}\right\} \quad (II.39b)$$

$$[M_f] = \text{ diag } \left\{1,1,\frac{I_0^{(f)}}{m_f}\frac{1}{H^2}\right\}$$

and

$$[C_g^{(f)}] = \text{ diag } \left\{0,0,\frac{-g}{\omega^2 H}\frac{c}{H}\right\}.$$

$m_f[M_f]$ is the mass matrix of the foundation and $m_f[C_g^{(f)}]$ can be thought of as a stiffness matrix of the generalized force $\{F_g^{(f)}\} = \{0,0,M_{0,g}^{(f)}/H\}$, where $M_{0,g}^{(f)}$ is the dynamic moment about O of the foundation gravity forces. The response $\{\Delta_0\} = \{V_0,\Delta_0,\varphi_0 H\}^T$ to a P-wave with unit displacement amplitude is equal to

$$\{\Delta\} = \frac{1}{k_\alpha b}[K]^{-1}\frac{b}{2\mu}\{F_0^{(s)}\} \quad (II.40)$$

where

$$[K] = [Q] + \frac{m_f\omega^2}{2\mu}([M_f] + [C_g^{(f)}) + \frac{m_b\omega^2}{2\mu}([K^{(b)}] + [C_g^{(b)}]) \quad (II.41)$$

is a dimensionless matrix, $k_\alpha b$ is a dimensionless wave number of the incident waves and $\frac{b}{2\mu}\{F_0^{(s)}\}$ is a dimensionless generalized force vector.

The solution of the interaction problem can be carried out in the following steps. First, the generalized force $\{F_0^{(s)}\}$ can be calculated (forces that act onto the half-space when the incident wave is scattered from the immobile foundation). This vector depends on the frequency of the incident waves, on the incident angle, and on the shape of the foundation. It does not depend on the mass of the foundation and on any of the characteristics of the superstructure. Second, the impedance matrix for the half-space, $[Q]$, can be calculated. It depends only on the shape of the foundation and does not depend either on the incident wave or on the presence of the superstructure. Third, the various impedance and mass matrices of the foundation and of the superstructure, $[M_b]$, $[M_f]$, $[C_g^{(b)}]$, $[C_g^{(f)}]$ and $[K^{(b)}]$, can be calculated, and the matrix $[K]$ constructed. At the end, the interaction equation (II.40) can be solved. This type of decomposition was introduced by Thau (1967). The advantage of the decomposition is that once $\{F_0^{(s)}\}$ and $[Q]$ are calculated, with little extra effort the interaction problem can be solved for any properties of the superstructure and for any value of the mass of the foundation.

II.2 Results and Analysis

It is of interest to see how the displacements of the foundation Δ, V and φ and the relative responses of the building

$$u_b^{\rm rel}(\xi) = u_b(\xi) - (\Delta + \varphi\xi)$$

and

$$v_b^{\rm rel}(\xi) = v_b(\xi) + V$$

depend on the frequency (wave length) and angle of incidence of the incident waves, and on the many physical parameters of the soil-structure system. These parameters are: the masses of the building and of the foundation, m_b and m_f, the rigidity of the half-space, μ, the shear and longitudinal wave velocities in the building and in the half-space, α_b, β_b, α and β, the height of the building, H, and its slenderness ratio, $\frac{W}{H}$, the depth of the foundation, h, and its width, $2a$, and the acceleration due to gravity g.

II.2.1 Dimensionless Parameters

It is convenient to use the following dimensionless parameters. The frequency of the excitation can be expressed in terms of the dimensionless frequencies $\eta = \frac{2a}{\beta T}$, where $T = \frac{2\pi}{\omega}$ is the period, or $\Omega = \frac{\omega a}{\beta} = \pi\eta$. The parameter η equals the number of wave lengths of the shear waves in the half-space contained in length equal to the width of the foundation. It can also be interpreted as dimensionless width of the foundation. The flexibility of the building relative to that of the half-space can be expressed through the parameter $\varepsilon = \frac{k_\beta^b H}{k_\beta a} = \frac{\beta H}{\beta_b a} = \frac{2H}{\beta_b T}/\eta$, which is equal to twice the ratio of the number of wave lengths of shear waves in the building contained in length H and the number of wavelengths of the shear waves in the soil contained in length $2a$ (η). Then, for given η and ε, there are $\frac{1}{2}\eta\varepsilon$ shear wave wavelengths of the building contained in its height. Larger values of ε correspond to flexible buildings, i.e. tall buildings and/or buildings with small β_b relative to β. Short and stiff buildings (relative to the stiffness of the half-space) will have smaller value of ε. As an example, in Appendix B, values for ε have been calculated for the former Imperial County Services Building in El Centro (Kojić et al. 1984) for different values of the soil shear wave velocity. Other dimensionless parameters are the mass ratios $\frac{m_b}{m_f}$ and $\frac{m_f}{m_s}$, where m_s is the mass (per unit length in the y-direction) of the soil replaced by the foundation, the geometric ratios $\frac{H}{a}$, $\frac{W}{H}$ and $\frac{h}{a}$, and the ratio of accelerations $\frac{g}{\omega_1^2 a}$ where ω_1 is the fundamental frequency of the shear vibrations of the building. It is equal to $\omega_1 = \beta_b\pi/2H$. The order of magnitude of $\frac{g}{\omega_1^2 a}$ is 10^{-4}, e.g., for the former Imperial County services building (Appendix B).

In all the examples considered in this report, the Poisson's ratio $\nu = 0.3333 \sim \frac{1}{3}$ both in the building and in the half-space, implying $\alpha/\beta = 2$ and $\alpha_b/\beta_b = 2$. Also, in all the examples $W = 2a$. The slenderness ratio $\frac{W}{H} = 1$ or 4, and the depth to half-width ratio of the foundation $\frac{h}{a} = 1$ or 0.5. The effect of the gravity forces is neglected, i.e. $\frac{g}{\omega_1^2 a} = 0$.

The mass ratios m_f/m_s and m_b/m_f are chosen so that $\rho_b/\rho_s \approx 0.2$ and $\rho_b \approx \rho_f$ (Luco, 1980). Also two additional values of m_b/m_f are taken for each combination of parameters h/a, H/a and ε - a twice smaller and a twice larger. The spectra of Δ, V, φ, u_b^{rel} and v_b^{rel} are calculated in the frequency domain $0 < \eta \leq 2$. In this chapter, incident P waves are considered with incident angles $\gamma = 0°, 30°, 60°$ and $85°$. The free-field displacement amplitudes on the surface, $|u^{ff}|$ and $|v^{ff}|$, as well as the amplitudes of the reflection coefficients, K_1 and K_2, and the angle of the reflected SV-wave, θ_β, for these incident angles and for $\nu = 0.3333$ are shown in Table II.1.

Table II.1

Free-field motion characteristics on the half-space surface for incident plane P-waves with unit amplitude and for Poissons ratio $\nu = 0.3333$

γ	$\lvert u^{ff}\rvert$	$\lvert v^{ff}\rvert$	$\lvert K_1\rvert$	$\lvert K_2\rvert$	θ_β
0°	0.000	2.000	1.00	0.00	0°
30°	0.963	1.741	0.76	0.44	14.48°
60°	1.395	1.117	0.40	0.48	25.66°
85°	0.517	0.301	0.74	0.15	19.74°

The fixed base natural frequencies for the building are $k_\beta^b H = (2n-1)\frac{\pi}{2}$, $n = 1, 2, \ldots$, for shear deformation, and $k_\alpha^b H = (2n-1)\frac{\pi}{2}$, $n = 1, 2, \ldots$, for longitudinal deformation. In terms of the dimensionless frequency Ω, these are at $\Omega = k_\beta a = \frac{1}{\varepsilon}(2n-1)\frac{\pi}{2}$ and at $\Omega = k_\beta a = \frac{1}{\varepsilon}\frac{\alpha_b}{\beta_b}(2n-1)\frac{\pi}{2}$, $n = 1, 2, \ldots$, respectively. For $\varepsilon = 2$ and 4, the first few fixed base natural frequencies are as follows:

	shear deformation	longitudinal deformation
$\varepsilon = 2$	$k_\beta a = \frac{\pi}{4}, \frac{3\pi}{4}, \frac{5\pi}{4}, \ldots$	$k_\beta a = \frac{\pi}{2}, \frac{3\pi}{2}, \frac{5\pi}{2}, \ldots$
$\varepsilon = 4$	$k_\beta a = \frac{\pi}{8}, \frac{3\pi}{8}, \frac{5\pi}{8}, \ldots$	$k_\beta a = \frac{\pi}{4}, \frac{3\pi}{4}, \frac{5\pi}{4}, \ldots$

The value $\varepsilon = 2$ would correspond, e.g., to a 10 story building with fundamental period $T_1 \approx (0.1)(10) = 1$ sec, height $H \approx 50$ m and width $W = 50$ m, situated on soil with shear wave velocity $\beta \approx 200$ m/s. The value $\varepsilon = 4$ would correspond to the same building on soil with $\beta \approx 400$ m/s. A 50 story building would have fundamental period $T_1 \approx (0.1)(.50) = 5$ sec and height $H \approx 250$ m, which would imply the shear wave velocity to be $\beta_b = 4H/T_1 \approx 200$ m/s. Then, if its base is $W \approx 80$ m, $\varepsilon = 4$ would correspond to the same building on soil with shear wave velocity by $\beta \approx 100$ m/s (e.g., in Mexico City).

II.2.2 Discussion of the Interaction Equations

How the chosen system parameters influence the interaction can be seen from equations (II.40) and (II.41). For example, larger values of ε correspond to shorter periods of the harmonic functions in $[K^{(b)}]$ which means that, in given interval of the dimensionless frequency (e.g., $0 < \eta \leq 2$), the fixed base natural frequencies of the building will be more dense. Rapid changes in the spectra of Δ and φ and u_b^{rel} are expected for frequencies in the vicinity of the resonant (shear) fixed-base frequencies of the building. The same is true for the spectra of V and v_b^{rel} for frequencies in the vicinity of the longitudinal fixed-base resonant frequencies. The reason is that as the fixed base resonant (natural) frequencies are approached, the terms in $[K^{(b)}]$ having $\tan \frac{\omega H}{\beta_b}$ $\left(\text{or} \tan \frac{\omega H}{\alpha_b}\right)$ become very large and suddenly change sign as those frequencies are crossed. Next, from equations (II.40) and (II.41) it can be seen that the inertia forces of the foundation are proportional to

$$\frac{m_f \omega^2}{2\mu} = \frac{m_f}{m_s} \frac{1}{2} \frac{A_f}{a^2} (k_\beta a)^2$$

and that the inertia forces in the building depend on

$$\frac{m_b \omega^2}{2\mu} = \frac{m_f}{m_s} \frac{m_b}{m_f} \frac{1}{2} \frac{A_f}{a^2} (k_\beta a)^2.$$

Therefore, away from the characteristic frequencies, the interaction forces are larger for larger frequencies of the excitation, for larger $\frac{m_f}{m_s}$ and $\frac{m_b}{m_s}$ and for deeper foundations. The larger $\frac{W}{H}$ is, the larger will be the moment of inertia of the building. Typically, $\frac{W}{H}$ has little effect on the interaction. The larger the ratio $\frac{H}{a}$ is, i.e. the higher the center of gravity of the building is, the larger is the moment (about O) of the inertia forces of the building and larger is the moment with which the building acts onto the foundation.

If the foundation is deeper, i.e. if $\frac{h}{a}$ is larger, the terms in the foundation rigid body motion influence matrix (in equations (II.27), (II.30c and d) and (II.31a)) corresponding to rotation will be larger. Because of the larger distances of the points on the foundation boundary from point O, the moment (about O) of the stresses of the free-field motion acting on the contact area between the foundation and the soil will be larger. However, the foundation driving forces are represented by integrals of those stresses and of their moment about O along the whole contact surface, which has larger area if the foundation is deeper (h/a is larger). The net result will depend on the wavelength of the incident waves relative to the size of the foundation. When the incident waves vary little along the contact surface, then, the resultant horizontal and vertical foundation driving force is larger when the contact area is larger, i.e. for deeper foundations. For wavelengths comparable to the foundation size, certain distributions of the stresses along the contact area many produce large rotation of the foundation. The value of η for which this happens will depend also on the depth of the foundation.

The foundation will act as a low pass filter for the short wavelengths of the motion of the soil, because it is rigid and therefore cannot follow the short wavelength motions of the

soil. In sections II.1.3 and II.1.4, it was shown that only the first two cylindrical waves of the expansion of the free-field motion actually "drive" the foundation. The foundation driving force therefore depends on the amplitude of the coefficients in the series multiplying those waves. If the incident wave has unit amplitude, for shorter incident waves those coefficients are smaller. "Shorter" and "longer" means relative to the size of the foundation, and so an incident wave would appear as "shorter" to a foundation that is deeper. Therefore, for given η a deeper foundation will filter more energy than a shallow foundation. This effect will be seen in the examples that follow.

A cylindrical foundation, without or with a rigid building, embedded into the elastic half-space and excited by in-plane waves, is like an "oscillator" with three degrees of freedom, with stiffness provided by the elastic medium and with damping caused by the radiation of energy into the semi-infinite medium. The characteristic frequencies of this oscillator depend on the rigidity of the elastic medium (μ), on the mass of the oscillator and on the shape of the foundation. The foundation will have two system frequencies: one for the coupled horizontal and rocking motion and one for the uncoupled vertical motion. By analogy with a single degree-of-freedom oscillator, the characteristic frequencies should be higher when the rigidity of the half-space is higher (μ is larger) and when the mass of the oscillator is smaller. The amplitudes of forced oscillations, caused by a periodic external force, would be larger if the amplitude of the force is larger and if the mass and the characteristic frequencies of the oscillator are smaller (the static displacements would be larger). At the characteristic frequencies the foundation response, relative to the foundation input motion, should be the largest. As the frequency of the outside force approaches infinity, the response should approach zero (the dynamic amplification factors approach zero).

II.2.3 Foundation Input Motion

Some authors, (e.g. Luco, 1980; and Luco et al., 1975), use the foundation input motion, rather than the foundation driving forces, as an excitation function in solving soil-structure interaction problems. Foundation input motion is called the response of a massless foundation under the action of the seismic excitation and in the absence of external forces, e.g. forces exerted by the structure. This motion depends on the characteristics of the incident wave motion (frequency, incident angle and type of incident waves) and also on the geometrical shape of the foundation. Then, the total ground motion is a superposition of the free-field motion and the scattered waves from the massless foundation without the building.

In Fig. II.5a, b and c, the amplitude spectra of the components of the foundation input motion Δ, φa and V are shown for a semi-cylindrical foundation and for incidence angles $\gamma = 0°, 30°, 60°$ and $85°$ for incident P-waves with unit displacement amplitude. It can be seen from these figures, that for vertically incident P-waves ($\gamma = 0°$) there is no horizontal component of motion and no rotation of the rigid foundation. The reason for this is the symmetry of the shape of the foundation and the symmetry of the incident wave

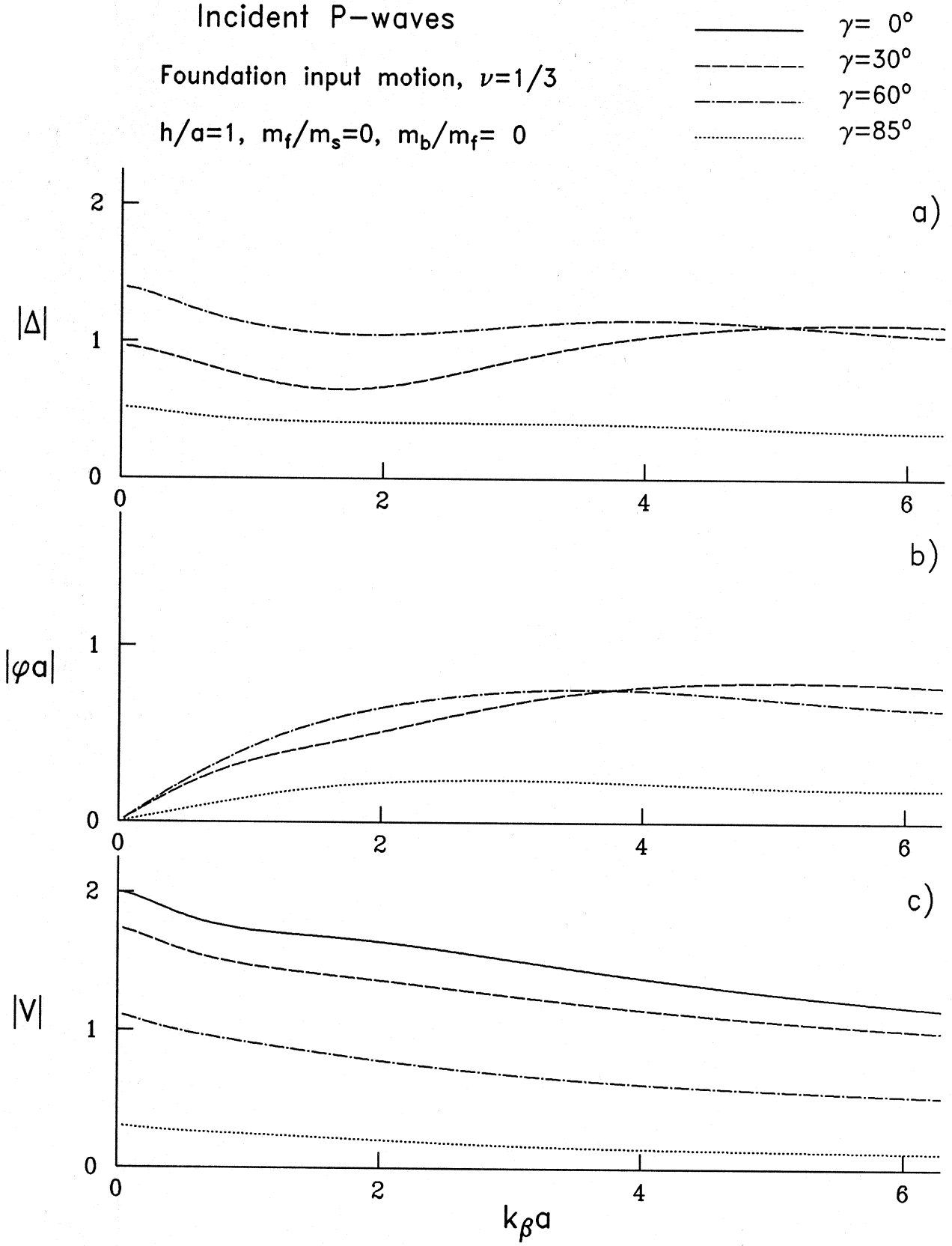
Incident P-waves
Foundation input motion, ν=1/3
h/a=1, m_f/m_s=0, m_b/m_f= 0
γ= 0°
γ=30°
γ=60°
γ=85°
a)
b)
c)
|Δ|
|φa|
|V|
0
1
2
0
2
4
6
$k_\beta a$

Figure II.5

motion about the plane $x = 0$. For incidence other than vertical, $|\Delta|$, $|\varphi a|$ and $|V|$ are non-zero and are frequency dependant. For long incident wavelengths, $|\Delta|$ and $|V|$ approach the free (half-space) surface displacement amplitudes, $|u^{ff}|$ and $|v^{ff}|$, and the rotation approaches zero. The displacement of the free-field motion on the half-space surface at $x = 0$ would be the input motion for the building if it had a surface foundation and if no differential motions occurred along its contact with the soil. From the spectra in Fig. II.5c it can be seen that for $\Omega = k_\beta a \in (0, 2\pi]$, as a result of the scattering of the incident waves, the input motion for embedded foundations has smaller vertical amplitudes than the input motion for surface foundations. This difference increases with decreasing wave length of the incident waves. For the horizontal amplitude of the foundation input motion, this is also the case for $\gamma = 60°$ and $85°$. For $\gamma = 30°$ this amplitude first decreases with frequency but then increases and exceeds $|u^{ff}|$ for $\Omega \geq 3.6$. The reason for the decrease of the amplitudes of the translational components of the response of the massless foundation, relative to the free-field motion amplitudes, is in the scattering of the incident waves and in the filtering effect of the rigid foundation. The "anomaly" in the transfer function of Δ for $\gamma = 30°$ and at $\eta \approx 2$ appears to be caused by a contribution to the translation of point O from the rotation of the massless foundation.

In the traditional seismic analyses of buildings, the building models are supported by a rigid base moving at all times only horizontally and vertically, following the free-field ground motion on the surface. In the models that do allow for soil-structure interaction, often the excitation it taken to consist only of horizontal and vertical translations, equal to the corresponding components of the free-field motion. The rotation of the base of such models is caused only by the moment of the inertia forces of the building about its base. The rotation of the free-field motion, and the induced rotation and the modification of the translational components of the input motion due to the embedment are neglected. In some analyses (with or without interaction) the building models are also subjected to rotational excitation equal to the point rotation of the free-field motion on the ground surface (Gupta, and Trifunac, 1990a,b). This rotation is proportional to the amplitude of the SV-wave generated by the mode conversion on the half-space surface and to the wave number of the shear waves in the soil (Trifunac, 1982). In terms of the quantities defined in this chapter, the free-field point rotation for incident plane P-wave (with unit amplitude) is

$$\varphi^{ff} = \frac{i}{2} K_2 \frac{\alpha}{\beta} \frac{\omega}{\beta} e^{ik_\alpha (x \sin\gamma - z\cos\gamma) - i\omega t}$$

where K_2 is the reflection coefficient defined in equation (II.15.b) and with values as given in Table II.1. For given incident angle, the amplitude of φ^{ff} increases linearly with frequency of the incident wave and regardless of the frequencies, there is a $\pi/2$ phase difference between φ^{ff} and the horizontal translation u^{ff}. The results in Fig. II.5 show that for the vertical component of motion the approximation of the foundation input motion by the free-field motion is conservative. For the horizontal component, this approximation is also acceptable. However, neglecting the rotation, a considerable contribution to the base excitation is neglected, and this may lead to nonconservative estimates of the forces in the building. Approximation of the rotation by the point rotation of the free-field motion is meaningful only for long wavelengths of the incident waves compared with the

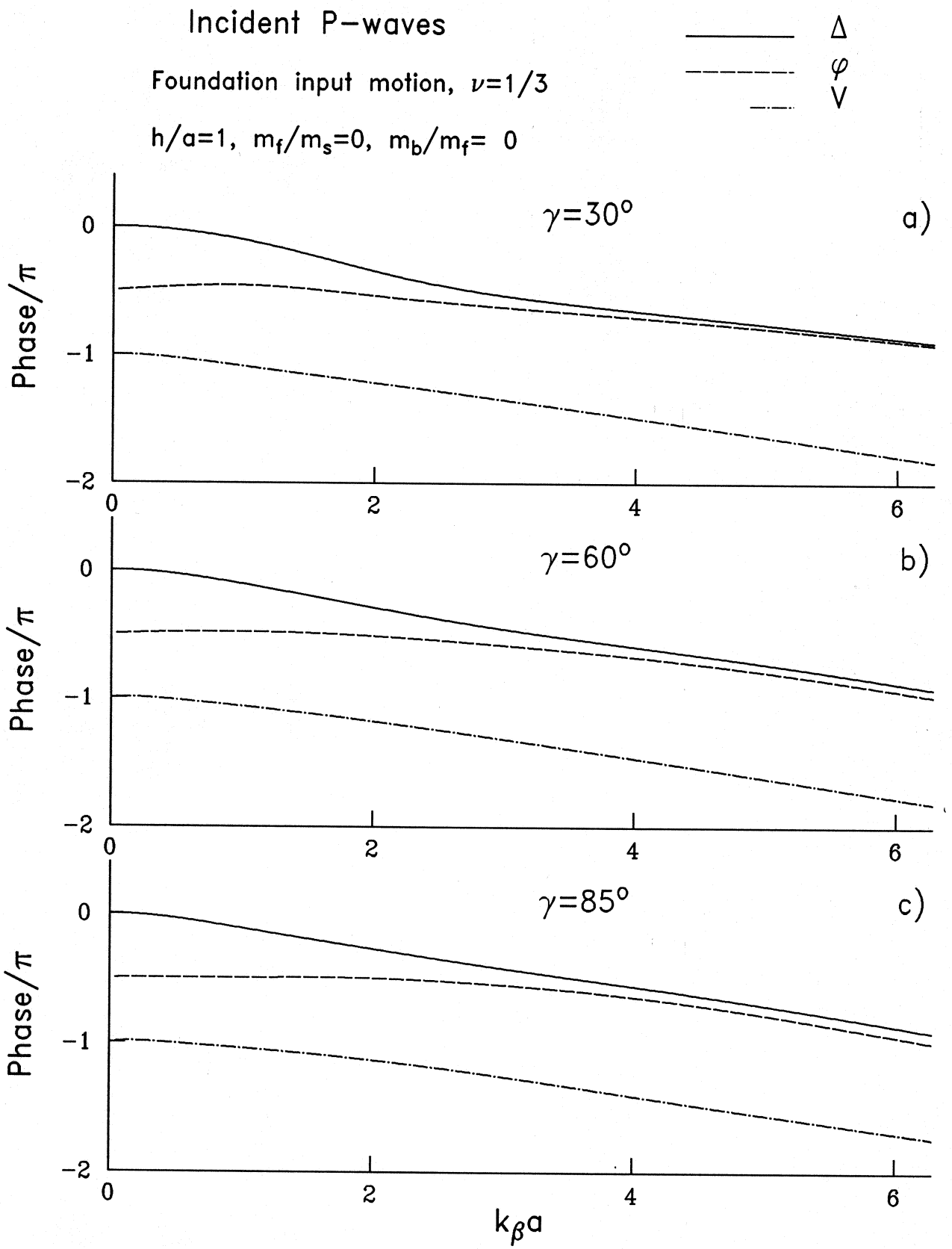
Incident P-waves
Foundation input motion, ν=1/3
h/a=1, m_f/m_s=0, m_b/m_f= 0
Δ
φ
V
γ=30°
a)
γ=60°
b)
γ=85°
c)
Phase/π
0
-1
-2
0
2
4
6
k_βa

Figure II.6

size of the foundation ($\eta < 0.3$), when the point rotation along the foundation boundary has practically the same phase. For shorter wave lengths, the amplitude of the input rotation is overestimated, and its phase relative to the phase of the translation is changed (Todorovska and Trifunac, 1990).

In Fig. II.6a, b and c, the phases of Δ, φ and V, calculated from

$$\text{Phase}(\cdot) = \tan^{-1}\left(\frac{\Im(\cdot)}{\Re(\cdot)}\right)$$

where $\Im$ and $\Re$ represent imaginary and real parts, are shown versus $k_\beta a$ for incident angles $\gamma = 30°$, $60°$ and $85°$. For low frequencies (long incident waves), Δ is in phase with the incident P-wave and the phase of φ is ahead of Δ by phase angle equal to $\pi/2$. For shorter wavelengths, the phase difference between Δ and φ decreases, and for $1 \leq \eta < 2$ the two are practically in phase (as the foundation input motion moves the foundation in the positive x-direction, it rotates it clockwise).

When the wavelength of the shear waves of the free-field motion is comparable with the size of the foundation, the wave passage effects become important. When the wavelength of the shear waves is much smaller than the size of the foundation, the differential motions along the foundation boundary average out and result in smaller rotation of the rigid foundation. This can be seen from Fig. II.5b and Fig. II.6. For very small η, φ increases almost linearly with η and the phase difference between the translation and the rotation is about $\pi/2$, i.e. φ behaves as φ^{ff}. For larger η, φ still increases but with a smaller rate and achieves a maximum. This is when the wave passage effects contribute most to the rotation. The SV-wave of the free-field motion is a propagating wave with phase velocities $c_x^\beta = \beta/\sin\theta_\beta$ and $c_z^\beta = \beta/\cos\theta_\beta$, where $\theta_\beta = \arcsin(\sin\gamma\beta/\alpha)$. When $\gamma = 60°$, e.g., $\theta_\beta = 25.7°$ and the rotation is maximum at $\eta \simeq 1$. For that wavelength of the SV-waves the ratio $2a/c_x^\beta T \simeq 0.43$ and $a/c_z^\beta T \simeq 0.45$. This means that the maximum occurs when the phase difference between the motion of the two corners of the foundation is about π. The phase difference between the motions of points at level $z = 0$ and $z = h$ (located on a same vertical line) is similar. When $\gamma = 30°$, $\theta_\beta = 14.5°$ and the rotation is maximum at $\eta \simeq 1.5$. Then $2a/c_x^\beta T \simeq 0.38$ and $a/c_z^\beta T \simeq 0.73$, i.e. the phase difference between the motion of the two corners is smaller than π, and between the top and the bottom points of the foundation about $3\pi/2$.

II.2.4 Soil-Foundation Interaction

In Fig. II.7 a, b and c, the transfer function amplitudes of the horizontal, rocking and vertical components of the response of a semi-cylindrical foundation, with mass ratio $\frac{m_f}{m_s} = 1$, are shown, for incident angles $\gamma = 0°, 30°, 60°$ and $85°$ and ignoring any other external forces. This would be the response of the foundation if the building is very "light" compared with the foundation, so that it's inertia forces are negligible. It is seen from these figures that, as in the case of a massless foundation, $|\Delta|$, $|\varphi a|$ and $|V|$ depend on γ and, as $\Omega \to 0$, $|\Delta| \to |u^{ff}|$, $|V| \to |u^{ff}|$ and $|\varphi a| \to 0$.

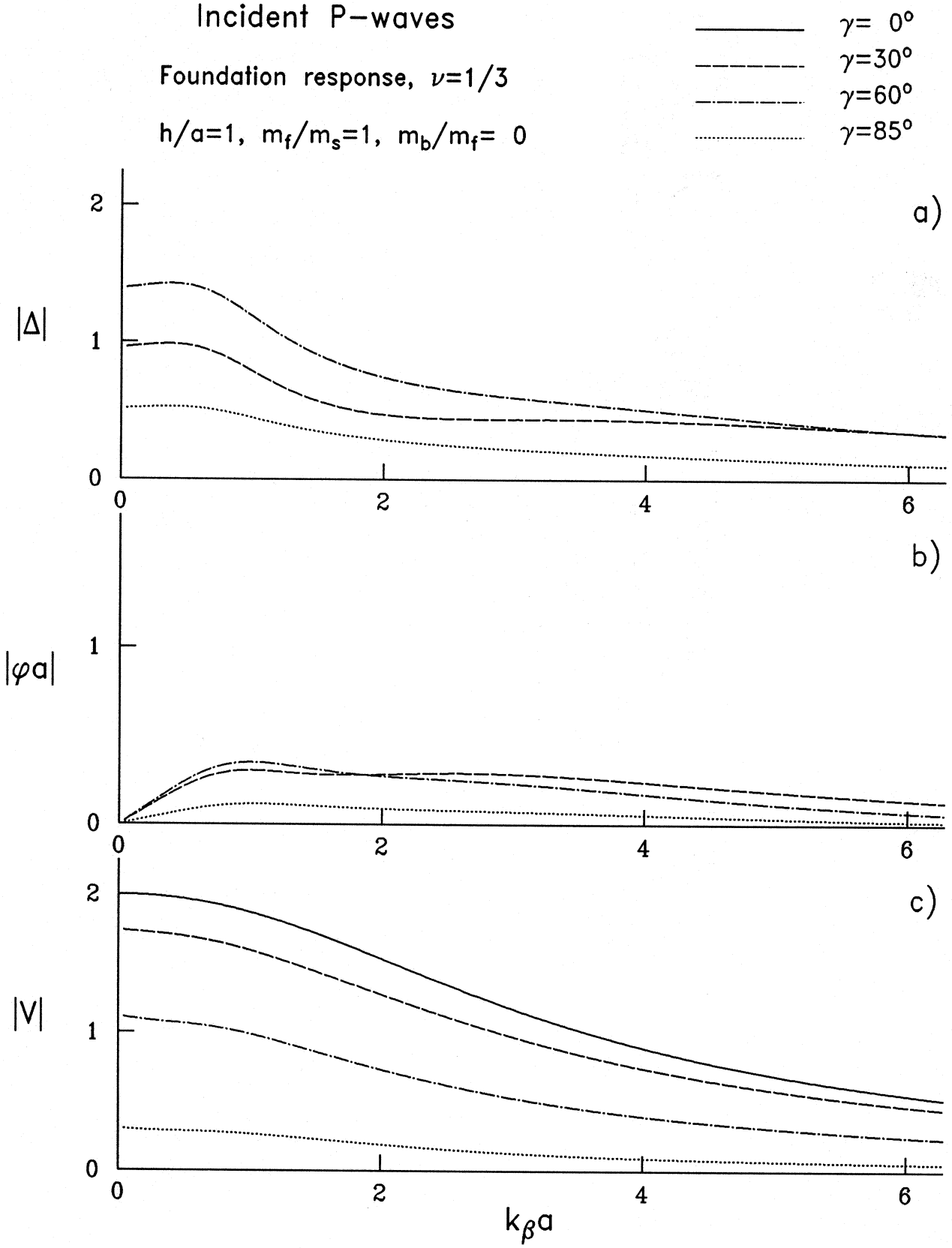
Incident P-waves
Foundation response, ν=1/3
h/a=1, m_f/m_s=1, m_b/m_f= 0
γ= 0°
γ=30°
γ=60°
γ=85°
a)
b)
c)
|Δ|
|φa|
|V|
k_βa
0
1
2
4
6

Figure II.7

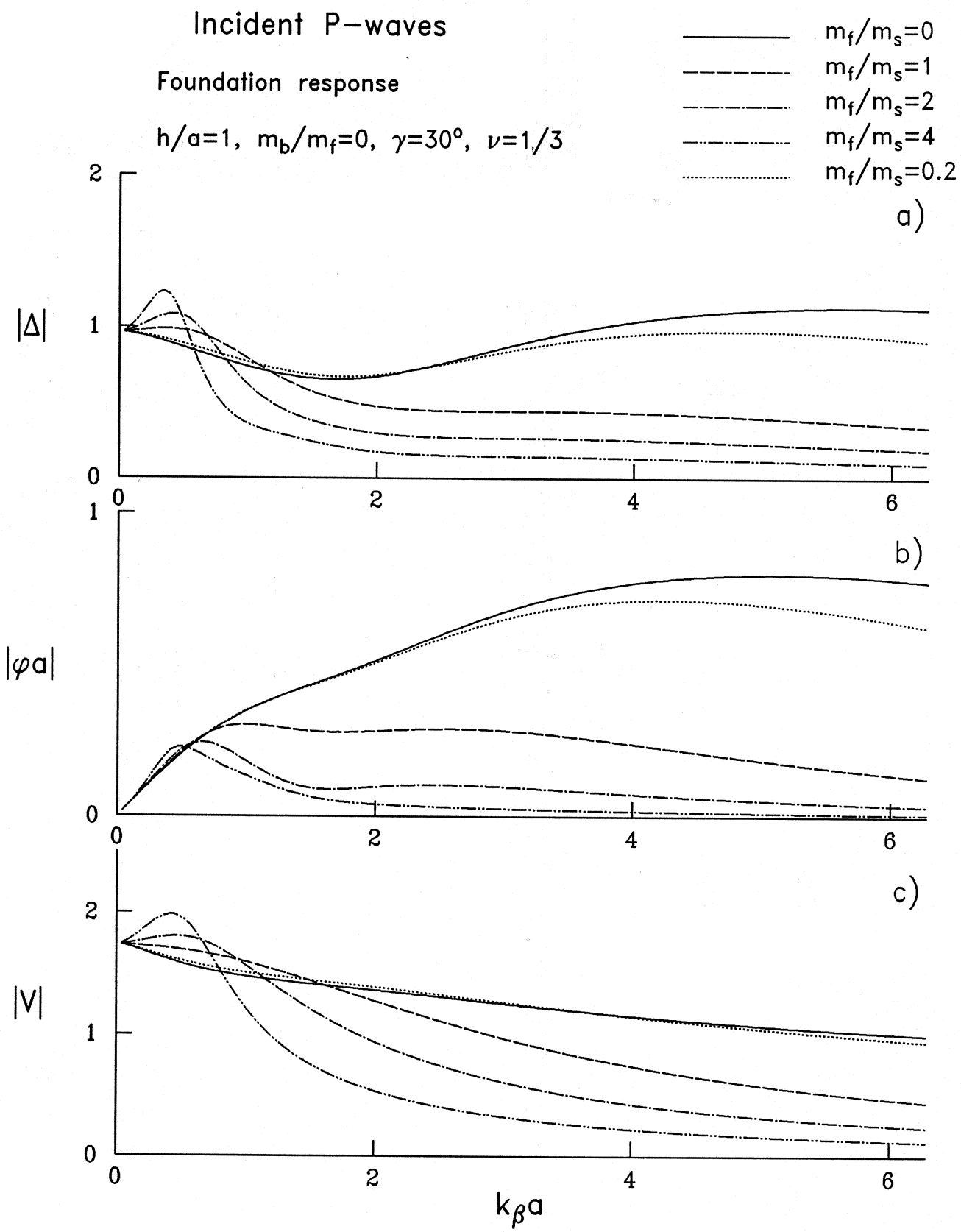
Incident P-waves
Foundation response
h/a=1, m_b/m_f=0, γ=30°, ν=1/3
m_f/m_s=0
m_f/m_s=1
m_f/m_s=2
m_f/m_s=4
m_f/m_s=0.2
a)
b)
c)
|Δ|
|φa|
|V|
$k_\beta a$
0
1
2
4
6

Figure II.8

In the lower frequency range ($\eta < 0.3$, $k_\beta a < 1$), Δ, φ and V have higher amplitudes than the foundation input motion, and that is in the vicinity of the system frequencies. These are "characteristic" frequencies of the interacting system. Yet, those cannot be called eigenvalues because they do not arise from a boundary value problem (the elastic medium, i.e. the half-space is unbounded). At those frequencies the amplitudes of the corresponding components of the foundation motion relative to the free-field motion are maximum. When the mass of the foundation is larger, the amplitudes of this relative motion are larger and the "characteristic" frequencies are lower (the soil acts as a softer medium). This is illustrated in Fig. II.8a, b and c where the amplitudes of the transfer functions of Δ, φ and V are shown for $m_f/m_s = 1, 2, 4$ and 0.2. The solid curves correspond to the foundation input motion ($m_f/m_s = 0$). At higher frequencies $|\Delta|$, $|V|$ and $|\varphi|$ are smaller than the amplitudes of the foundation input motion, and decrease more rapidly with frequency when m_f/m_s is larger.

The foundation has two system frequencies: one of the coupled horizontal and rocking motion, η^{sys}, and one of the vertical motion, η_V. The former depends on the horizontal and rocking foundation frequencies, η_H and η_R. η_V, η_H and η_R can be calculated from the real parts of the diagonal terms of the foundation impedance matrix (Luco, 1980a). Those three frequencies can be thought of in the following way. The vertical frequency would be the frequency of free oscillations of the foundation if it is given an initial vertical displacement. The horizontal frequency would be the frequency of the free oscillation of the foundation if it is given an initial horizontal displacement and it is prevented to rotate. Similarly, the rocking frequency would be the frequency of the free oscillation of the foundation when it is given an initial twist and is prevented to move horizontally. If the foundation is allowed to move horizontally and to rotate, but it cannot move vertically, η^{sys} will be the frequency of its free oscillations. Because of the radiation of energy into the unbounded soil medium those free oscillations would die out with time.

II.2.5 Building-Foundation-Soil Interaction

II.2.5.1 Rigid building

An extreme case occurs when the building is very stiff compared with the soil ($\varepsilon \to 0$) so that its elastic deformations are negligible. Then the building moves as a rigid body welded to the foundation. In Fig. II.9a, b and c, the amplitudes of the transfer functions of Δ, φa and V are shown in the frequency range $\Omega \in (0, 2\pi)$ for rigid buildings ($\varepsilon = 0$) with slenderness ratio $\frac{W}{H} = 1$ and mass ratios $\frac{m_b}{m_f} = 1, 2$ and 4, on semi-cylindrical rigid foundations with mass ratio $\frac{m_f}{m_s} = 0.2$ and for an incident P-wave with angle of incidence $\gamma = 60°$. For comparison, the case $\frac{m_b}{m_f} = 0$ is also shown in the figures. In Fig. II.10 the phases of those transfer functions are shown. Parts a, b and c correspond to $m_b/m_f = 1, 2$ and 4. The transfer functions of the base motion of the rigid building have similar shape as the transfer functions of the foundation in Fig. II.8. From the phase spectra in Fig. 10, it can be seen that for very low frequencies there is a difference of $\pi/2$ between the phases of Δ and φ (same as between u^{ff} and φ^{ff}). As the frequency increases the phase of φ

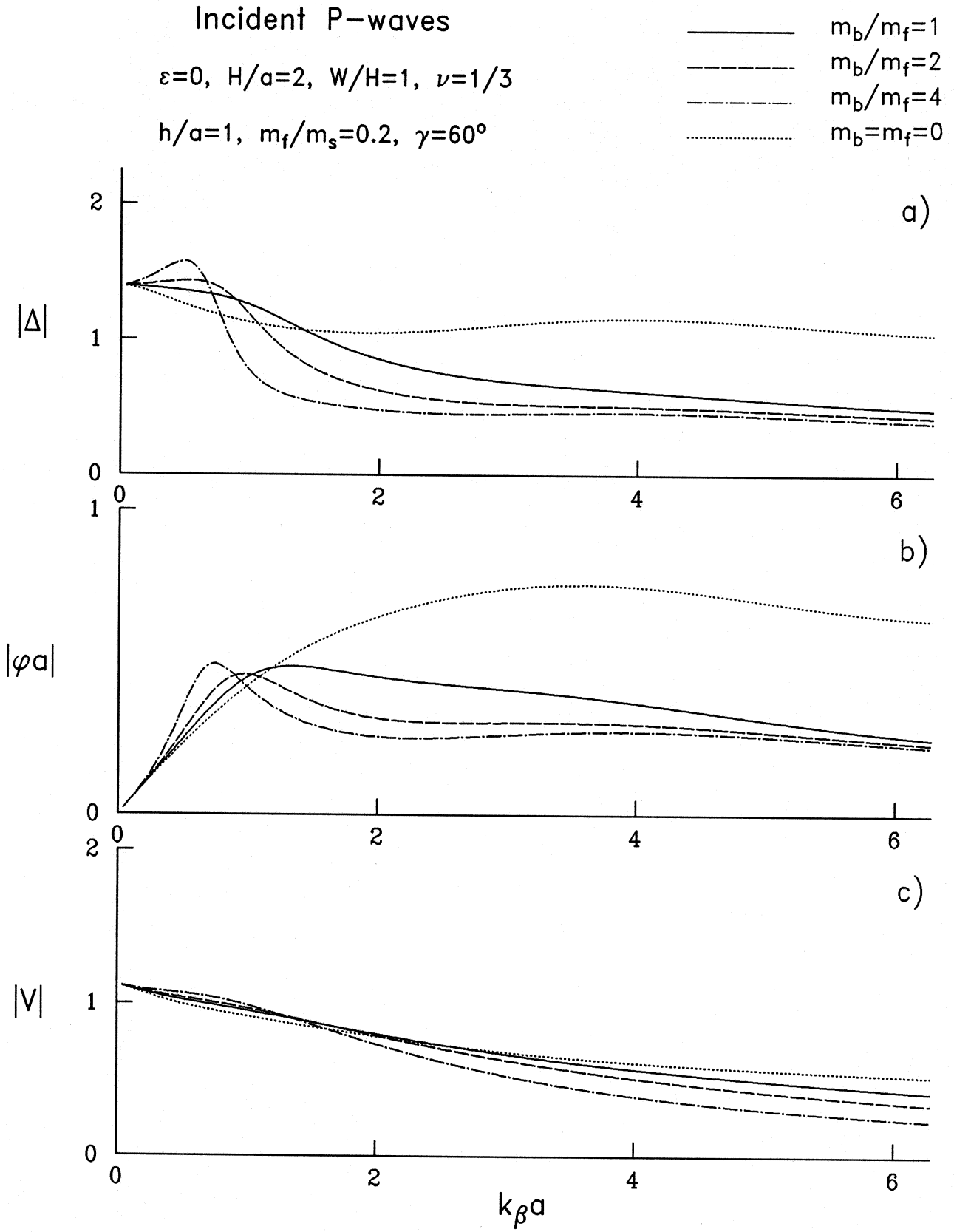
Incident P-waves
ε=0, H/a=2, W/H=1, ν=1/3
h/a=1, m_f/m_s=0.2, γ=60°
m_b/m_f=1
m_b/m_f=2
m_b/m_f=4
m_b=m_f=0
a)
b)
c)
|Δ|
|φa|
|V|
k_βa
0
1
2
4
6

Figure II.9

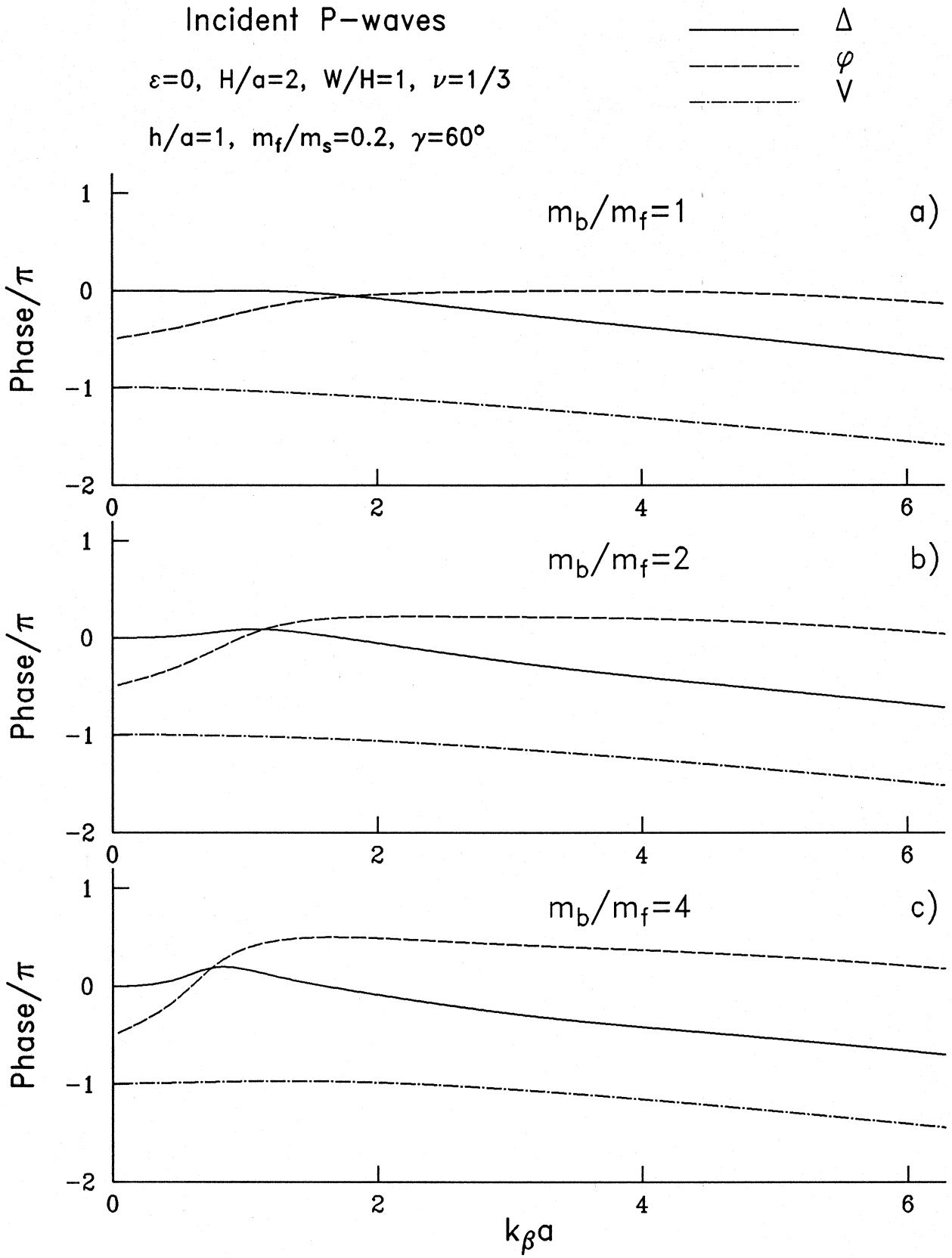
Incident P-waves
ε=0, H/a=2, W/H=1, ν=1/3
h/a=1, m_f/m_s=0.2, γ=60°
Δ
φ
V
m_b/m_f=1
a)
m_b/m_f=2
b)
m_b/m_f=4
c)
Phase/π
1
0
−1
−2
0
2
4
6
k_βa

Figure II.10

approaches the phase of Δ and at some frequency the two phase curves cross each other. The frequency at which Δ and φ have same phase decreases when m_f/m_s increases. This "characteristic" frequency is in the vicinity of the rocking and the translational frequencies, which are very close. At those frequencies, when the translational and the rotational responses are maximum, as the foundation moves to the right it rotates clockwise.

II.2.5.2 Effect of the Incident angle

Figures II.11a through II.11e illustrate the dependance of the amplitude spectra of Δ, φ, u_b^{rel}, V and v_b^{rel} (for unit amplitude of the incident wave) on the incident angle γ, for a flexible building ($\varepsilon = 4$), with slenderness ratio $\frac{W}{H} = 1$, on a semi-cylindrical rigid foundation, and with mass ratios $\frac{m_b}{m_f} = 2$ and $\frac{m_f}{m_s} = 0.2$. The different dashed lines correspond to $\gamma = 0°$, $30°$, $60°$ and $85°$. When $\gamma = 0$, the horizontal motion of the foundation, the rotation, and, consequently, the horizontal component of the building relative response are zero. In the vicinity of the fixed-base natural frequencies of the building, $|\Delta|$, $|\varphi a|$ and $|V|$ have large variations, having sharp local minima and maxima. $|u_b^{\text{rel}}|$ and $|v_b^{\text{rel}}|$ also have peaks in the vicinity of those frequencies. The general behavior of the curves $|V|$ and $|v_b^{\text{rel}}|$ is similar to the horizontal foundation and relative building responses for incident SH-waves (Trifunac, 1972), where there is no rotation of the base. $|V|$ is zero close to the fixed-base longitudinal natural frequencies of the building. It is not so for $|\Delta|$, because the horizontal motions of the soil-structure system are coupled with the rocking motions. The amplitudes of $|V|$ and $|v_b^{\text{rel}}|$ are proportional to the vertical amplitudes of the free-field motion on the half-space surface. For oblique incidence, for low frequencies ($k_\beta a < 3$), the amplitudes of Δ and φa are proportional to $|u^{ff}|$. However, for higher frequencies that is not always the case. For example, even though the horizontal free-field displacement amplitudes $|u^{ff}|$ are larger by a factor of about 1.5 when $\gamma = 60°$ relative to $\gamma = 30°$, at some frequency the base horizontal amplitudes $|\Delta|$ and the base rotation amplitudes $|\varphi|$ become the same ($k_\beta a \approx 5$ and $k_\beta a \approx 3.5$, respectively), and for frequencies higher than those the relationship even reverses. The same can be said for the amplitudes of the horizontal relative building response $|u_b^{\text{rel}}|$. Those are close at $k_\beta a \approx 4$ and for higher frequencies $|u_b^{\text{rel}}|$ is even higher for $\gamma = 60°$ relative to $\gamma = 30°$. This effect reflects the behavior of $|\Delta|$ and $|\varphi|$ of the foundation input motion at those angles (Fig. II.5), and it is ignored in analysis that take only the free-field translations as base excitation. Such analyses may underestimate the forces in the building and the base rotation at higher frequencies for $\gamma = 30°$, for example. Because the model in this report neglects the coupling of the vertical motions with the base rotation, $|V|$ and $|u_b^{\text{rel}}|$ are proportional to $|v_b^{\text{rel}}|$ in the whole frequency range considered.

Because of the interaction, the transfer function of the building relative responses is modified relative to those of the fixed-base model. (1) At the resonant frequencies of the fixed-base model, the relative responses are finite (in the fixed-base model these amplitudes are unbounded). (2) There, the relative response has peaks but at frequencies shifted relative to the fixed base frequencies. The first peak of $|u_b^{\text{rel}}|$ is most affected by

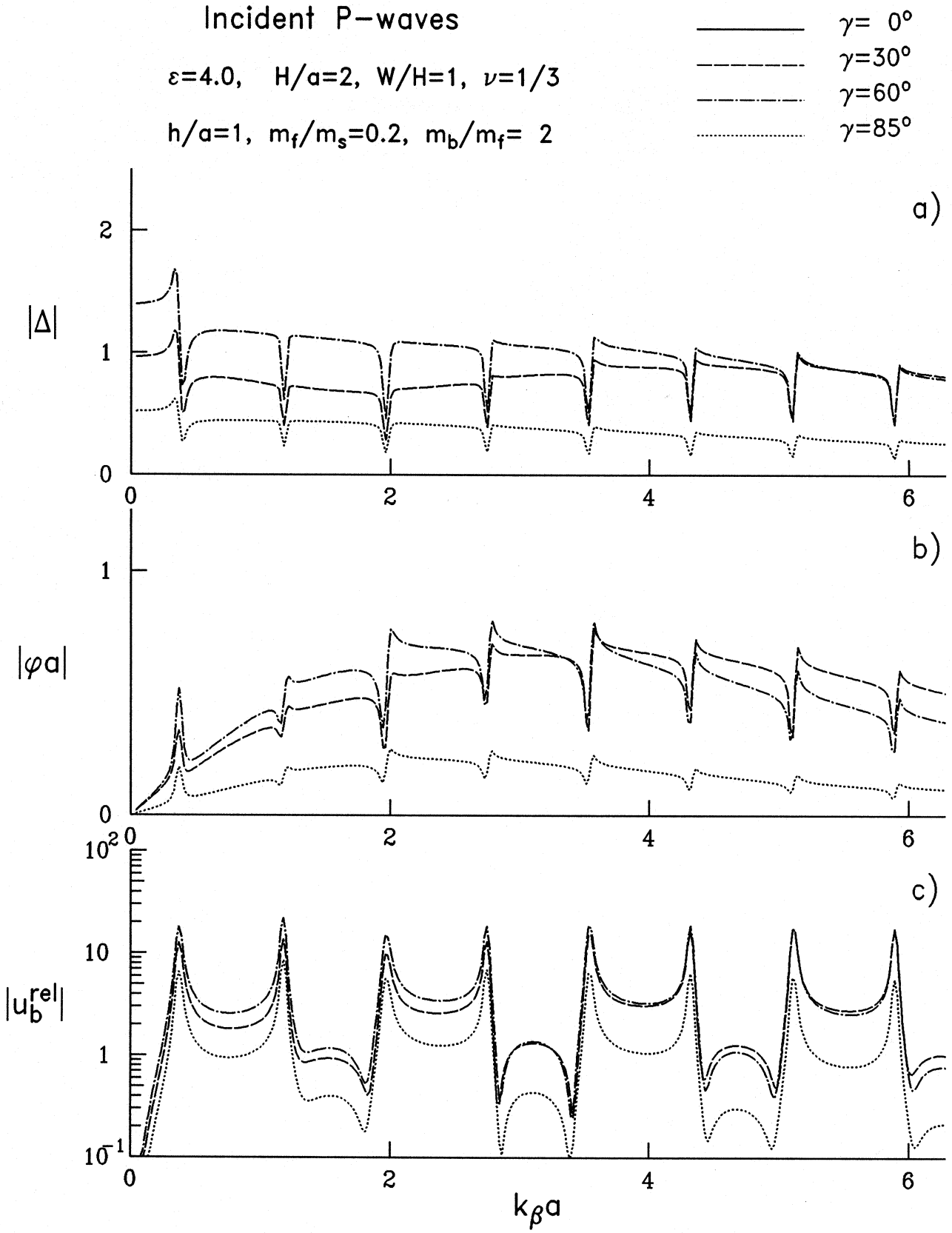

Figure II.11 a), b) and c)

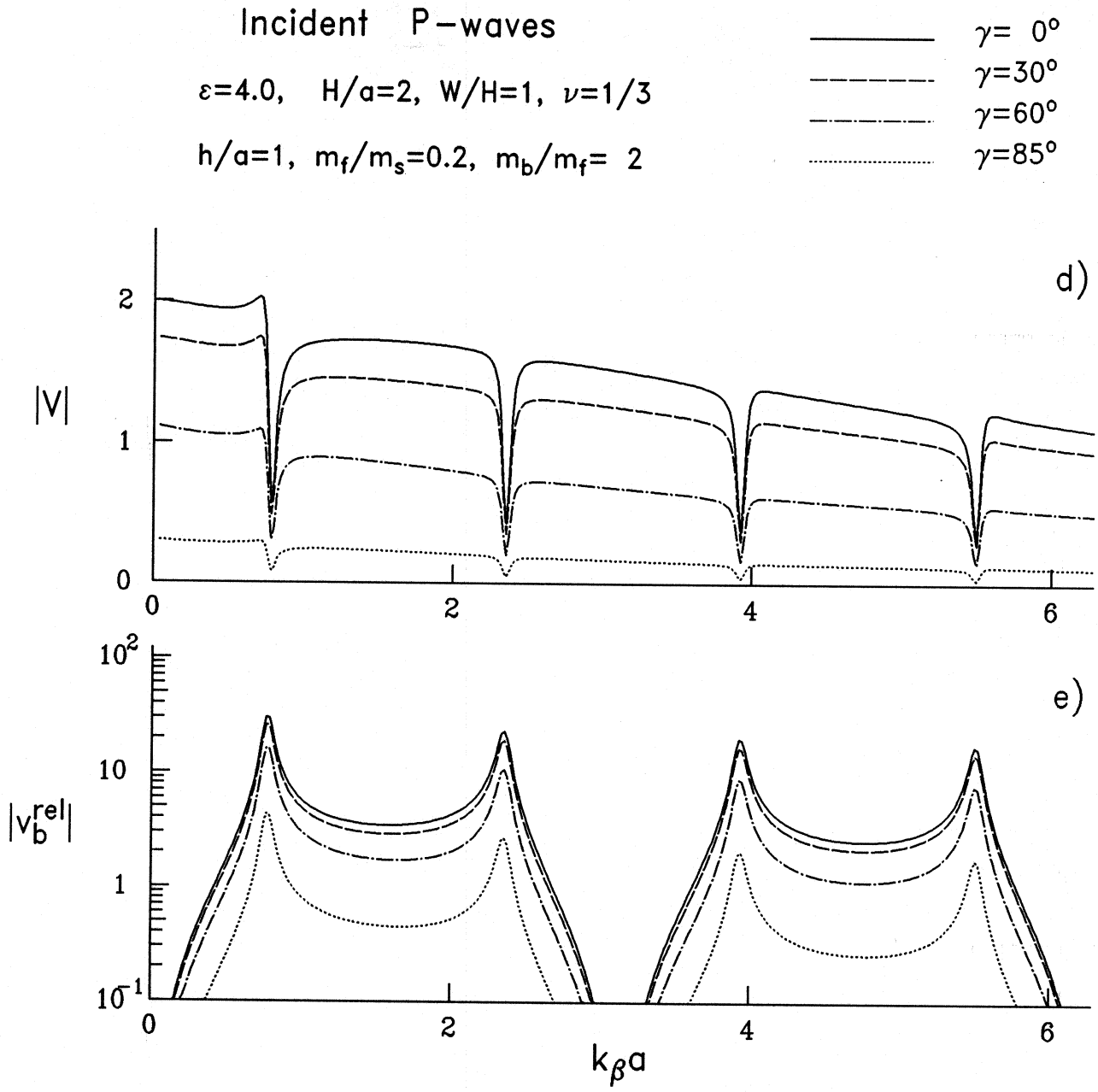

Figure II.11 d) and e)

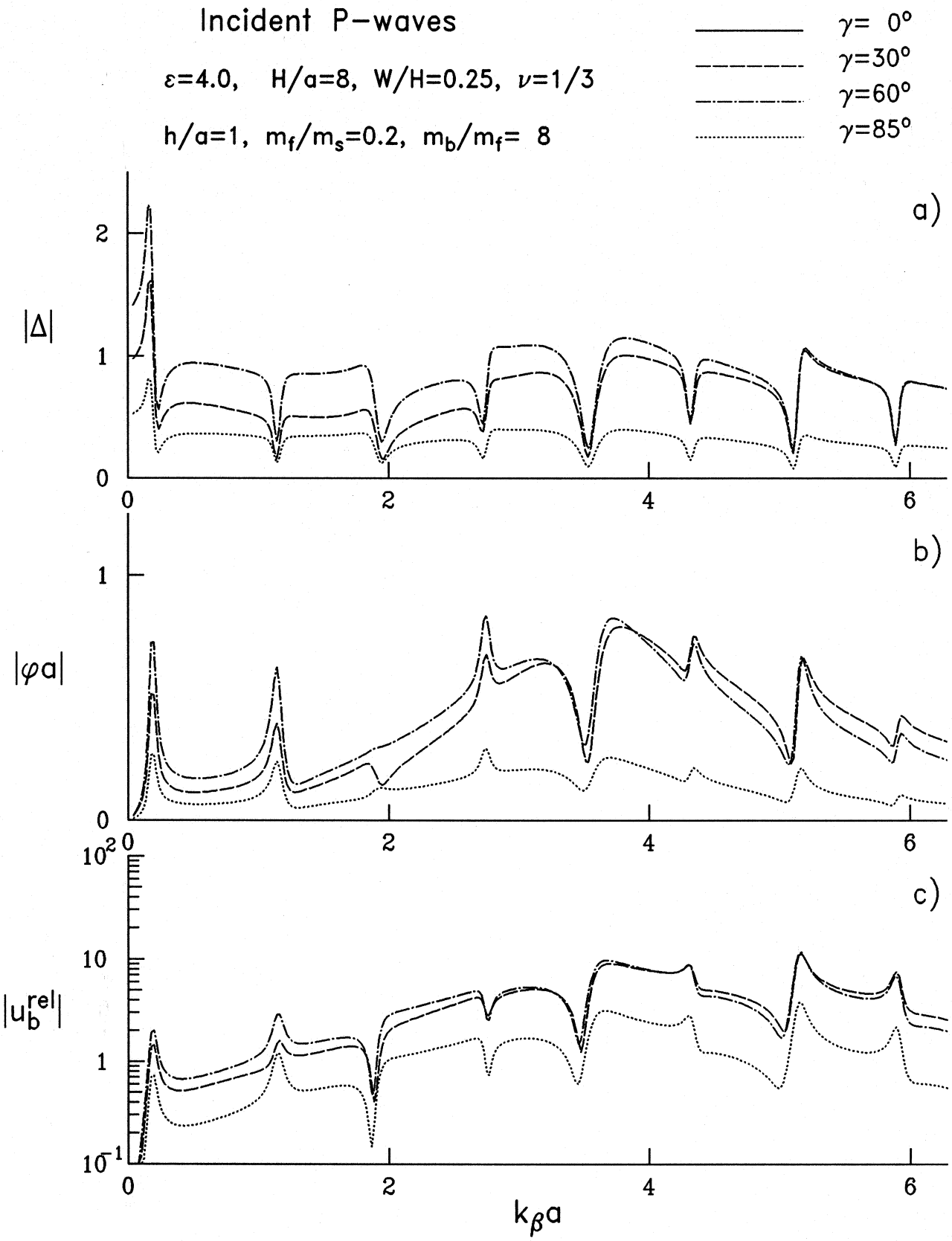

Figure II.12 a), b) and c)

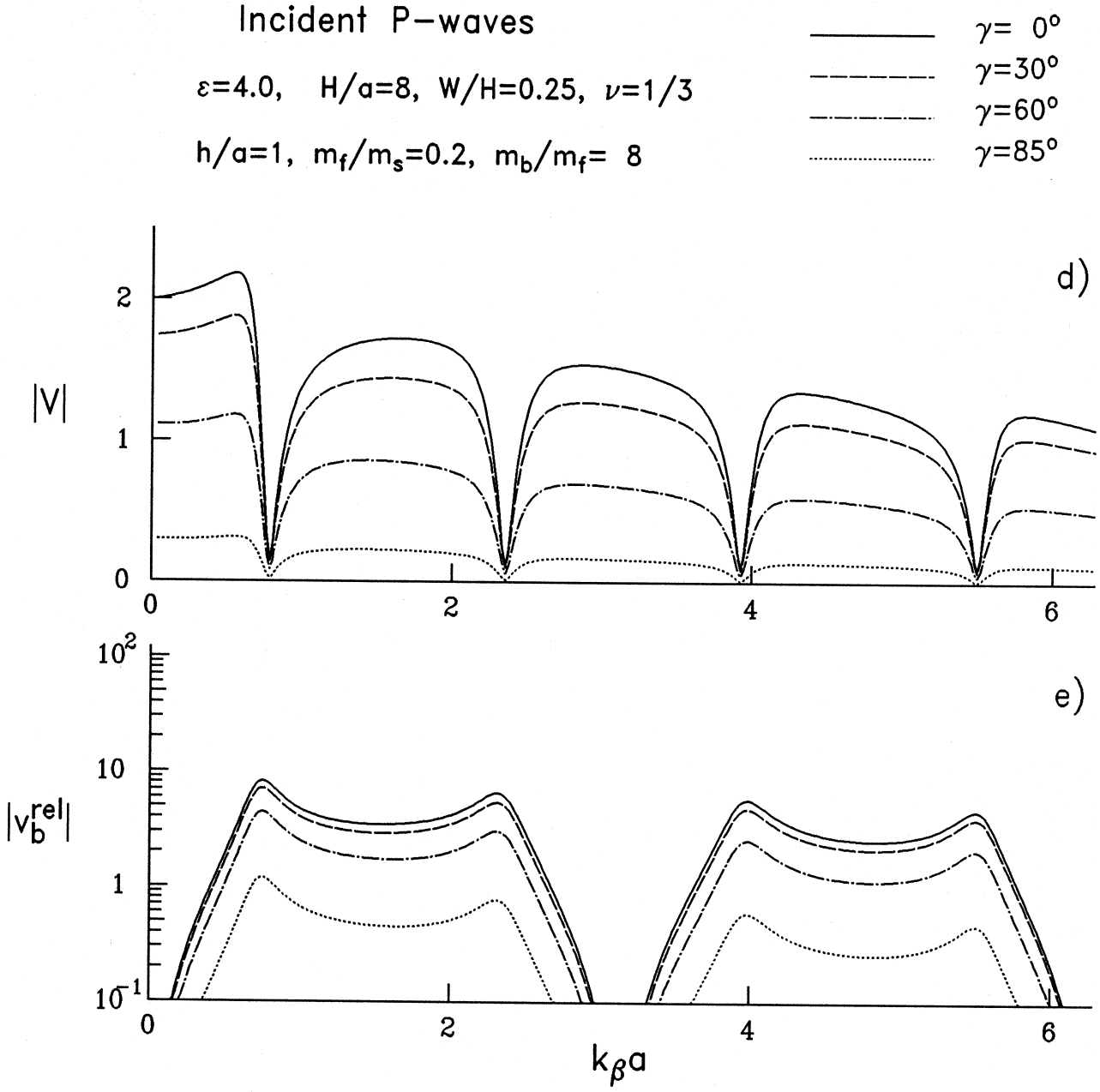

Figure II.12 d) and e)

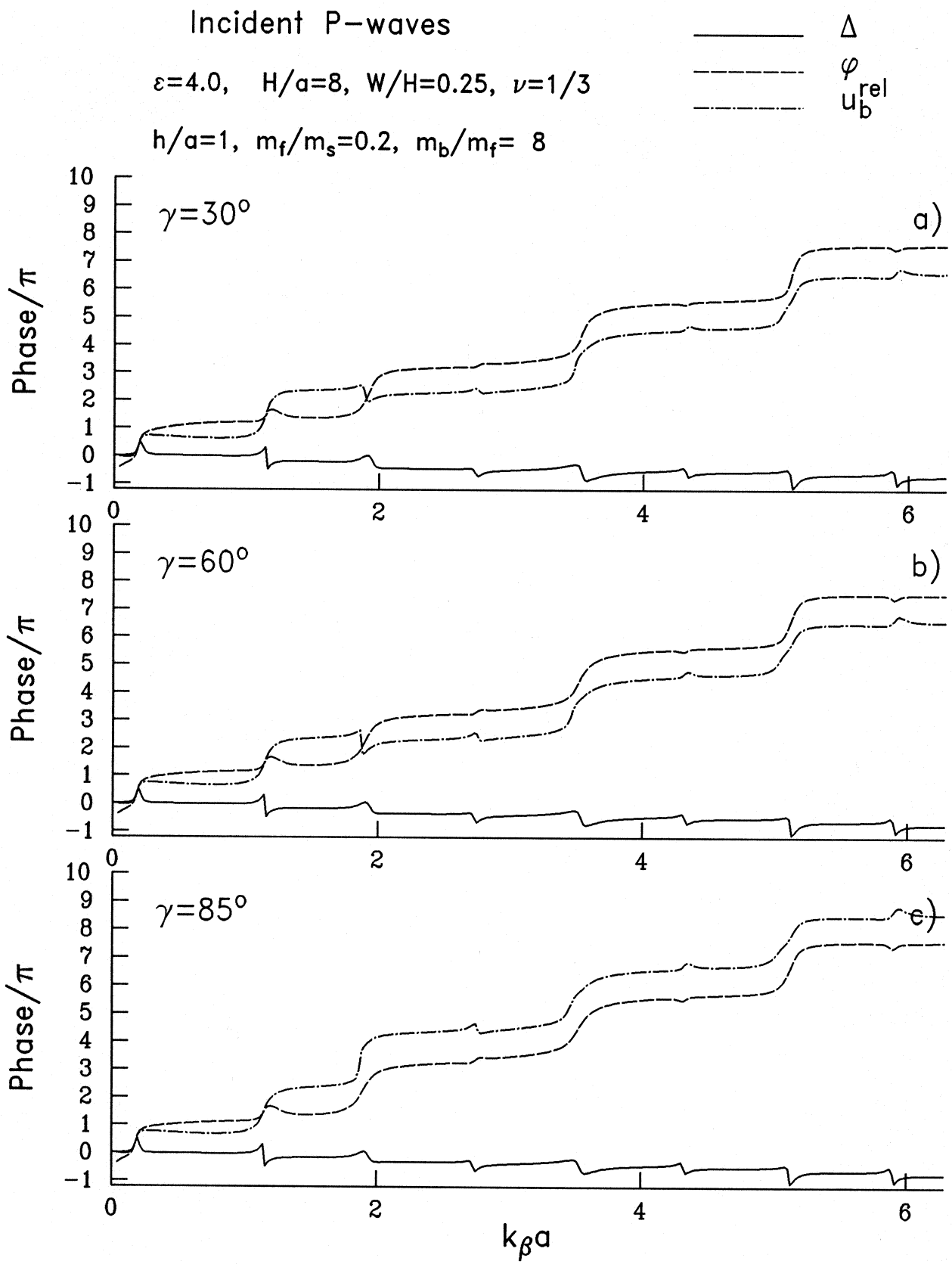
Incident P-waves
ε=4.0, H/a=8, W/H=0.25, ν=1/3
h/a=1, m_f/m_s=0.2, m_b/m_f= 8
Δ
φ
u_b^rel
γ=30°
a)
γ=60°
b)
γ=85°
c)
Phase/π
k_βa

Figure II.13

the interaction. It is always at frequency that is lower than the fundamental frequency of the fixed-base model.

II.2.5.3 Effect of the Size of the Building

In Fig. II.12a, b and c, the same quantities are shown as in Fig. II.11, but for a higher and heavier building ($H/a = 8$, $W/H = 0.25$, $m_b/m_f = 8$, $\varepsilon = 4$, $m_f/m_s = 0.2$). The different curves correspond again to different incident angles ($\gamma = 0°$, $30°$, $60°$ and $85°$). $|\Delta|$ and $|\varphi|$ now have different "backbone" curves than the same curves in Fig. II.11. For the higher building, the "backbone" curves for $|\varphi|$ are lower for frequencies < 2.5. Δ and φ are in fact a superposition of the foundation input motion and the additional motion of the foundation, relative to the foundation input motion, due to the inertia forces of the building, with amplitudes proportional to the mass of the building. When the building is heavier, those additional displacements reduce the resultant amplitudes of the foundation input motion. (The density of the foundation is small relative to the density of the soil and its inertia forces do not play a significant role in the interaction). Comparing the curves in Fig. II.11 and Fig. II.12, it can be concluded that, when the building is heavier, (1) the first peak in the response is shifted more towards lower frequencies relative to the first fixed-base natural frequency. (2) The first peaks of $|\Delta|$ and $|\varphi|$ are higher, but (3) the peaks of the relative building response $|u_b^{\text{rel}}|$ are lower. (4) The peaks of the relative vertical response $|v_b^{\text{rel}}|$ are also lower for the heavier building. The reduction of the peak relative responses is caused by the soil flexibility and by the radiation of the vibrational energy of the building into the soil. It is especially pronounced in the relative horizontal response for the heavier building where some of the peaks are practically lost (e.g. the third, fourth and fifth peaks).

In Fig. II.13a, b and c, the phases of the transfer functions of Δ, φ and u_b^{rel} have been plotted for the higher building ($H/a = 8$, $W/H = 0.25$, $m_b/m_f = 8$, $\varepsilon = 4$, $m_f/m_s = 0.2$ and $h/a = 1$) for incident angles $\gamma = 30°$, $60°$ and $85°$. As $k_\beta a \to 0$, Phase $(\Delta) \to 0$ and Phase $(\varphi) \to -\frac{\pi}{2}$, and the phase of u_b^{rel} is same as the phase of Δ. At the first peak frequency, both Δ, φ and u_b^{rel} have same phase. That is not the case for the higher order peaks. For example, at the frequency of the second peak u_b^{rel} and φ have almost opposite phases. Between the first peaks, the phase difference between Δ and φ is $\approx \pi$, and between u_b^{rel} and Δ also $\approx \pi$.

II.2.5.4 Effect of the Relative Stiffness

The relative stiffness of the building and of the soil is controlled by the parameter $\varepsilon = \frac{\beta H}{\beta_b a}$. Leaving all the other parameters unchanged and decreasing ε would correspond to placing the same building on softer soil. Increasing ε would be equivalent to placing he same building on harder soil. To see the effects of ε on the response of the building-soil system, and also of the building mass, in Fig. II.14 and Fig. II.15 the amplitudes of the transfer functions of Δ, φ, and u_b^{rel}, and of V and v_b^{rel} are shown for the same buildings ($H/a = 2$, $W/H = 1$, $h/a = 1$, $\gamma = 30°$, $m_f/m_s = 0.2$, $m_b/m_f = 1, 2$ and 4), but on

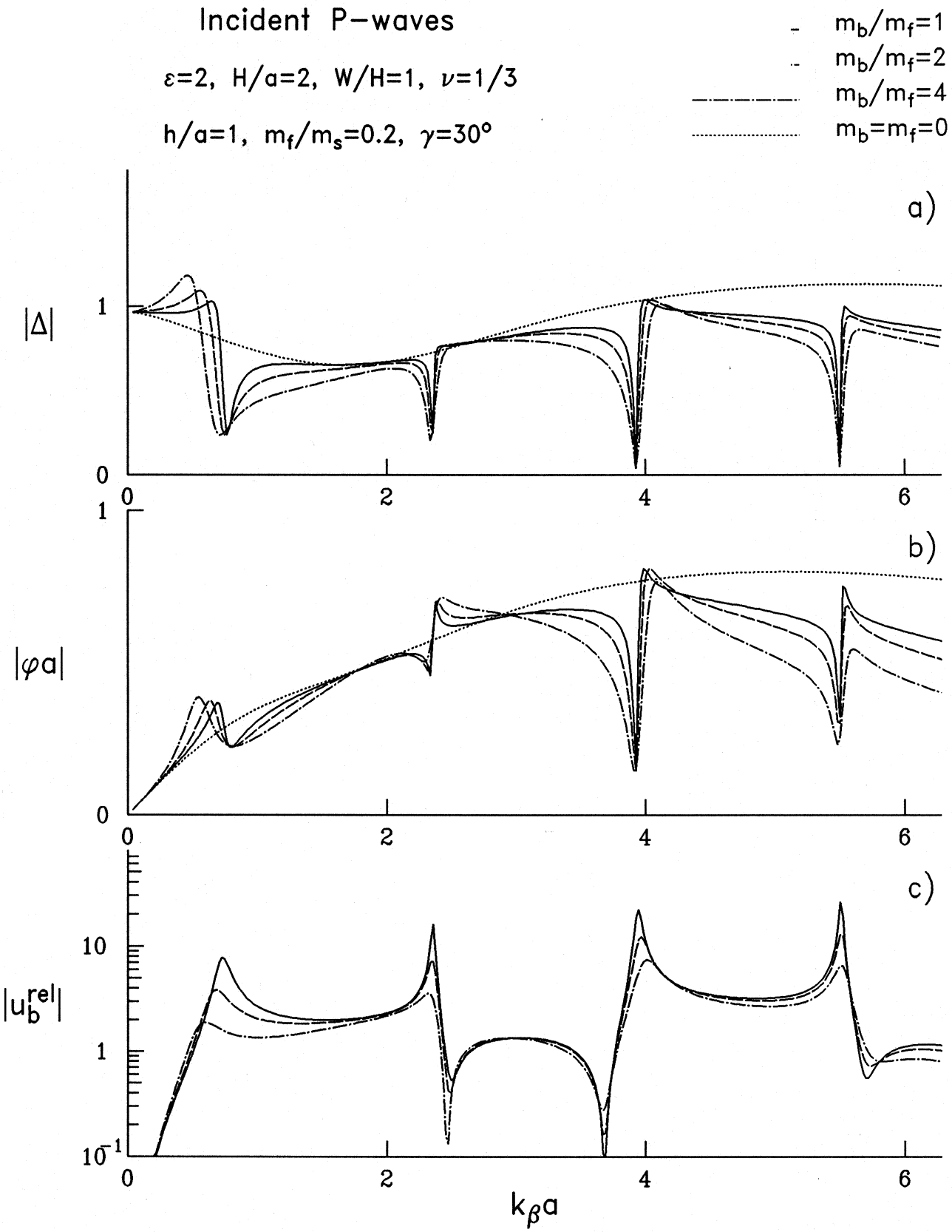

Figure II.14 a), b) and c)

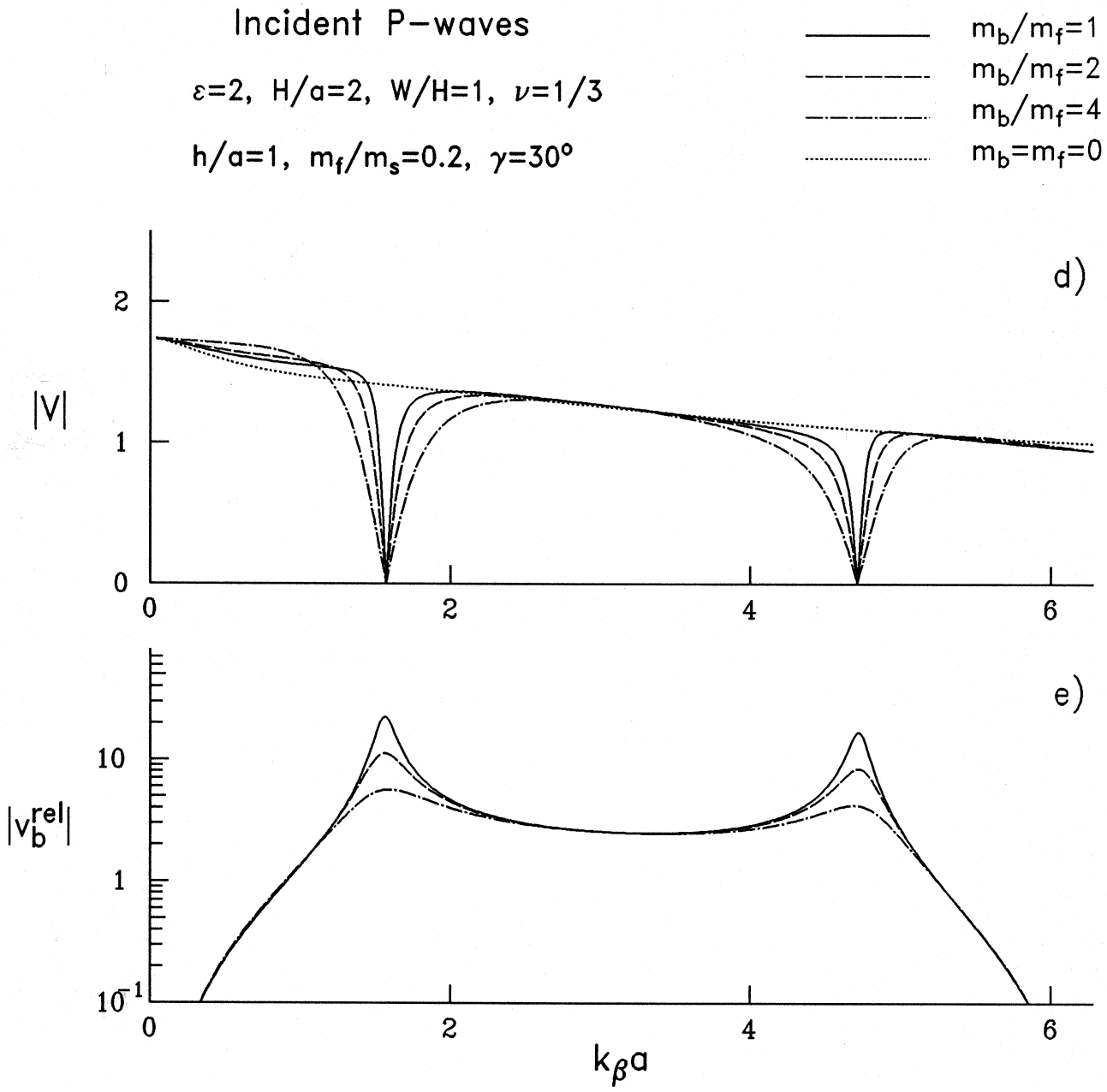

Figure II.14 d) and e)

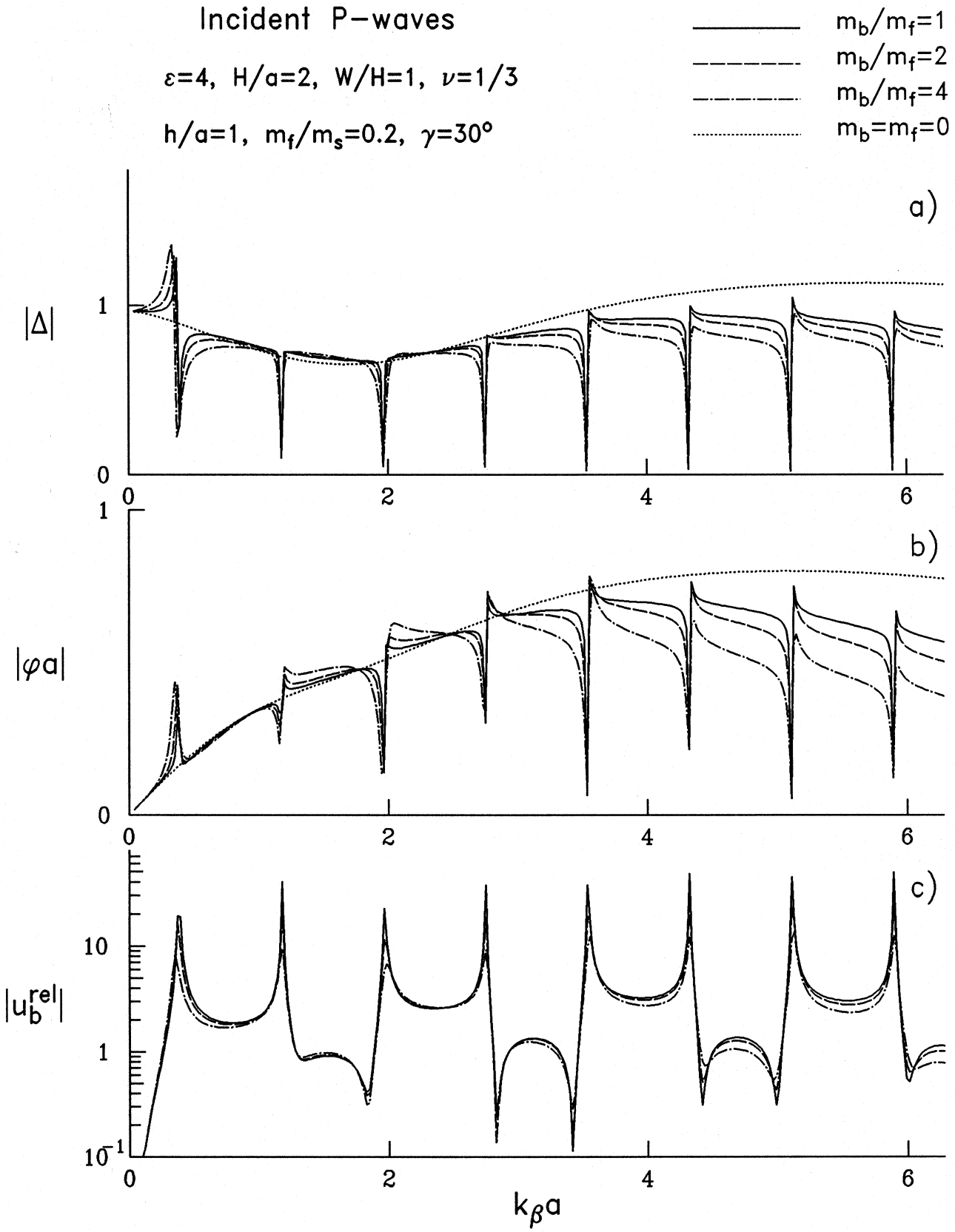

Figure II.15 a), b) and c)

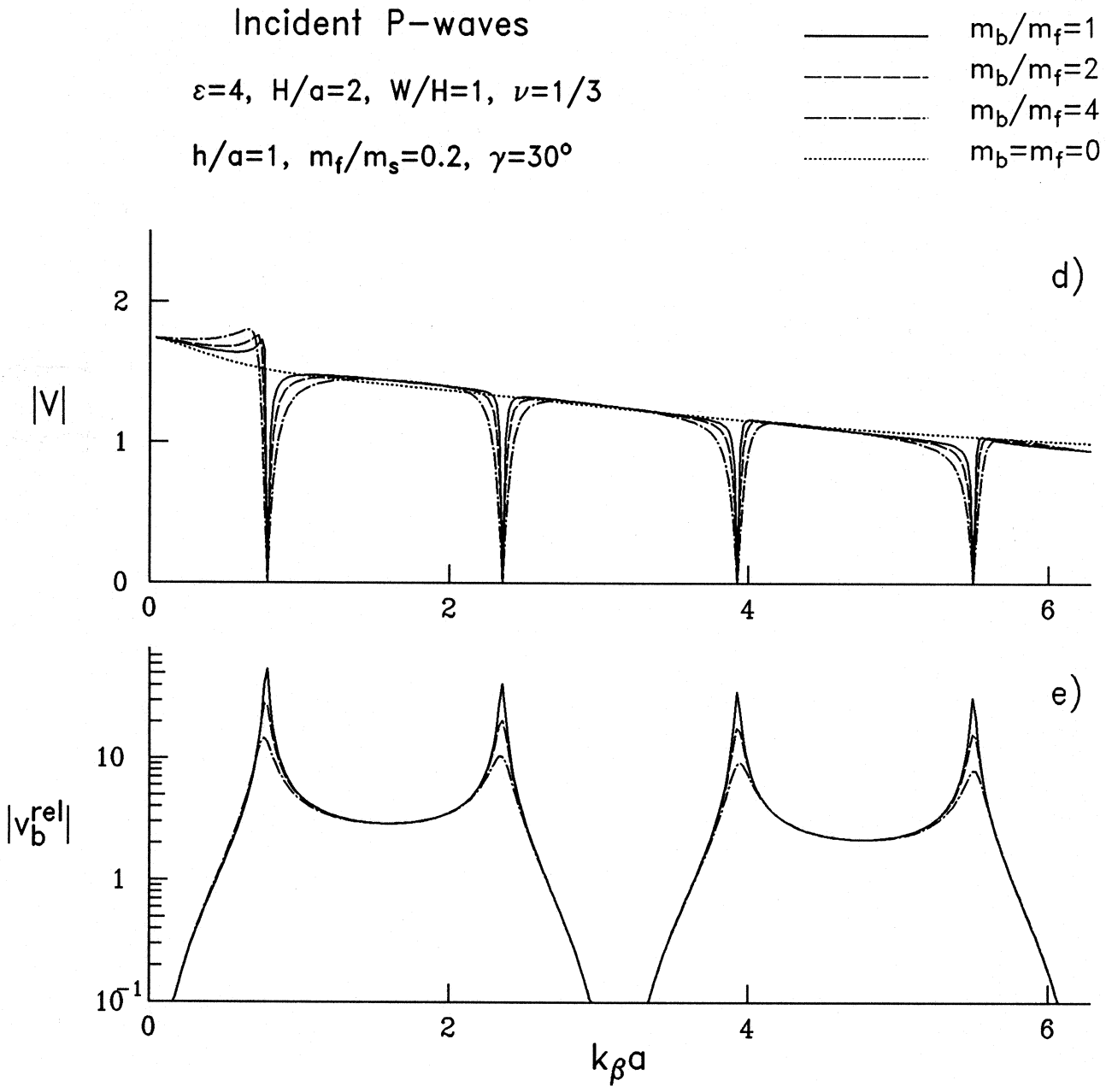

Figure II.15 d) and e)

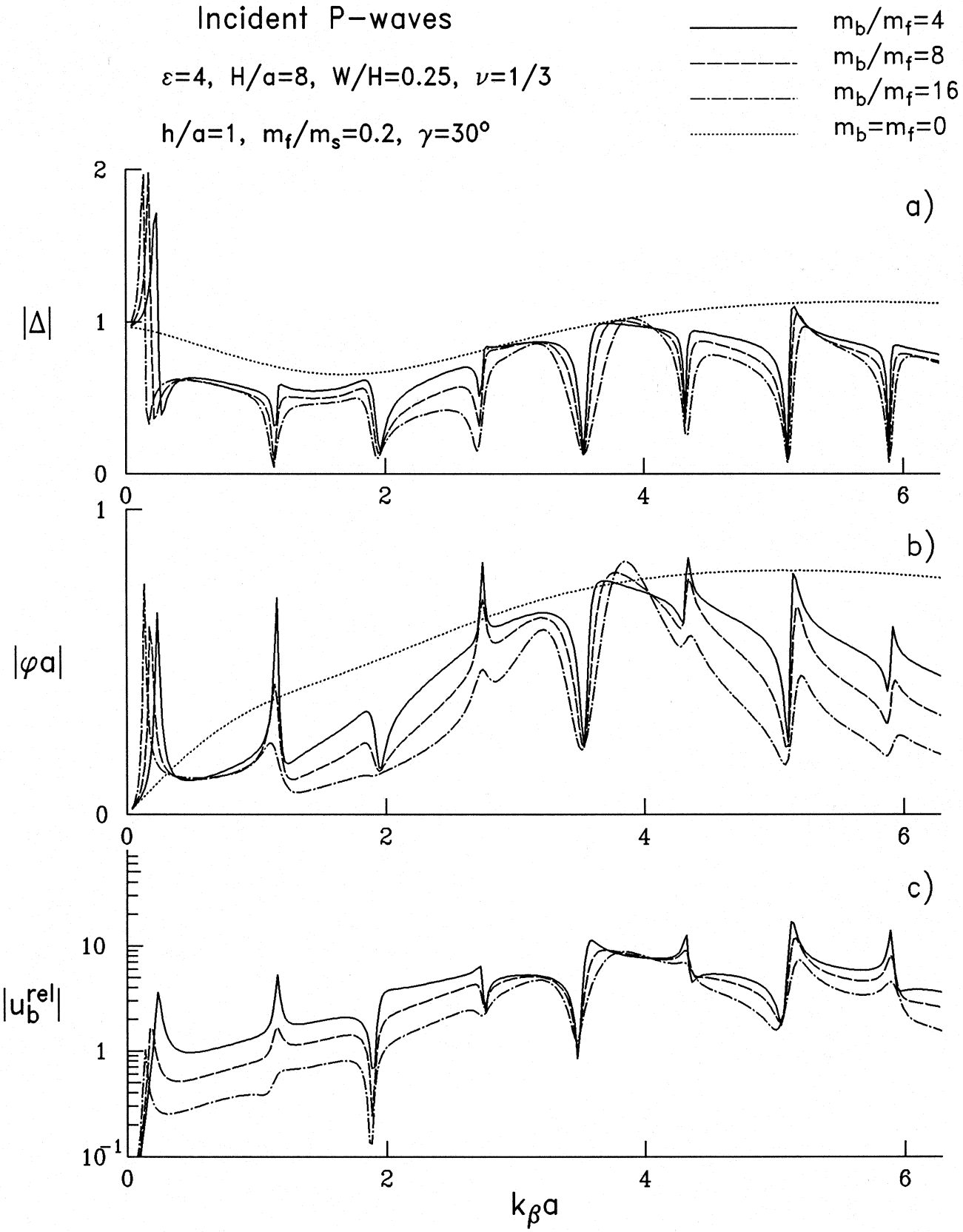

Figure II.16 a), b) and c)

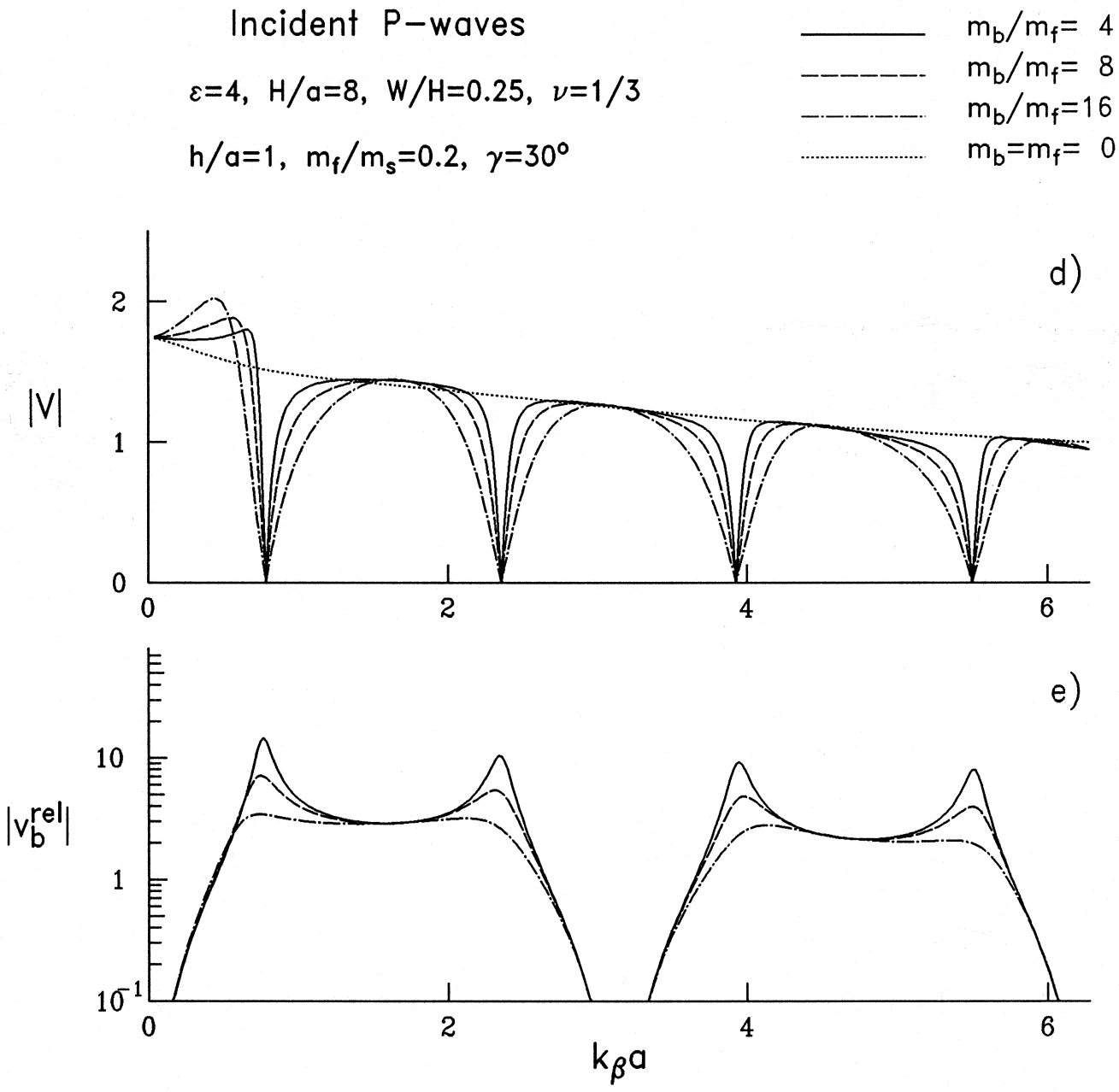

Figure II.16 d) and e)

different soil. In Fig. II.14 the soil is softer ($\varepsilon = 2$) than in Fig. II.15 ($\varepsilon = 4$). Those results lead to the following conclusions. (1) In the same interval of wavelengths of the incident waves compared with the size of the foundation ($0 < \eta = \frac{2a}{\lambda_\beta} \leq 2$), more modes of vibration of the building will be excited if it is situated on stiffer soil. (2) When $\varepsilon = 2$, the first shear fixed-base natural frequency of the building is at $\eta = 1/4$ ($k_\beta a = \pi/4$), and when $\varepsilon = 4$ it is at $\eta = 1/8$ ($k_\beta a = \pi/8$). The first peak of $|u_b^{\rm rel}|$ of the building on flexible soil is at $\eta \approx 0.22$ when $\varepsilon = 2$, and at $\eta \approx 0.12$ when $\varepsilon = 4$. The reduction of the first frequency is about 12% when the soil is softer ($\varepsilon = 2$) and about 4% when the soil is harder ($\varepsilon = 4$). (3) The peaks of $|u_b^{\rm rel}|$ and $|v_b^{\rm rel}|$ are significantly lower when he soil is softer ($\varepsilon = 2$). This is especially the case for the first peak of $|u_b^{\rm rel}|$. (4) The shift of the first peak of the longitudinal building vibrations is not so large as for the shear vibrations for which there is coupling of the translational and the rotational motions.

The different dashed lines in Fig. II.14 and Fig. II.15 correspond to different values of m_b/m_f, but for ε kept constant (the ratio β/β_b is also constant and the fixed-base resonant frequencies are the same). Then, larger m_b/m_s (i.e. increasing ρ_b/ρ) implies smaller μ/μ_b. The results show that when the building is heavier and the rigidity of the soil is smaller, so that the fixed base resonant frequencies are unchanged, the reduction of the first peak frequency of $|u_b^{\rm rel}|$, relative to the first fixed-base frequency, is more pronounced. Then the peaks of $|\Delta|$ and $|\varphi|$ are higher but the relative building response $|u_b^{\rm rel}|$ is smaller. The same holds for the vertical foundation and relative building responses, V and $v_b^{\rm rel}$. The amount of the building energy radiated into the soil is also larger.

The curves in Fig. II.16 are for a heavier and a higher building ($H/a = 8$, $W/H = 0.25$, $\varepsilon = 4$, $m_f/m_s = 0.2$, $h/a = 1$, $\gamma = 30°$). The different dashed lines correspond to $m_b/m_f = 4, 8$ and 16. In this figure the reduction of the peaks of the relative building response is even more pronounced. It can be concluded from Fig. II.15 and Fig. II.16 that the reduction of the peaks of $|u_b^{\rm rel}|$ is associated with large rotations of the base. When the peak relative response is lower the rotation is larger. Some of the higher order peaks in part c of this figure are almost lost. The reason for this is the significant reduction of $u_b^{\rm rel}$ at the peak frequencies, because of the interaction, and the large base rotation that causes larger amplitudes of $u_b^{\rm rel}$ away from the peak frequencies.

II.2.6 Interaction for Shallow Embedment

In the rest of this chapter examples will be presented for buildings on shallow foundations ($h/a = 0.5$), and the effect of the depth of the embedment will be discussed. To keep the same value of the ratio of the density of the building and the density of the soil ($\rho_b/\rho_s \approx 0.2$), since the area of the foundation with $h/a = 0.5$ is approximately half of that of the area of the semi-circular foundation ($h/a = 1$), the ratio m_b/m_f will be taken twice larger than in the previous examples. The following examples are arranged in the same order as in the first part of the chapter. For comparison, the same examples presented for $h/a = 1$ will be repeated but for $h/a = 0.5$. In Fig. II.17, the amplitude spectra of the foundation input motion are shown for angels $\gamma = 0$, 30°, 60° and 85°. In Fig. II.18 and Fig. II.20, the amplitudes of the transfer functions of foundation response are shown

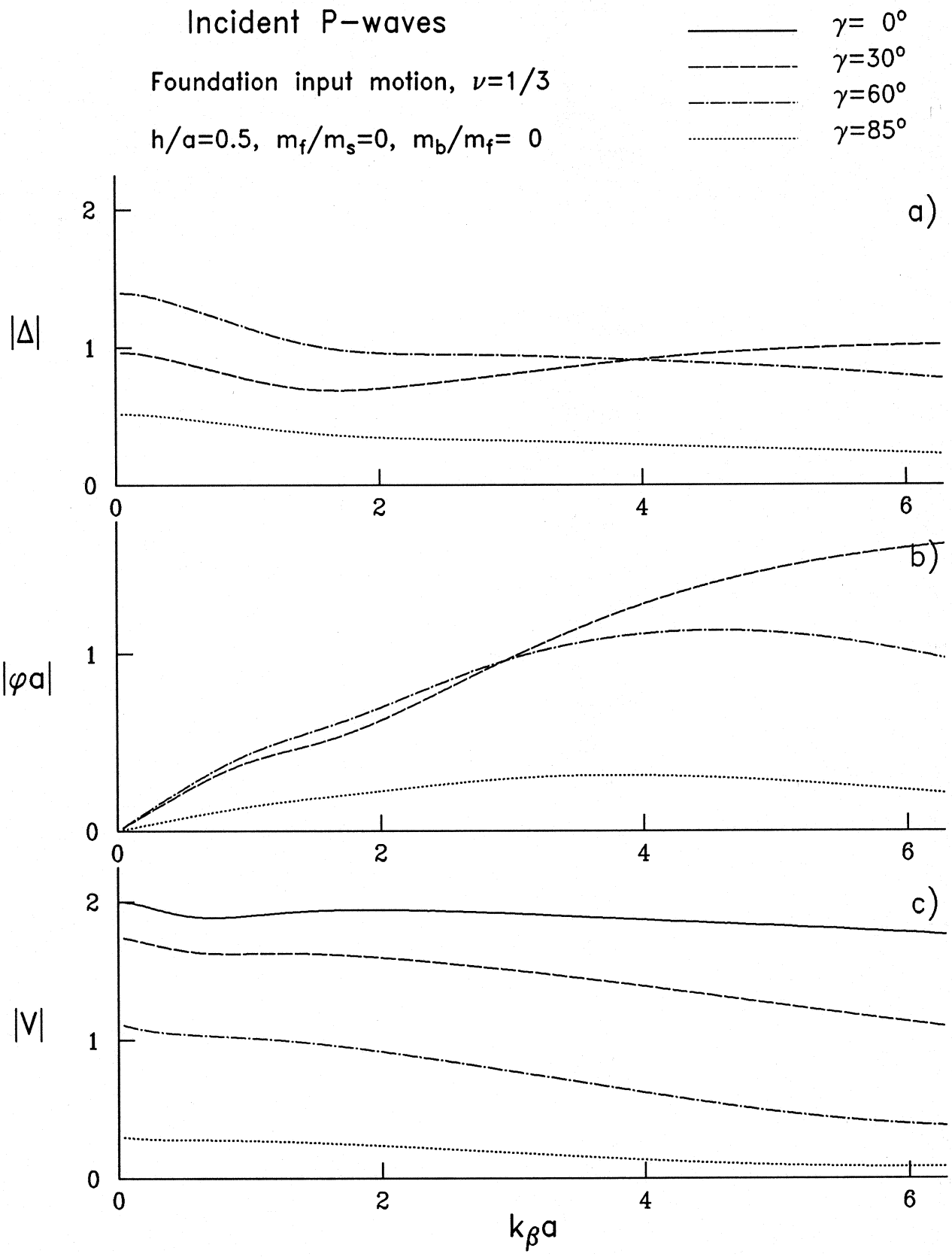
Incident P−waves
Foundation input motion, ν=1/3
h/a=0.5, m_f/m_s=0, m_b/m_f= 0
γ= 0°
γ=30°
γ=60°
γ=85°
a)
b)
c)
|Δ|
|φa|
|V|
0
1
2
0
2
4
6
k_βa

Figure II.17

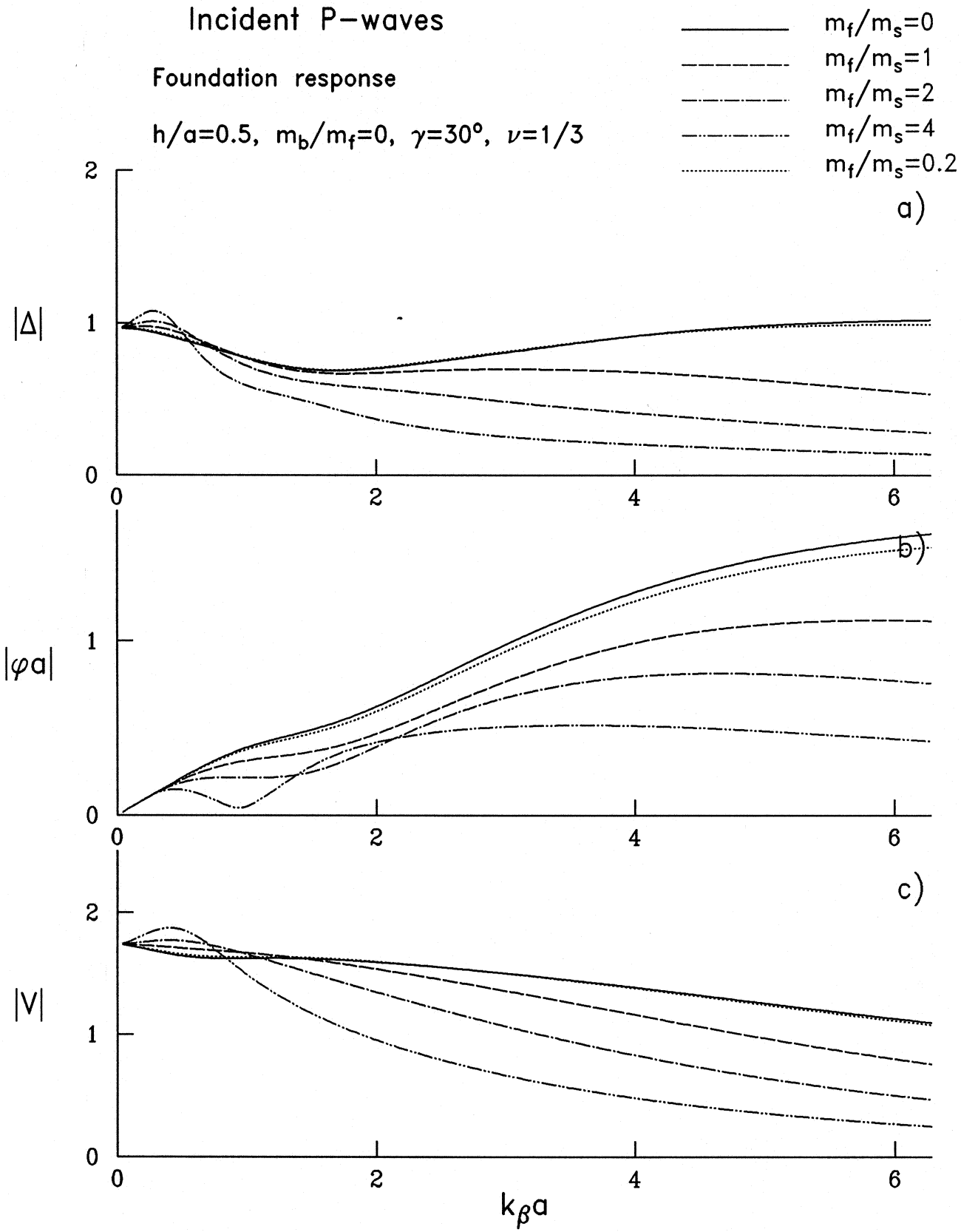
Incident P−waves
Foundation response
h/a=0.5, m_b/m_f=0, γ=30°, ν=1/3
m_f/m_s=0
m_f/m_s=1
m_f/m_s=2
m_f/m_s=4
m_f/m_s=0.2
a)
b)
c)
|Δ|
|φa|
|V|
$k_\beta a$
0
1
2
4
6

Figure II.18

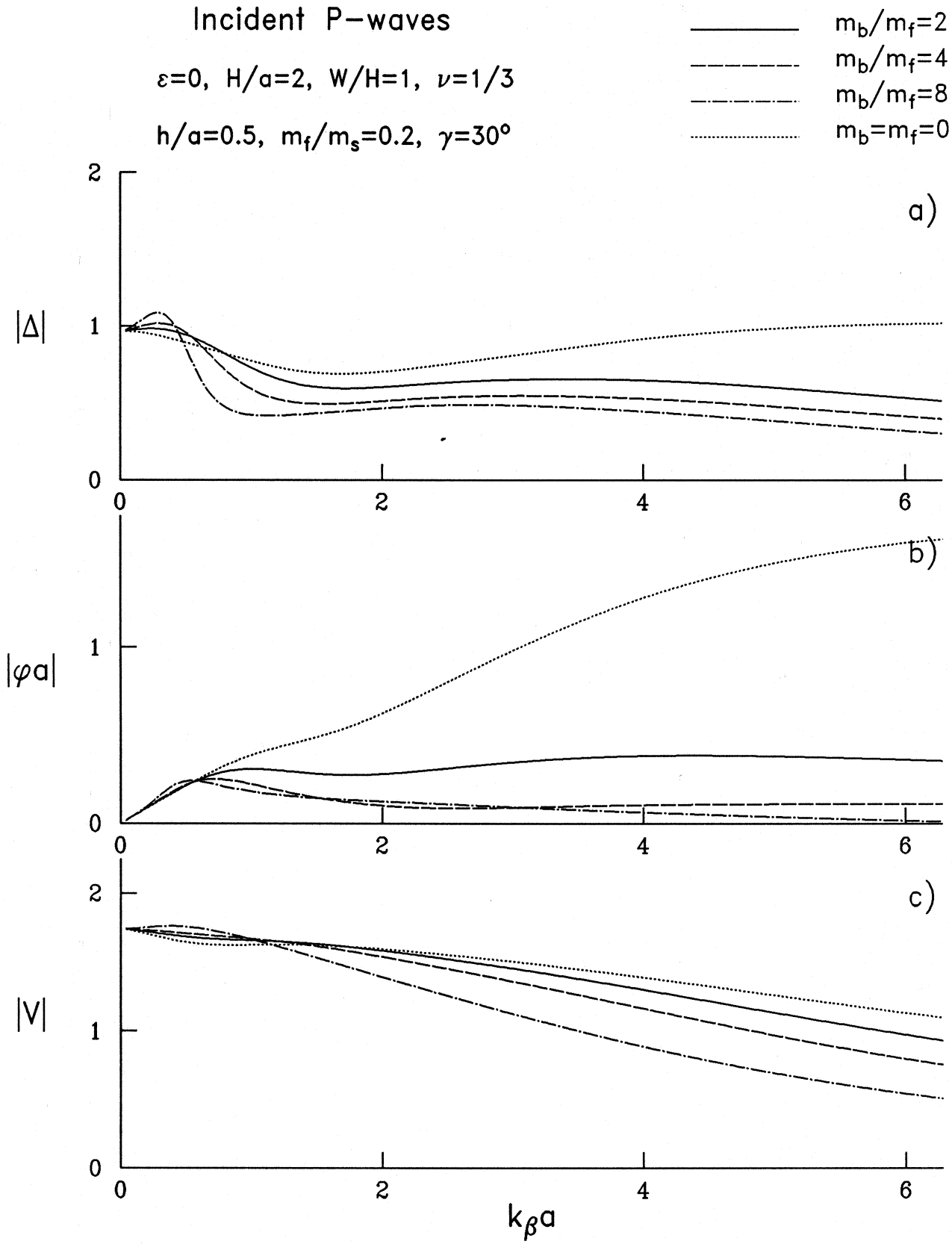
Incident P−waves
ε=0, H/a=2, W/H=1, ν=1/3
h/a=0.5, m_f/m_s=0.2, γ=30°
m_b/m_f=2
m_b/m_f=4
m_b/m_f=8
m_b=m_f=0
a)
b)
c)
|Δ|
|φa|
|V|
k_βa
0
1
2
4
6

Figure II.19

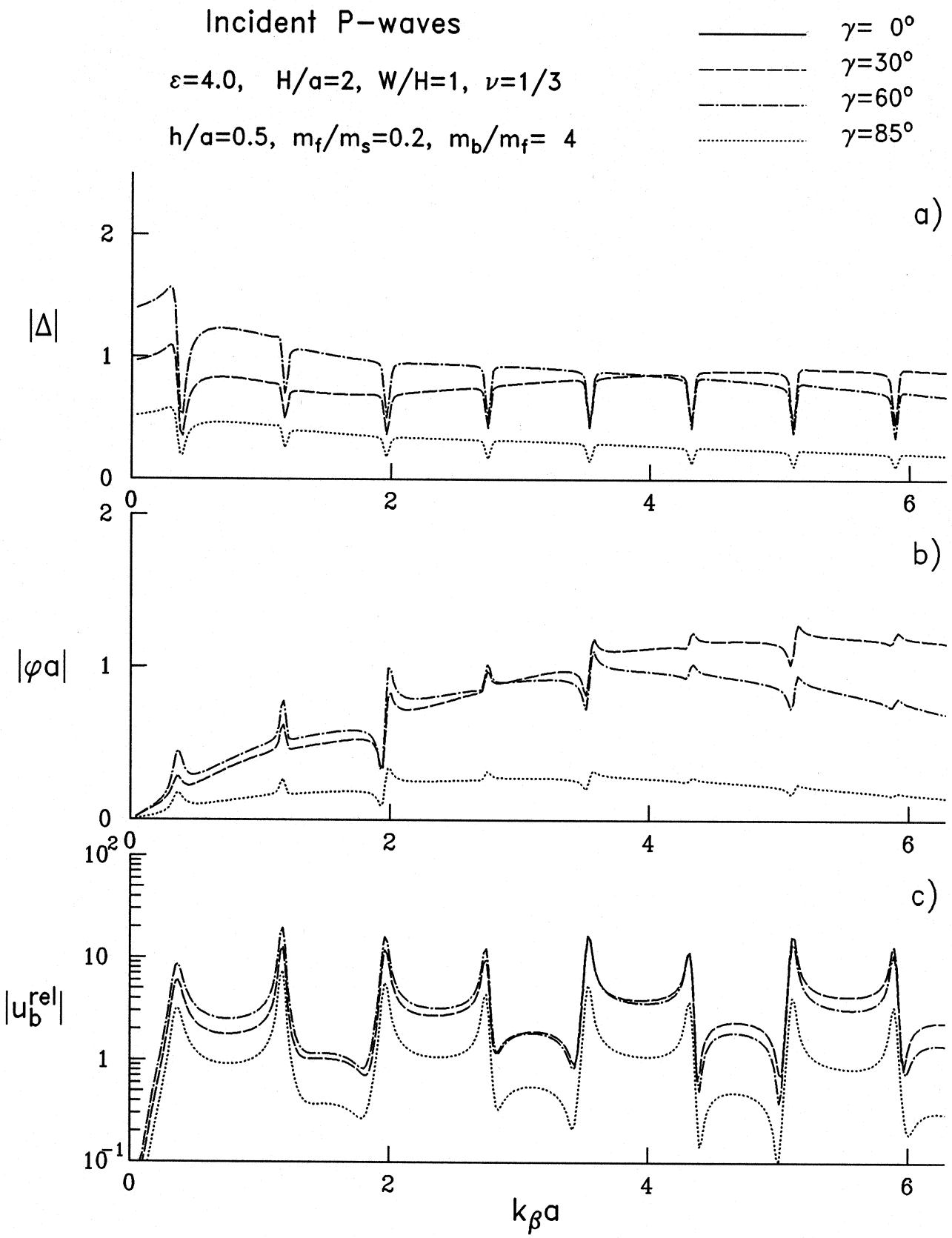

Figure II.20 a), b) and c)

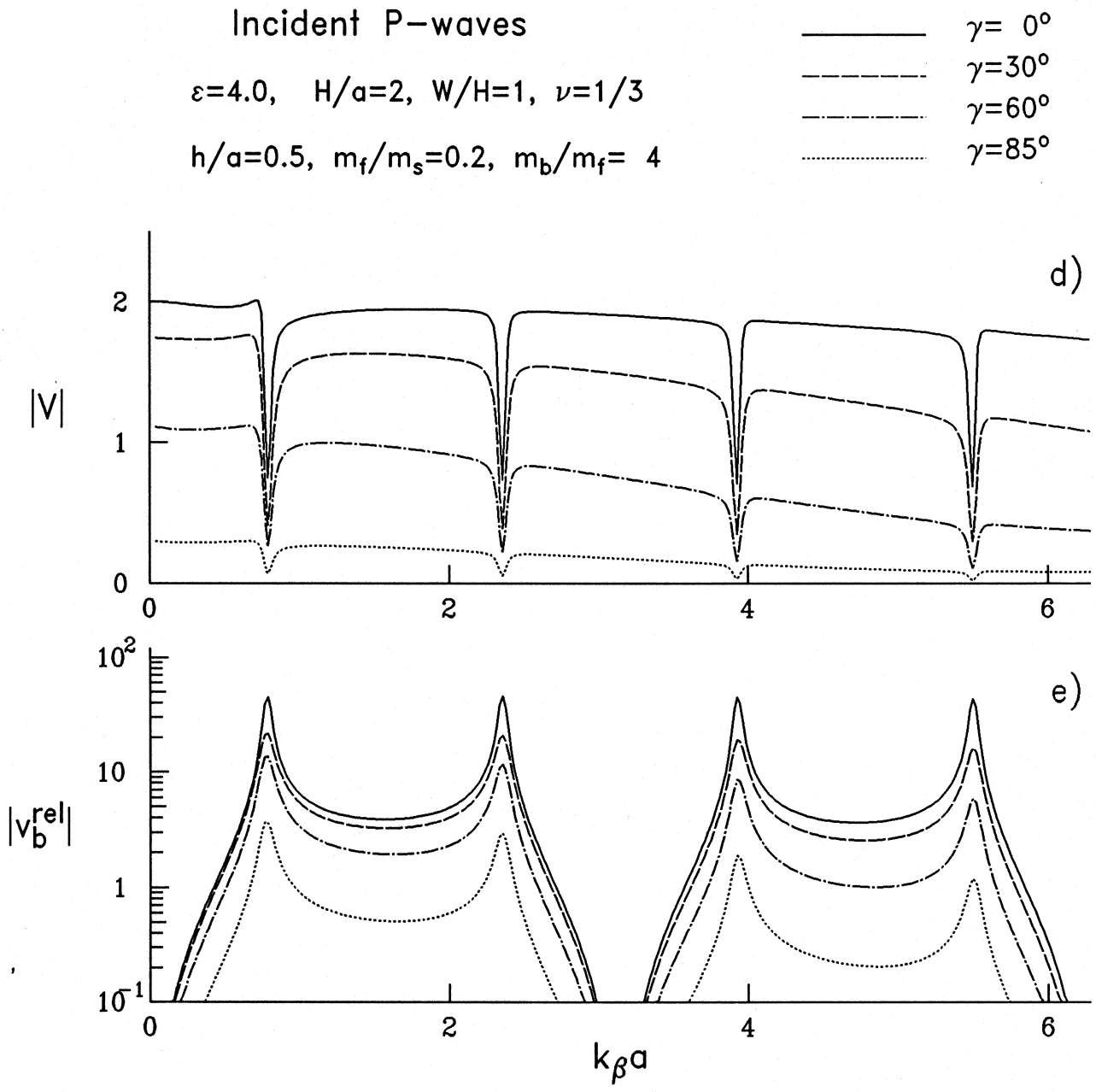

Figure II.20 d) and e)

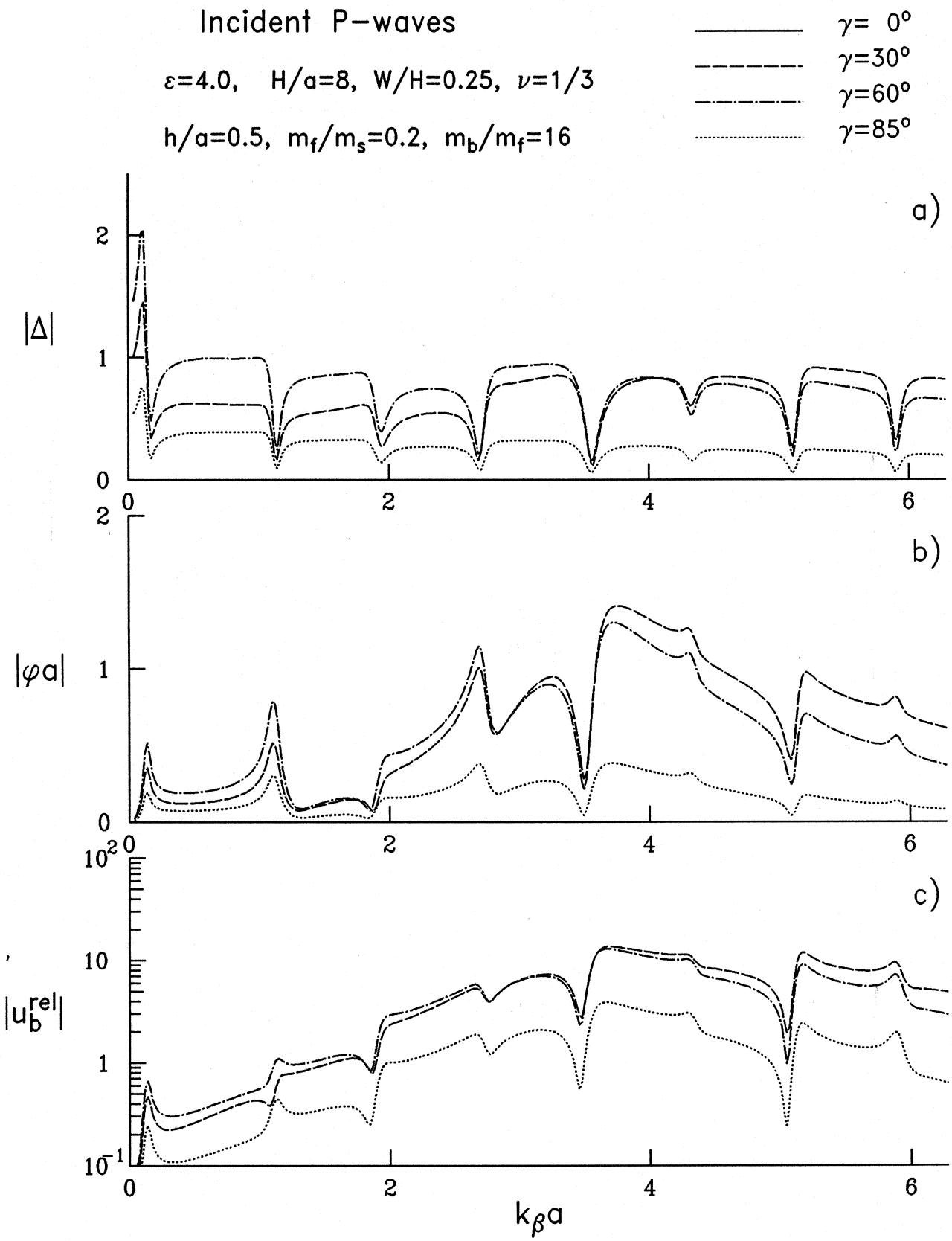

Figure II.21 a), b) and c)

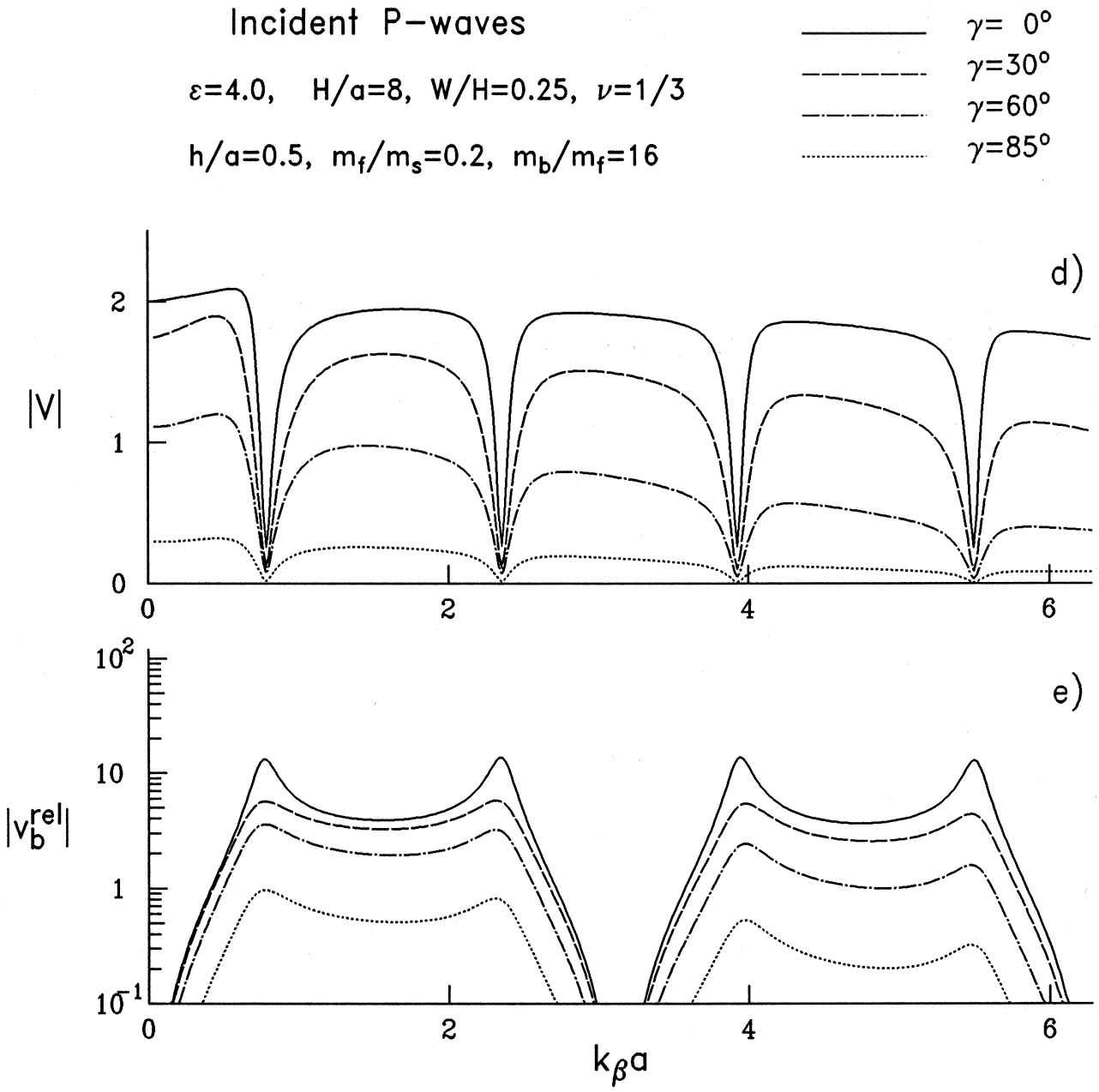

Figure II.21 d) and e)

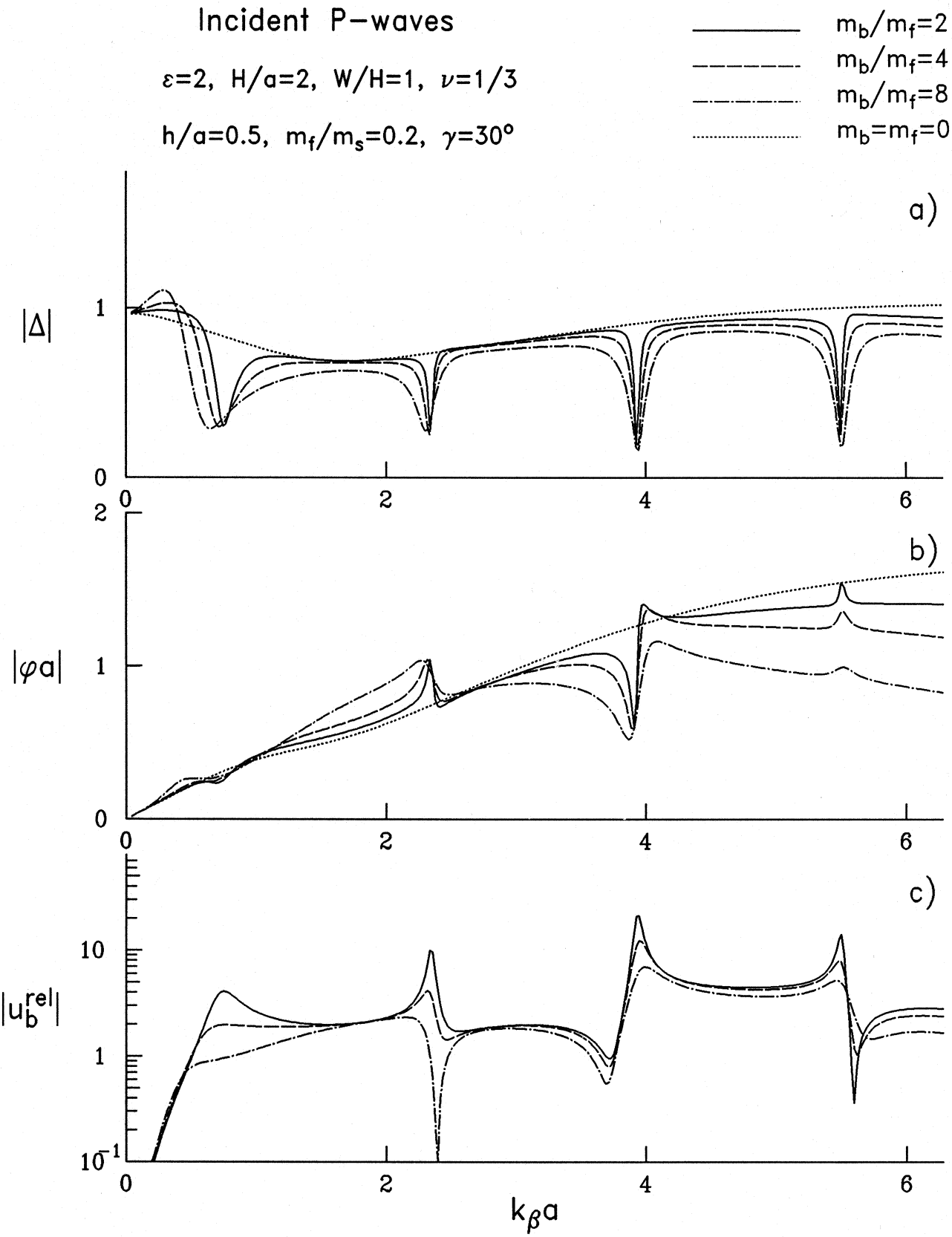

Figure II.22 a), b) and c)

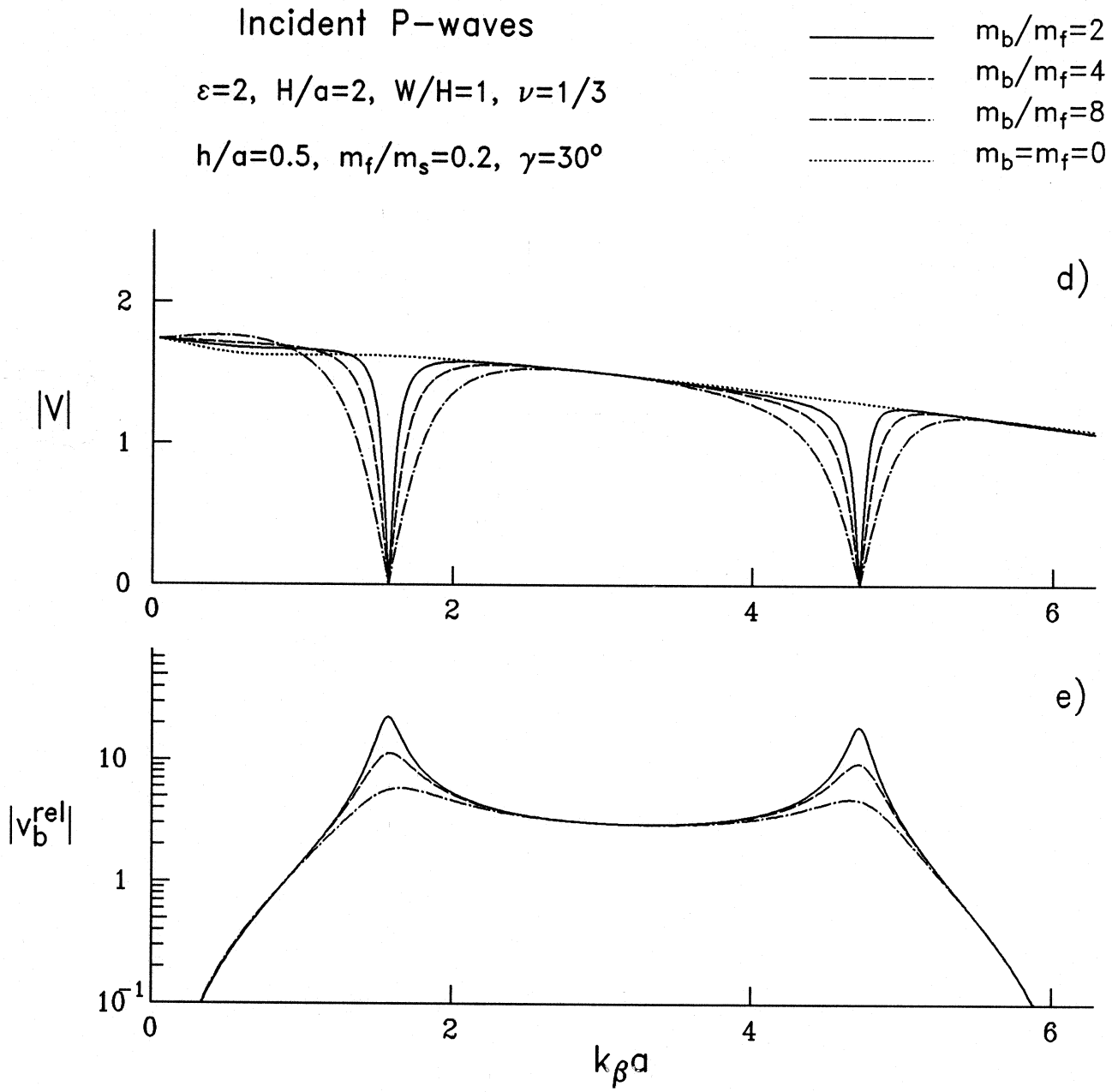

Figure II.22 d) and e)

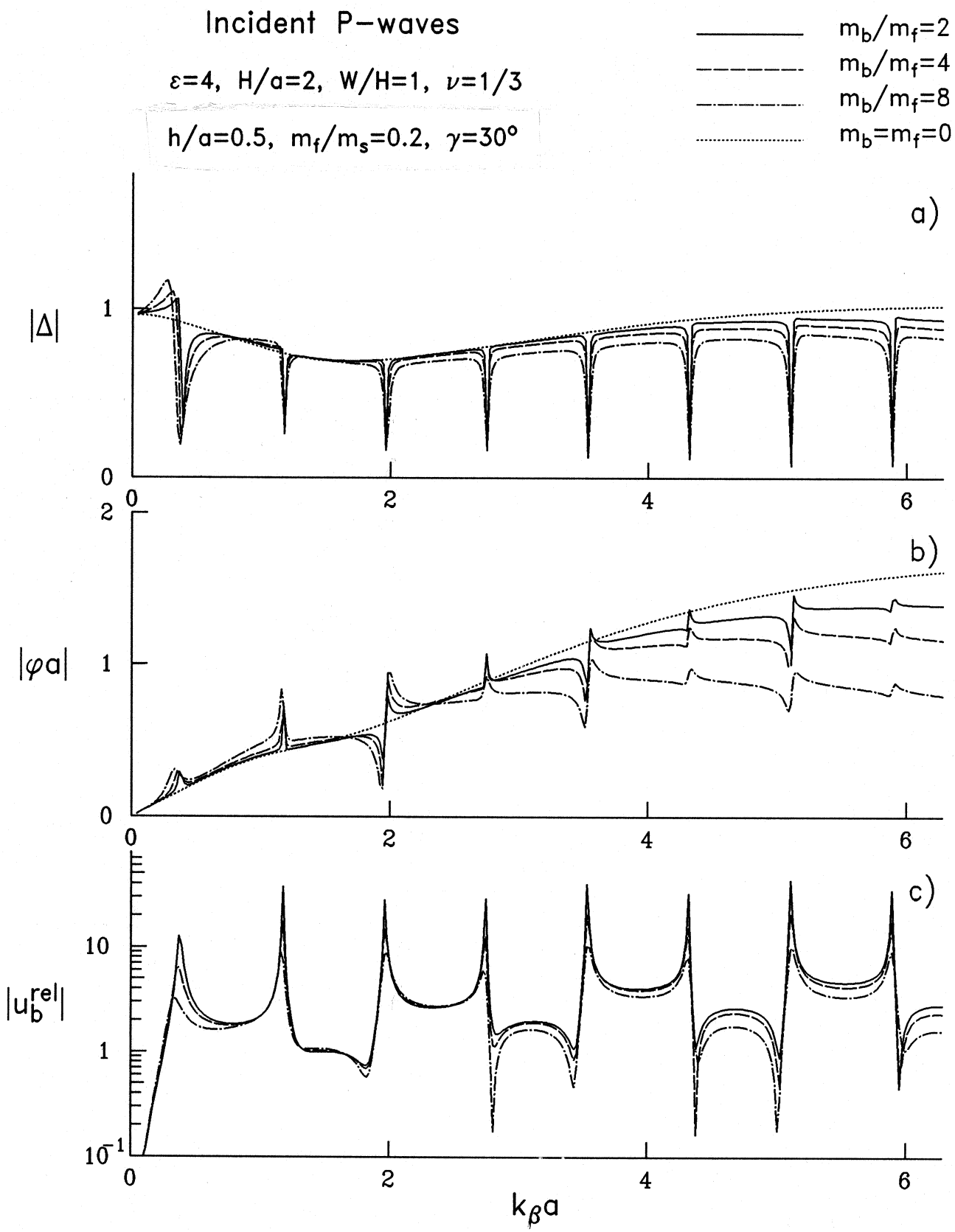

Figure II.23 a), b) and c)

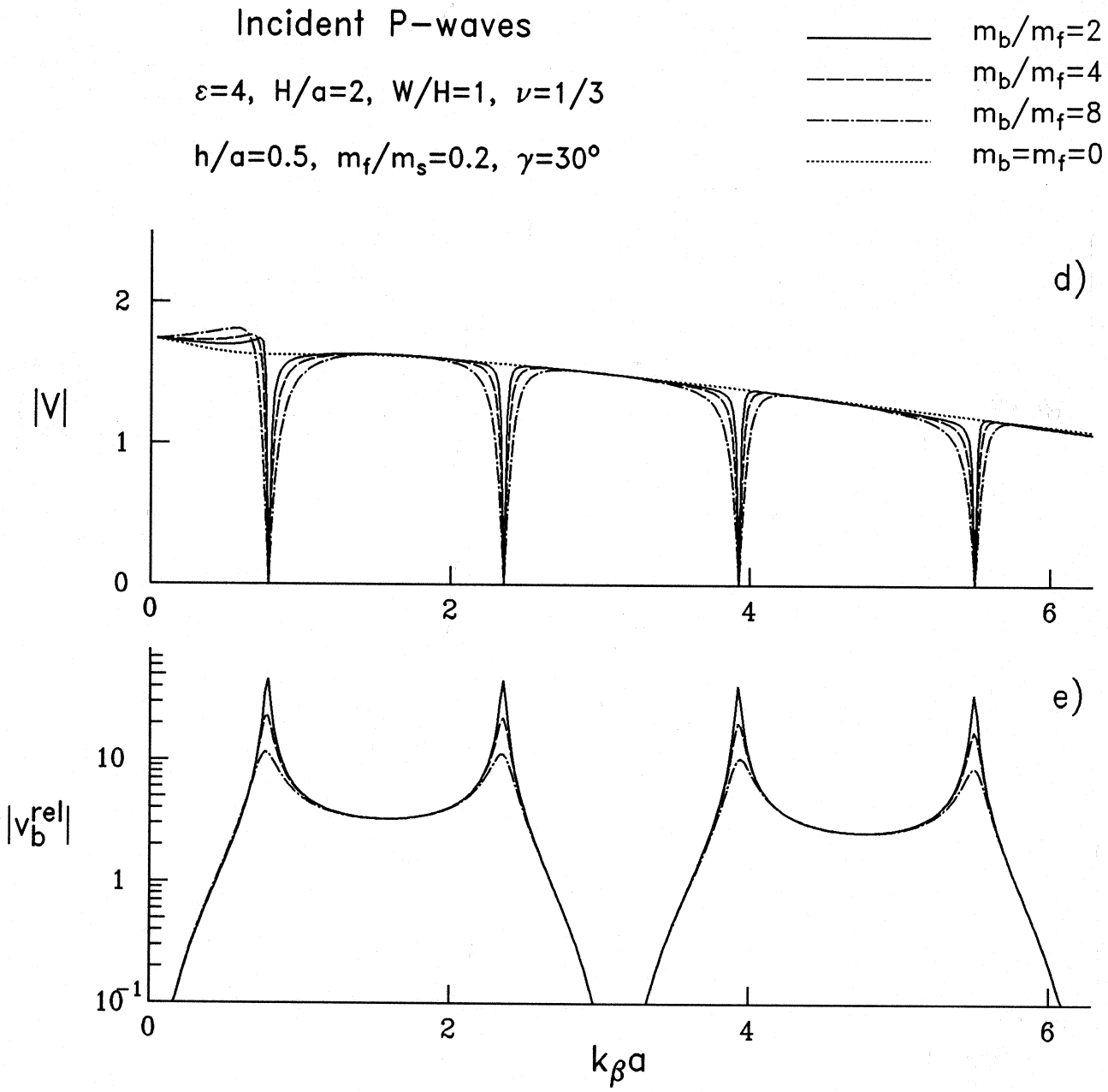

Figure II.23 d) and e)

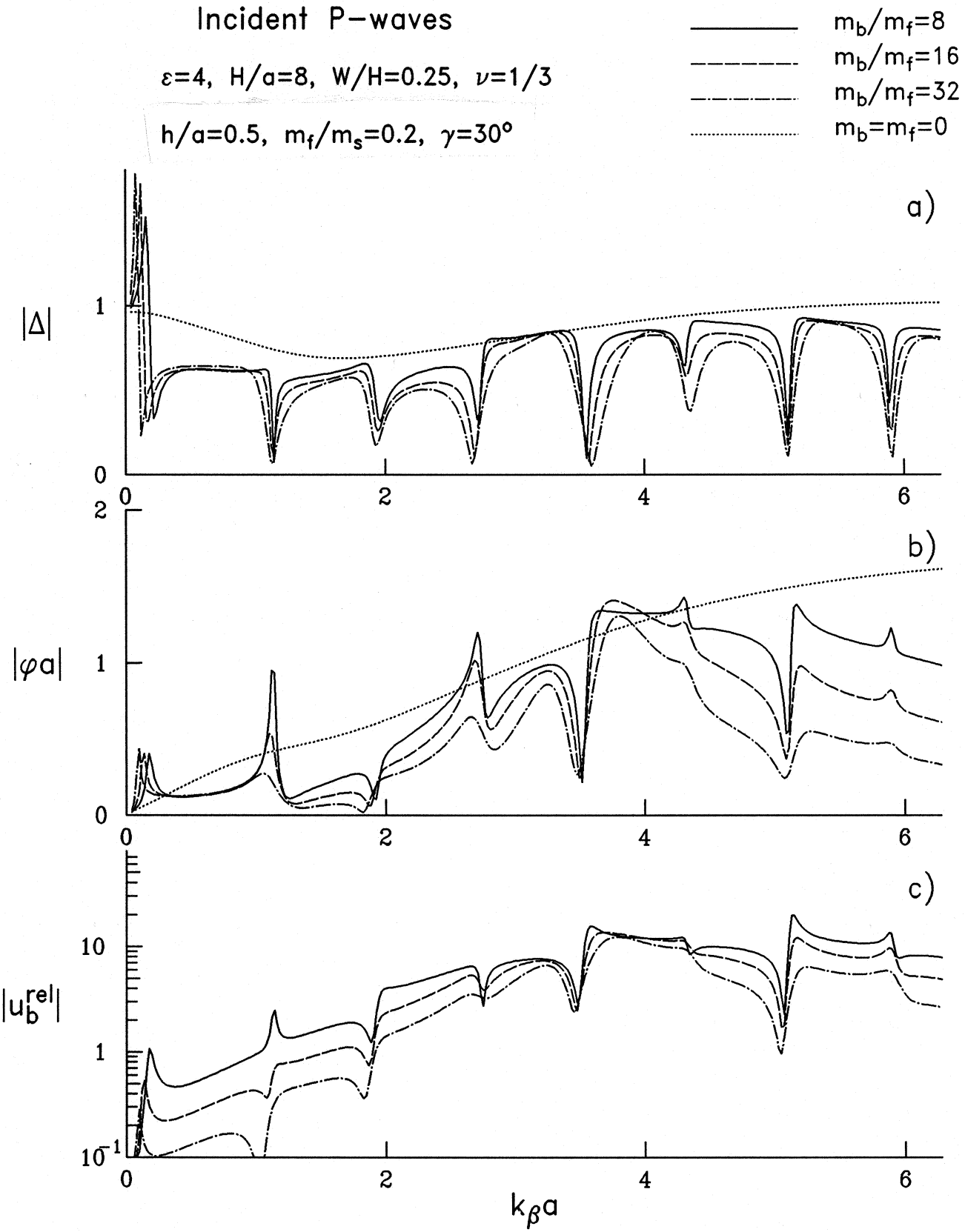

Figure II.24 a), b) and c)

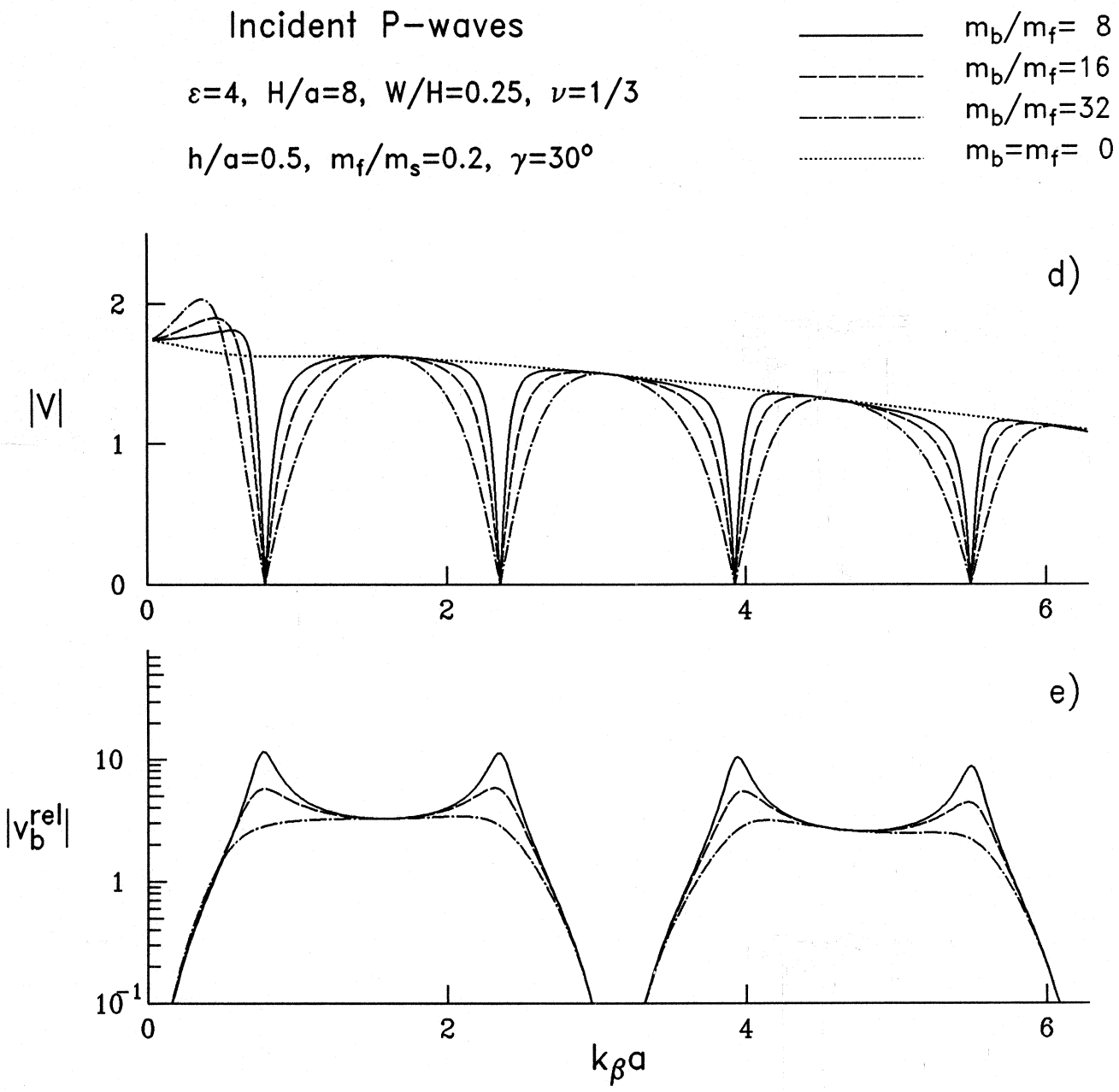

Figure II.24 d) and e)

for $\gamma = 30°$ and $m_f/m_s = 1$, 2, 4 and 0.2. In Fig. II.19, the amplitudes of the transfer functions of the base motion of a rigid building are shown for $\gamma = 30°$ ($\varepsilon = 0$, $H/a = 2$, $W/H = 1$, $m_f/m_s = 0.2$) and for $m_b/m_f = 2$, 4 and 8. In Fig. II.20, the transfer functions of the building base and building relative responses are shown for a flexible building ($\varepsilon = 4$, $m_f/m_s = 0.2$, $m_b/m_f = 4$, $H/a = 2$, $W/H = 1$), for incident angles $\gamma = 0°$, 30°, 60° and 85°. In Fig. II.21, the same is shown, for the same incident angles, but for a taller building ($m_b/m_f = 16$, $H/a = 8$, $W/H = 0.25$, $m_f/m_s = 0.2$ and $\varepsilon = 4$). Fig. II.22, II.23 and II.24 are similar to Fig. II.14, II.15 and II.16. The only difference is in the values of the m_b/m_f, which are twice larger for the shallow foundation, in order to preserve approximately the same value of the mass of the building.

II.2.6.1 Foundation Input Motion

For low frequencies of the incident waves Δ, φ and V do not depend much on the embedment. For higher frequencies, Δ has larger amplitudes and V has smaller amplitudes when the embedment is deeper. For the shallow foundation, in a broader frequency range ($\eta \in (0,2)$ and $\eta \in (0,3)$), $|\varphi a|$ versus $k_\beta a$ is almost a straight line. The rotation amplitudes for low frequencies are larger for a deeper foundation, but for higher frequencies become much bigger for the shallow foundation, especially for $\gamma = 30°$ (two times). So are the rotational amplitudes of the foundation responses when $m_b/m_f = 0$. (Fig. II.18). These effects were anticipated as shown earlier in the discussion (section II.2.2).

II.2.6.2 Building-Soil Interaction

During the building-soil interaction, the soil appears as "softer" if the foundation is shallower. It can be more "easily" deformed by the forces from the building. This can be seen from the larger reduction of the frequency and amplitude of the first peak of the relative horizontal response when the foundation is shallower. In the presented results, for a shallow foundation, the first peaks of $|\Delta|$ and $|\varphi|$ are also smaller. The reduction of the relative response may be because of the larger apparent flexibility of the soil and/or the smaller amplitudes of the foundation driving fores (see section II.2.2). This implies that neglecting the depth of the embedment may cause nonconservative estimates for the forces in the building, and also for the base rotation, whose large amplitudes may cause failure of the soil surrounding the foundation. For higher frequencies, the base rotation has larger amplitudes when the foundation is shallow. Also the relative building response u_b^{rel} is larger. This may be because of the larger base rotation of the foundation input motion. This is especially so far the examples with $\gamma = 30°$ and 60°.

The amplitudes of the vertical foundation motion and of v_b^{rel} are in general larger when the foundation is shallow, because the vertical component of the foundation input motion is, then, larger (which is related to the filtering effect of the foundation as discussed earlier).

CHAPTER III

SOIL-STRUCTURE INTERACTION FOR INCIDENT PLANE SV-WAVES

III.1 The Model

In this chapter, the response of the model in Fig. II.1 to incident plane SV-waves will be analyzed.

III.1.1 The Free-field Motion

Let the incident plane SV wave have unit potential with the following representation

$$\psi^i = \exp[ik_\beta(x\sin\theta_\beta - z\cos\theta_\beta) - i\omega t] \qquad (III.1)$$

where ω is the circular frequency, $k_\beta = \omega/\beta$ is the wave number of the shear waves in the half-space and $i = \sqrt{-1}$. As it reflects from the surface of a stress-free half-space, two other waves are generated: another plane SV-wave with angle of reflection $\theta_\beta = \gamma$ and a P-wave with angle of reflection θ_α (which can be real or complex, depending on the value of the incident angle γ). As in Todorovska and Lee (1990,1991), those two waves have potentials ψ^r and ϕ^r, respectively, with the following mathematical representations

$$\phi^r = K_1 \exp[ik_\alpha(x\sin\theta_\alpha + z\cos\theta_\alpha) - i\omega t] \qquad (III.2)$$

$$\psi^r = K_2 \exp[ik_\beta(x\sin\theta_\beta + z\cos\theta_\beta) - i\omega t] \qquad (III.3)$$

where $k_\alpha = \omega/\alpha$ is the wave number of the P-waves in the half-space. The reflection coefficients are

$$K_1 = \frac{-2(\alpha/\beta)^2 \sin 2\theta_\beta \cos 2\theta_\beta}{\sin 2\theta_\alpha \sin 2\theta_\beta + (\alpha/\beta)^2 \cos^2 2\theta_\beta}, \qquad (III.4a)$$

$$K_2 = \frac{\sin 2\theta_\alpha \sin 2\theta_\beta - (\alpha/\beta)^2 \cos^2 2\theta_\beta}{\sin 2\theta_\alpha \sin 2\theta_\beta + (\alpha/\beta)^2 \cos^2 2\theta_\beta} \qquad (III.4b)$$

where θ_α and θ_β are related by the Snell's law

$$\frac{\sin\theta_\alpha}{\alpha_s} = \frac{\sin\theta_\beta}{\beta_s} \qquad (III.5)$$

which implies that θ_α is real valued only if $\gamma \le \theta_{\text{crit}}$, where $\theta_{\text{crit}} = \sin^{-1}\left(\frac{\beta}{\alpha}\right)$. When $\gamma > \theta_{\text{crit}}$, θ_α becomes complex

$$\theta_\alpha = \frac{\pi}{2} - i\cosh^{-1}\left(\frac{\alpha}{\beta}\sin\theta_\beta\right)$$

and the reflected P-wave is an inhomogeneous (surface) wave. Then ϕ^r can be written as

$$\phi^r = K_1 \exp[-\gamma_1 z + ikx - i\omega t] \qquad (III.6)$$

where $\gamma_1 = \sqrt{k^2 - k_\alpha^2}$ is a real valued quantity and $k = k_\alpha \sin\theta_\alpha = k_\beta \sin\theta_\beta > k_\alpha$ is the horizontal wave number of the incident and of the reflected waves.

III.1.2 Displacements and Forces in the Half-space and Dynamic Equilibrium of the Foundation

III.1.2.1 Incidence Below Critical Angle

For incidence below critical angle, all the equations for the displacements and forces are essentially the same as for incident P-waves except that the free-field potentials now are

$$\phi^r(r_1, \theta_1) = \sum_{n=0}^{\infty} J_n(k_\alpha r_1) \left(A_{0,n} \cos n\theta_1 + B_{0,n} \sin n\theta_1\right) \exp\left(-i\omega t\right) \qquad (III.7)$$

and

$$\psi^{i+r}(r_1, \theta_1) = \sum_{n=0}^{\infty} J_n(k_\beta r_1) \left(C_{0,n} \sin n\theta_1 + D_{0,n} \cos n\theta_1\right) \exp\left(-i\omega t\right) \qquad (III.8)$$

with

$$A_{0,n} = \epsilon_n i^n \cos n\theta_\alpha \left((-1)^n e^{ik_\alpha d \cos\theta_\alpha} + K_1 e^{-ik_\alpha d \cos\theta_\alpha}\right) \qquad (III.9a)$$

$$B_{0,n} = \epsilon_n i^n \sin n\theta_\alpha \left(-(-1)^n e^{ik_\alpha d \cos\theta_\alpha} + K_1 e^{-ik_\alpha d \cos\theta_\alpha}\right) \qquad (III.9b)$$

$$C_{0,n} = \epsilon_n K_2 e^{-ik_\beta d \cos\theta_\beta} i^n \sin n\theta_\beta \qquad (III.10a)$$

$$D_{0,n} = \epsilon_n K_2 e^{-ik_\beta d \cos\theta_\beta} i^n \cos n\theta_\beta \qquad (III.10b)$$

where $\epsilon_0 = 1$ and $\epsilon_n = 2$ for $n \geq 1$. (Lee and Cao 1989). Therefore, only the case of incidence beyond critical angle will be considered in the further discussion.

III.1.2.2 Incidence Beyond Critical Angle

For incidence beyond critical angle, when θ_α is complex, the series in equation (III.7) diverges and some other form of expansion of the displacements and the stresses, that the P-potential produces along the arc $r_1 = b$, $-\theta_0 \leq \theta_1 \leq \theta_0$, is required. The method used in this work is a modification of the method used by Lee and Cao (1989) in their paper on scattering of plane SV-waves from shallow circular canyons. They expanded ϕ^r along $r_1 = b$ in finite Fourier series of θ_1 with period 2π. In the calculation of the coefficients of those series they assigned the value 0 to ϕ^r in the region above the half-space. (Note that by eq. (III.6), along $r_1 = b$, ϕ^r grows very fast as $\theta_1 = \pm\pi$ and may take values that cause overflow in the computer memory.) They assumed that the coefficients of this

expansion must be products of some constant coefficients and $J_n(k_\alpha b)$, since the radial part of the potential ϕ^r must satisfy the Bessel differential equation and can have only the Bessel J_n functions as solution. Those constant coefficients were the coefficients of the Fourier-Bessel series expansion of ϕ^r. Then, they calculated the displacements and stresses by differentiating the series representing the potentials. Because the function that they approximated had jumps at $\theta_1 = \pm\theta_0$, the finite Fourier series could oscillate significantly about the exact function in the neighborhood of the boundary points. Those oscillations propagated through the whole region $0 \leq \theta \leq 2\pi$, and therefore the amplitudes and the derivatives of the series did not represent very accurately the amplitudes and the derivatives of the actual potential. The amplitudes of these oscillations became larger for shorter wavelengths of the incident wave.

To overcome this disadvantage, in this work a modified version of the method of Lee and Cao is used. The displacements and the stresses at $r_1 = b$ are first calculated directly by differentiating the expression for ϕ^r as a function or r_1 and θ_1, and then those are expanded in finite Fourier series of θ_1. In polar coordinates $\phi^r(r_1, \theta_1)$ is

$$\phi^r = K_1 \exp[-ik_\alpha d \cos\theta_\alpha + ik_\alpha r_1 \cos(\theta_1 - \theta_\alpha) - i\omega t] \qquad (III.11)$$

If $u^\phi_{r_1}, u^\phi_{\theta_1}, \tau^\phi_{r_1 r_1}$ and $\tau^\phi_{r_1\theta_1}$ are the displacements and the stresses induced by ϕ^r only, then

$$u^\phi_{r_1}(r_1, \theta_1) = \frac{\partial \phi}{\partial r_1} \qquad (III.12a)$$

$$u^\phi_{\theta_1}(r_1, \theta_1) = \frac{1}{r}\frac{\partial \phi}{\partial \theta_1} \qquad (III.12b)$$

$$\tau^\phi_{r_1 r_1}(r_1, \theta_1) = \lambda\left(\frac{\partial u^\phi_{r_1}}{\partial r_1} + \frac{u^\phi_{r_1}}{r_1} + \frac{1}{r}\frac{\partial u^\phi_{\theta_1}}{\partial \theta_1}\right) + 2\mu\frac{\partial u^\phi_{r_1}}{\partial r_1} \qquad (III.13a)$$

and

$$\tau^\phi_{r_1\theta_1}(r_1, \theta_1) = \mu\left(\frac{\partial u^\phi_{\theta_1}}{\partial r_1} - \frac{u^\phi_{\theta_1}}{r_1} + \frac{1}{r_1}\frac{\partial u^\phi_{r_1}}{\partial \theta_1}\right). \qquad (III.13b)$$

This implies

$$u^\phi_{r_1}(b, \theta_1) = \frac{1}{b}K_1 ik_\alpha b \cos(\theta_1 - \theta_\alpha) \exp[\gamma d + ik_\alpha b \cos(\theta_1 - \theta_\alpha) - i\omega t] \qquad (III.14a)$$

$$u^\phi_{\theta_1}(b, \theta_1) = -\frac{1}{b}K_1 ik_\alpha b \sin(\theta_1 - \theta_\alpha) \exp[\gamma d + ik_\alpha b \cos(\theta_1 - \theta_\alpha) - i\omega t] \qquad (III.14b)$$

$$\tau^\phi_{r_1 r_1}(b, \theta_1) = -\frac{2\mu}{b^2}K_1(k_\alpha b)^2\left[\frac{1}{2}\left(\frac{\alpha}{\beta}\right)^2 - \sin^2(\theta_1 - \theta_\alpha)\right] \exp[\gamma d + ik_\alpha b \cos(\theta_1 - \theta_\alpha) - i\omega t] \qquad (III.15a)$$

and

$$\tau^{\phi}_{r_1\theta_1}(b,\theta_1) = -\frac{2\mu}{b^2}K_1(k_\alpha b)^2\sin(\theta_1-\theta_\alpha)\cos(\theta_1-\theta_\alpha)\exp[\gamma d + ik_\alpha b\cos(\theta_1-\theta_\alpha) - i\omega t]. \tag{III.15b}$$

Then, one can search for analytical extensions, in the region above the half-space, that would satisfy the following conditions: (1) have comparable amplitudes everywhere in the interval $[0,2\pi]$, (2) be continuous and have continuous slope at $\theta_1 = +\theta_0$ and at $\theta_1 = 2\pi - \theta_0$, and (3) be also continuous at $\theta_1 = \pi$. Let the function to be extended be denoted by $f(\theta)$. Then the extension was constructed by the following steps:

1. to satisfy condition (1), in the region $\theta \in [\theta_0, \pi]$ f was extended symmetrically about $\theta_1 = +\theta_0$, and in the region $\theta \in (\pi, 2\pi - \theta_0)$ symmetrically about $\theta_1 = 2\pi - \theta_0$;

2. to satisfy condition (2), the function constructed in step 1. was set to be $f(\theta_1) = 2f(\theta_0) - f(\theta_1)$ in the region $\theta \in [\theta_0, \pi]$, and $f(\theta_1) = 2f(2\pi - \theta_0) - f(\theta_1)$ in the region $\theta \in (\pi, 2\pi - \theta_0)$;

3. condition (3) is automatically satisfied by the real parts of u_{r_1} and $\tau_{r_1 r_1}$ and the imaginary parts of u_{θ_1} and $\tau_{r_1\theta_1}$, which are symmetric about $\theta_1 = 0$. The imaginary parts of u_{r_1} and $\tau_{r_1 r_1}$ and the real parts of u_{θ_1} and $\tau_{r_1\theta_1}$, which are antisymmetric about $\theta_1 = 0$, were forced to satisfy this requirement, and without violating the first two requirements, by multiplication of the function constructed in step 2. by $\cos(\theta_1 - \pi/2)$, in the region $\theta \in [\theta_0, \pi]$, and by $-\cos(\theta_1 - \pi/2)$ in the interval $\theta \in [\theta_0, \pi]$.

Under those conditions the corresponding finite Fourier series closely represented the free-field motion everywhere along the canyon walls.

The finite Fourier series, representing those displacements and stresses, at $r_1 = b$ are

$$u^*_{r_1}(b,\theta_1) = \frac{1}{b}\sum_{n=0}^{N}(A^{u_r}_{0,n}\cos n\theta_1 + B^{u_r}_{0,n}\sin n\theta_1)\exp(-i\omega t) \tag{III.16a}$$

$$u^*_{\theta_1}(b,\theta_1) = \frac{1}{b}\sum_{n=0}^{N}(A^{u_\theta}_{0,n}\sin n\theta_1 + B^{u_\theta}_{0,n}\cos n\theta_1)\exp(-i\omega t) \tag{III.16b}$$

$$\tau^*_{r_1 r_1}(b,\theta_1) = \frac{2\mu}{b^2}\sum_{n=0}^{N}(A^{\tau_r}_{0,n}\cos n\theta_1 + B^{\tau_r}_{0,n}\sin n\theta_1)\exp(-i\omega t) \tag{III.17a}$$

and

$$\tau^*_{r_1\theta_1}(b,\theta_1) = \frac{2\mu}{b^2}\sum_{n=0}^{N}(A^{\tau_\theta}_{0,n}\sin n\theta_1 + B^{\tau_\theta}_{0,n}\cos n\theta_1)\exp(-i\omega t). \tag{III.17b}$$

The coefficients $\{A^{u_r}_{0,n}\}^N_{n=0}$, $\{B^{u_r}_{0,n}\}^N_{n=0}$, $\{A^{u_\theta}_{0,n}\}^N_{n=0}$, $\{B^{u_\theta}_{0,n}\}^N_{n=0}$, $\{A^{\tau_r}_{0,n}\}^N_{n=0}$, $\{B^{\tau_r}_{0,n}\}^N_{n=0}$, $\{A^{\tau_\theta}_{0,n}\}^N_{n=0}$, $\{B^{\tau_\theta}_{0,n}\}^N_{n=0}$ can be calculated as in Hamming (1962) or as in Lee and Cao

(1989). This does not require any numerical integration, but only straightforward application of available formulae.

In the following discussion, only the expressions related to the displacements and the forces in the half-space that are different when $\gamma > \gamma_{crit}$, will be mentioned. The new expressions, relating the coefficients of the scattered waves with the displacements of the free-field motion and the components of the rigid body motion of the foundation, are

$$\left\{ \begin{array}{c} \vdots \\ \left\{ \begin{array}{c} A_{1,n} \\ C_{1,n} \end{array} \right\} \\ \vdots \end{array} \right\} = [W^+]^{-1} \left\{ \begin{array}{c} \vdots \\ \left\{ \begin{array}{c} A^u_{0,n} \\ C^u_{0,n} \end{array} \right\} \\ \vdots \end{array} \right\} - b[X^+] \left\{ \begin{array}{c} V_0 \\ \Delta_0 \\ \varphi_0 H \end{array} \right\} \qquad (III.18a)$$

$$\left\{ \begin{array}{c} \vdots \\ \left\{ \begin{array}{c} B_{1,n} \\ D_{1,n} \end{array} \right\} \\ \vdots \end{array} \right\} = [W^-]^{-1} \left\{ \begin{array}{c} \vdots \\ \left\{ \begin{array}{c} B^u_{0,n} \\ D^u_{0,n} \end{array} \right\} \\ \vdots \end{array} \right\} - b[X^-] \left\{ \begin{array}{c} V_0 \\ \Delta_0 \\ \varphi_0 H \end{array} \right\} \qquad (III.18b)$$

where

$$\left\{ \begin{array}{c} A^u_{0,n} \\ C^u_{0,n} \end{array} \right\} = \left\{ \begin{array}{c} A^{u_r}_{0,n} + \mathcal{D}^{(1)}_{12}(n,b) C_{0,n} \\ A^{u_\theta}_{0,n} + \mathcal{D}^{(1)}_{22}(n,b) C_{0,n} \end{array} \right\} \qquad (III.19a)$$

and

$$\left\{ \begin{array}{c} B^u_{0,n} \\ D^u_{0,n} \end{array} \right\} = \left\{ \begin{array}{c} B^{u_r}_{0,n} + \mathcal{D}^{(1)}_{12}(n,b) D_{0,n} \\ B^{u_\theta}_{0,n} + \mathcal{D}^{(1)}_{22}(n,b) D_{0,n} \end{array} \right\}. \qquad (III.19b)$$

The coefficients on the left-hand-side of eqs. (III.19) a and b are the coefficients of the Fourier series in θ_1 of the total free-field displacement at $r_1 = b$. $A_{0,n}$, $B_{0,n}$, $C_{0,n}$ and $D_{0,n}$ are as in eq. (III.10) a and b, and the matrices $[W^+]$, $[W^-]$, $[X^+]$ and $[X^-]$, and the coefficients $\mathcal{D}^{(1)}_{ij}$, i,j =1, 2, are as in eq. (II.21). The new expression for the generalized

force vector $\{F_0^{(s)}\}$ of the foundation driving forces is then

$$\begin{aligned}\left\{F_0^{(s)}\right\} = &\left[\frac{2\mu}{b}\left[\cdots\left[\tilde{L}^+(n)\right]_{3\times 2}\cdots\right]\right.\left\{\begin{array}{c}\vdots\\ \left\{\begin{array}{c}A^\tau_{0,n}\\ C^\tau_{0,n}\end{array}\right\}\\ \vdots\end{array}\right\}\\ &+\frac{2\mu}{b}\left[\cdots\left[\tilde{L}^+(n)\right]_{3\times 2}\cdots\right]\left\{\begin{array}{c}\vdots\\ \left\{\begin{array}{c}B^\tau_{0,n}\\ D^\tau_{0,n}\end{array}\right\}\\ \vdots\end{array}\right\}\\ &-\frac{2\mu}{b}[S^+]\left\{\begin{array}{c}\vdots\\ \left\{\begin{array}{c}A^u_{0,n}\\ C^u_{0,n}\end{array}\right\}\\ \vdots\end{array}\right\}\\ &-\frac{2\mu}{b}[S^+]\left\{\begin{array}{c}\vdots\\ \left\{\begin{array}{c}B^u_{0,n}\\ D^u_{0,n}\end{array}\right\}\\ \vdots\end{array}\right\}e^{-i\omega t}\end{aligned} \qquad (III.20)$$

where

$$[S^\pm] = [T^\pm][W^\pm]^{-1} \qquad (III.21)$$

and where

$$[\tilde{L}(n)^+] = \int_{-\theta_0}^{\theta_0}\begin{bmatrix}\cos\theta_1 & -\sin\theta_1\\ \sin\theta_1 & \cos\theta_1\\ \frac{d}{H}\sin\theta_1 & -\frac{b}{H}+\frac{d}{H}\cos\theta_1\end{bmatrix}\begin{bmatrix}\cos n\theta_1 & \cos n\theta_1\\ \sin n\theta_1 & \sin n\theta_1\end{bmatrix}d\theta_1 \qquad (III.22a)$$

$$[\tilde{L}(n)^-] = \int_{-\theta_0}^{\theta_0}\begin{bmatrix}\cos\theta_1 & -\sin\theta_1\\ \sin\theta_1 & \cos\theta_1\\ \frac{d}{H}\sin\theta_1 & -\frac{b}{H}+\frac{d}{H}\cos\theta_1\end{bmatrix}\begin{bmatrix}\sin n\theta_1 & \sin n\theta_1\\ \cos n\theta_1 & \cos n\theta_1\end{bmatrix}d\theta_1. \qquad (III.22b)$$

After integration

$$[\tilde{L}^+(n)] = \begin{bmatrix}I_1 & -I_4\\ 0 & 0\\ 0 & 0\end{bmatrix} \qquad (III.23a)$$

and

$$[\tilde{L}(n)^-] = \begin{bmatrix}0 & 0\\ I_4 & I_1\\ \frac{d}{H}I_4 & -\frac{b}{H}I_5+\frac{d}{H}I_1\end{bmatrix} \qquad (III.23b)$$

where I_1, I_4 and I_5 (functions of n) are same as in the analysis for incident P-waves. Also, in eq. (III.20)

$$\left\{ \begin{array}{l} A^{\tau}_{0,n} \\ C^{\tau}_{0,n} \end{array} \right\} = \left\{ \begin{array}{l} A^{\tau_r}_{0,n} + \mathcal{E}^{(1)}_{12}(n,b)C_{0,n} \\ A^{\tau_\theta}_{0,n} + \mathcal{E}^{(1)}_{22}(n,0)C_{o,n} \end{array} \right\} \qquad (III.24a)$$

and

$$\left\{ \begin{array}{l} B^{\tau}_{0,n} \\ D^{\tau}_{0,n} \end{array} \right\} = \left\{ \begin{array}{l} B^{\tau_r}_{0,n} + \mathcal{E}^{(1)-}_{12}(n,b)C_{0,n} \\ B^{\tau_\theta}_{0,n} + \mathcal{E}^{(1)}_{22}(n,0)C_{o,n} \end{array} \right\} \qquad (III.24b)$$

where the coefficients in the left-hand-side are the Fourier coefficients in the expansion of $\tau_{r_1 r_1}$ and $\tau_{r_1 \theta_1}$ of the total far-field motion at $r_1 = b$, and where $\mathcal{E}^{(1)}_{ij}$, $i,j = 1,2$, are the same as in the corresponding P-wave problem. The equilibrium equation for the foundation remains the same as for incident P-waves if the incident SV-wave has unit amplitude potential. If the displacement amplitude of the SV-wave is unity, then the generalized displacement in (II.39b) has to be normalized by $k_\beta b$ instead of by $k_\alpha b$, i.e.

$$\{\Delta\} = \frac{1}{k_\beta b}[K]^{-1}\frac{b}{2\mu}\{F^{(s)}_0\} \qquad (III.25)$$

III.2 Results and Analysis

As in the analysis for incident P-waves, in all of the following examples $\nu = 0.3333$. Also, it is assumed that $W = 2a$ and the effect of the gravity forces is neglected. Essentially the same building models will be analyzed as in Chapter II, first on a semi-cylindrical foundation ($\frac{h}{a} = 1$) and then on a shallow foundation $\frac{h}{a} = 0.5$. In all the following examples the incident SV wave has unit displacement amplitude.

III.2.1 The Foundation Input Motion

The amplitudes of the free-field motion, $|u^{ff}|$ and $|v^{ff}|$, as well as the point rotation φ^{ff} (Trifunac, 1982) depend on the angle of incidence γ and the Poisson's ratio ν. The point rotation is a linear function of ω and of the amplitude of the SV-waves, and, in terms of the variables defined in this chapter,

$$\varphi^{ff} = \frac{i}{2}(1 + K_2)\frac{\omega}{\beta}e^{ik_\beta(x\sin\gamma - z\cos\gamma) - i\omega t}$$

where K_2 is the reflection coefficient as defined in equation (III.4b).

The features of the free-field motion on the half-space surface are summarized in Table III.1. The critical angle for $\nu = 1/3$, exactly, is equal to 30°. Since in our examples $\nu = 0.3333 < 1/3$, γ_{crit} is slightly larger than 30°, ($\gamma_{crit} = 30.0025°$). When $\gamma = \gamma_{crit}$ the reflected P-wave has largest possible amplitude for a given value of the Poisson's ratio,

Table III.1

Free-field motion characteristics on the half-space surface for incident plane SV-wave with unit displacement amplitude and for Poisson ratio $\nu = 0.3333$

γ	$\lvert u^{ff}\rvert$	$\lvert v^{ff}\rvert$	$\lvert K_1\rvert$	$\lvert K_2\rvert$	$\lvert 1+K_2\rvert$	Comments
0°	2	0	0	1	0	No reflected P-wave
30°	3.392	0.042	3.39	0.96	0.04	Reflected P-wave propagates horizontally
45°	0	1.414	0.80	1	2.	No reflected P-wave
60°	0.459	1.124	0.80	1	1.95	Reflected P-wave is inhomogeneous
85°	0.169	0.295	0.34	1	0.59	Reflected P-wave is inhomogeneous

it propagates horizontally, and the incident and the reflected SV-waves have opposite phases (their vertical displacement components cancel each other), and, consequently, there is no vertical component of motion. The incident angle $\gamma = 45°$ is a characteristic angle for SV-wave incidence. Then, $|u^{ff}| = 0$ and there is no reflected P-wave regardless of the value of the Poisson's ratio. When $\gamma > \gamma_{crit}$ the reflected P-wave is inhomogeneous and, then, the reflected P- and SV-waves are, in general, not in phase with the incident wave (K_1 and K_2 are complex). The point rotation is zero both for vertical and for critical angle incidence. For vertical incidence, there is no reflected P-wave. In the table, the amplitude of v^{ff} is not exactly zero at $\gamma = 30°$ because γ_{cirt} is slightly larger than 30°. The point rotation φ^{ff} is zero for vertical incidence and practically equal to zero for $\gamma = 30°$. It is largest when $\gamma = 45°$ and 60°. Then $|1 + K_2| \approx 2$, while for $\gamma = 85°$ it is about four times smaller. The comparison of those values with the largest values of the rotation for incident P-wave with same displacement amplitude, shows that the incident SV-waves can produce much larger point rotations (four times).

In Fig. III.1 a, b and c, the amplitudes of the components of the foundation input motion are shown for five values of the incident angle ($\gamma = 0°, 30°, 45°, 60°$ and 85°) in the frequency domain $\Omega \in (0, 2\pi]$. It can be seen that, as $\Omega \to 0$, $|\Delta| \to |u^{ff}|$, $|V| \to |v^{ff}|$ and $|\varphi a| \to 0$ for all incident angles. As Ω increases, $|\Delta|$ and $|V|$ tend to decrease, in general, and the rotation is non-zero. Exceptions are made by $|\Delta|$ when $\gamma = 45°$ and by $|V|$ when $\gamma = 30°$. Both increase relative to their values for $\Omega \to 0$. Reasons for the decreasing $|\Delta|$ and $|V|$ with increasing frequency are (1) the filtering effect of the embedment and (2) the scattering of the incident waves from the rigid foundation. The reason for the increase of $|\Delta|$ and $|V|$ (when $\gamma = 45°$ and 30°, respectively) is in: (1) the scattering of the waves from the rigid foundation that creates components of motion in those directions and (2)

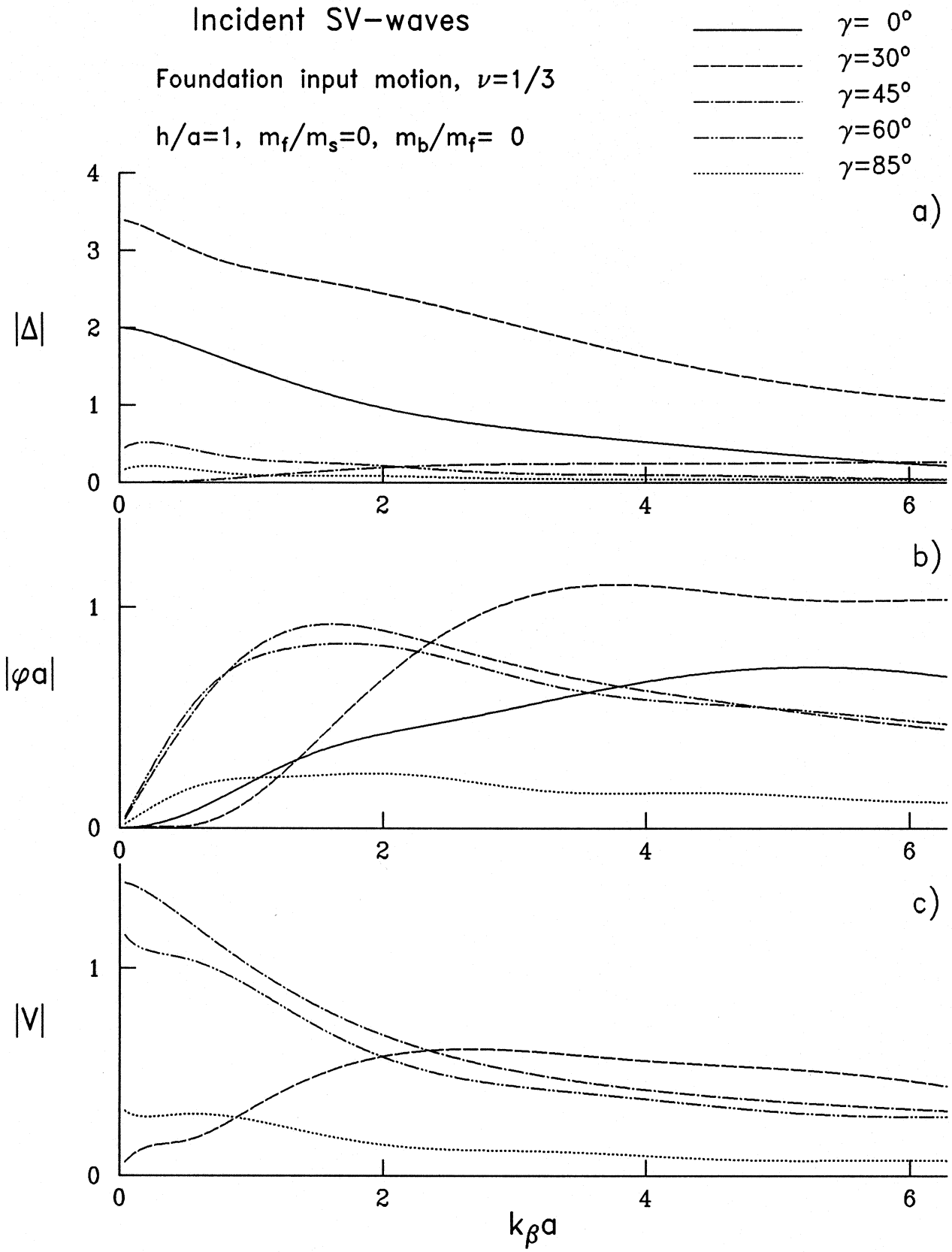
Incident SV−waves
Foundation input motion, ν=1/3
h/a=1, m_f/m_s=0, m_b/m_f= 0
γ= 0°
γ=30°
γ=45°
γ=60°
γ=85°
a)
b)
c)
|Δ|
|φa|
|V|
0
1
2
3
4
6
k_β a

Figure III.1

in the rotation of the foundation about the instantaneous axis of rotation that in general does not pass through O. The rocking amplitudes, in the frequency interval considered, first increase from zero to some maximum value and then start decreasing with increasing frequency.

Several factors influence the rotational amplitudes: (1) the point rotation of the free-field motion, (2) the wave passage effects, and (3) the filtering property of the embedment. This can be explained as follows. The point rotation of the free-field motion plays an important role when the wave length of the incident wave is much longer than the size of the foundation. For example, in Fig. III.1 b, for small frequencies (long wavelengths), the rocking amplitudes are significantly higher for $\gamma = 45°, 60°$ and $85°$ ($\varphi^{ff} \neq 0$) than for $\gamma = 0°$ and $30°$ ($\varphi^{ff} = 0$). For shorter wavelenghts, the effect of this factor is less significant because of the spatial variations in the phases along the contact between the soil and the foundation, as explained in section II.2.3. The wave passage effects due to the embedment play an important role in the rocking of the foundation for wavelengths that are comparable with the size of the foundation, since it enables the incident wave to drive consistently different points on the foundation surface to move in different directions. For example, for $\gamma = 0°$ and $30°$, the rocking response is not zero, even though the point rotation of the free-field motion is zero. When $\gamma = 0$, the free-field motion, which is horizontal, is a standing SV-wave in the vertical direction with an antinode at the surface. If $\eta = 0.5$, then, the bottom point of the foundation is sitting on the first node while the upper part moves horizontally. This tends to rotate the foundation, about it's "bottom point". As η increases the location of the first node is at smaller depth and the axis about which the foundation rotates changes. When $\eta = 1$, the top and the bottom move in opposite directions. A similar situation occurs when $\gamma = 30°$. Than, the SV-wave motion, also horizontal, is practically a standing wave, but with vertical phase velocity different from β. Since then $|v^{ff}| = 0$, the rotation is affected by the difference in phase along the vertical. The scattered waves also contribute to the rotation. When $\gamma = 0$, the scattered waves are also anti-symmetric relative to the axis of symmetry. Their amplitude and effect on the rotation also depend on the incident angle and on the wavelength.

In the frequency domain $\Omega \in (0, 2\pi]$, which is equivalent to $\eta \in (0, 2]$, for a vertically incident SV-wave, the rotation is maximum at about $\eta = 1.7$ ($\varphi a \approx .74$). Then, $a/c_z^\beta T \approx 0.85$ and $2a/c_x^\beta T = 0$. When $\gamma = 30°$, the maximum is at $\eta \approx 1.2$ ($\varphi a \simeq 1.1$). Then, $a/c_z^\beta T \approx 0.43$ and, when $\gamma = 45°$, $60°$ and $85°$ ($\gamma > \gamma_{crit}$), it is near $\eta = 0.5$ ($\varphi a \approx 0.9$, 0.8 and 0.25, respectively). When $\gamma = 60°$ and $45°$ the rocking amplitudes are similar. Then, for $\gamma = 45°$, $2a/c_x^\beta T = 0.36$ and $a/c_z^\beta T \approx 0.18$, and for $\gamma = 60°$, $2a/c_x^\beta T = 0.43$ and $a/c_z^\beta T \approx 0.13$. Then, the difference in the phase of the vertical motion of the corners probably contributes most to the rotation.

In Fig. III.2, the spectra of the phases of the foundation input motion are shown. When $\gamma = 0°$ and $60°$, as $k_\beta a \to 0$, Δ and φ are in phase. As the wavelength of the incident waves decreases, the phase difference between them slowly increases. It appears that when $\gamma = 30°$, as $k_\beta a \to 0$, the phase difference between Δ and φ approaches $\pi/2$. However, since then $|\varphi a|$ and its slope approach zero, this is of no interest for our analysis. To help visualize the rotation, in Fig. III.3 a, b, c, d and e, the displacement amplitudes

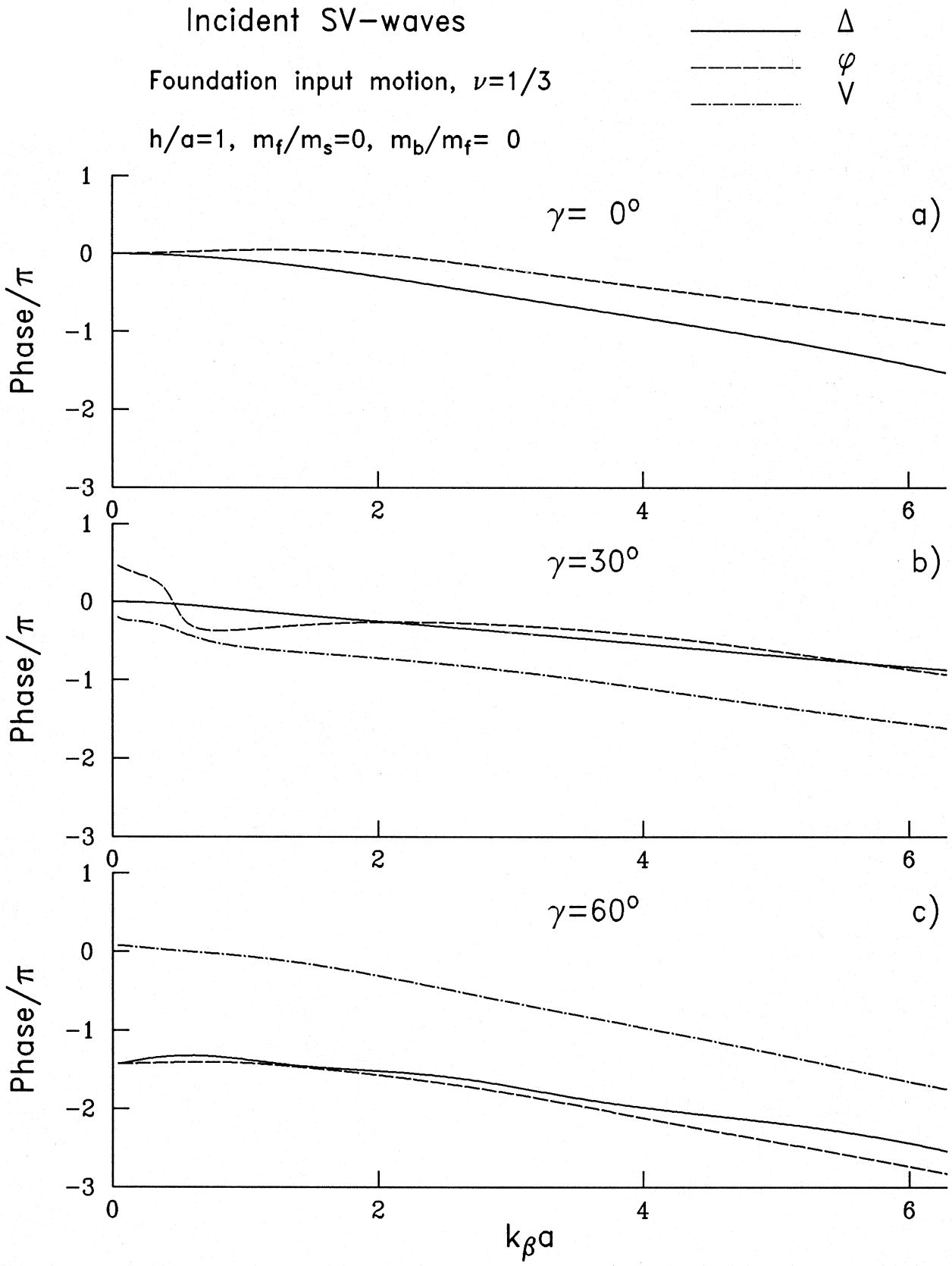
Incident SV−waves
Foundation input motion, ν=1/3
h/a=1, m_f/m_s=0, m_b/m_f= 0
Δ
φ
V
γ= 0°
a)
γ=30°
b)
γ=60°
c)
Phase/π
1
0
−1
−2
−3
0
2
4
6
k_β a

Figure III.2

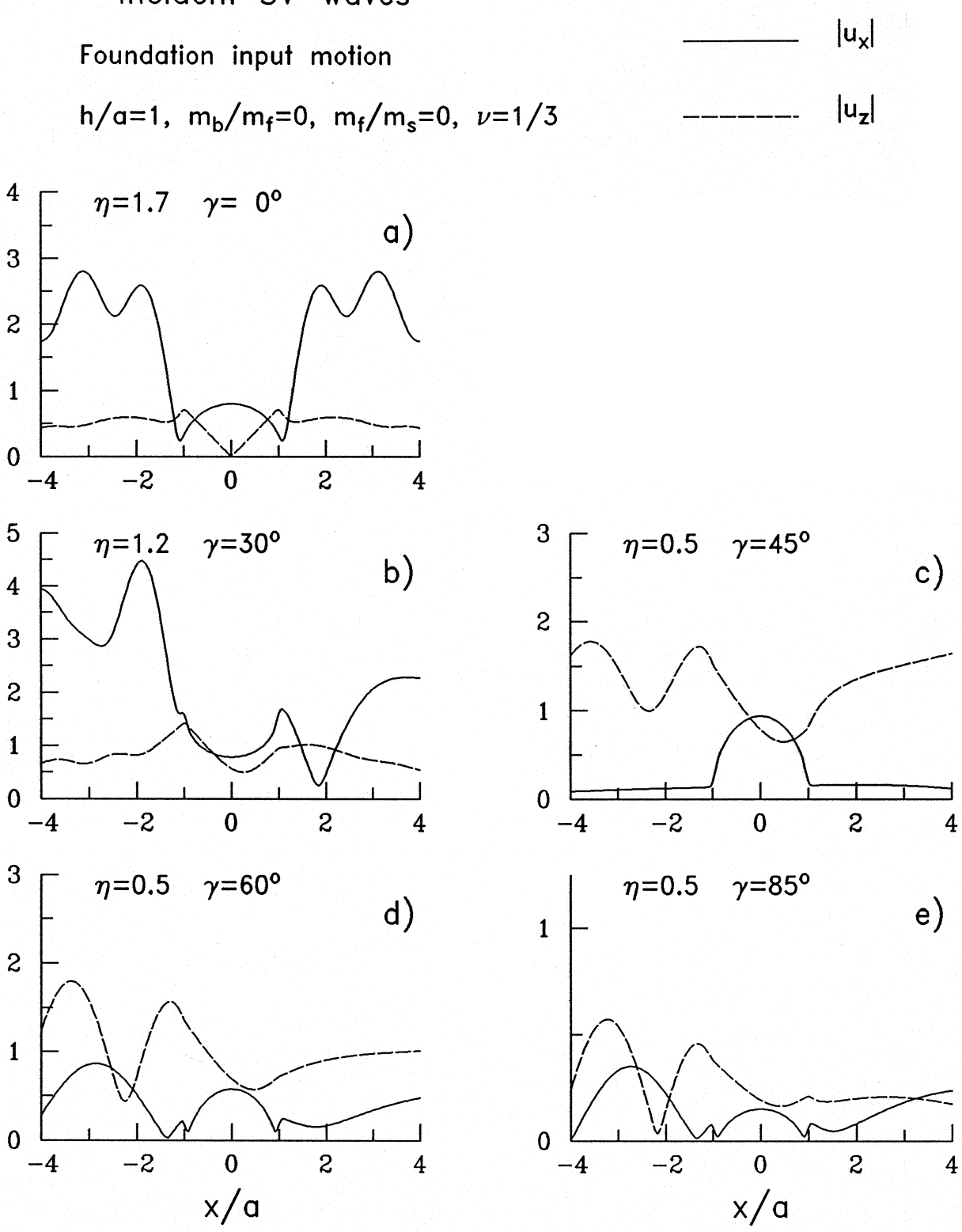
Incident SV-waves
Foundation input motion
h/a=1, m_b/m_f=0, m_f/m_s=0, ν=1/3
$|u_x|$
$|u_z|$
η=1.7 γ= 0° a)
η=1.2 γ=30° b)
η=0.5 γ=45° c)
η=0.5 γ=60° d)
η=0.5 γ=85° e)
x/a
x/a

Figure III.3

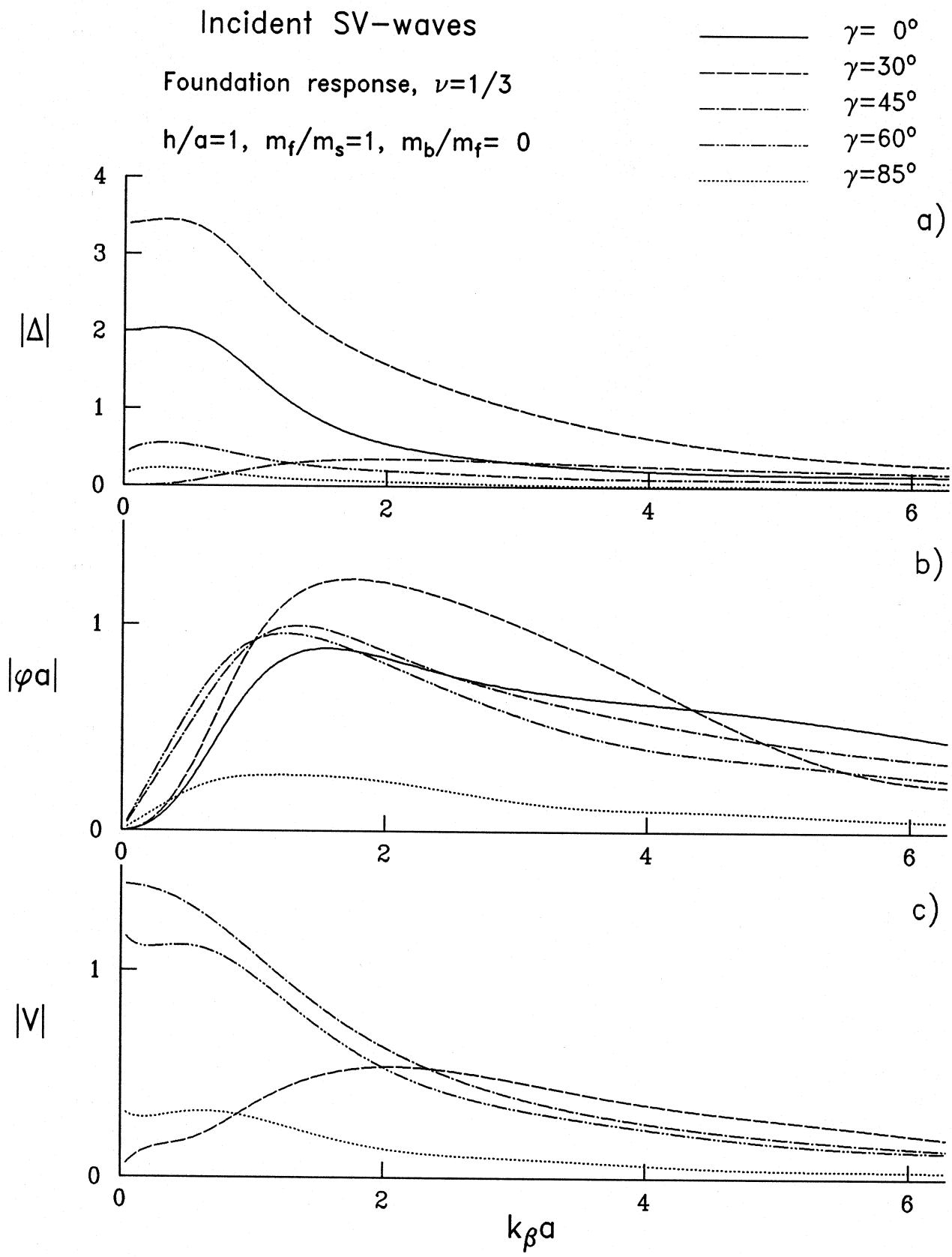
Incident SV−waves
Foundation response, ν=1/3
h/a=1, m_f/m_s=1, m_b/m_f= 0
γ= 0°
γ=30°
γ=45°
γ=60°
γ=85°
a)
b)
c)
|Δ|
|φa|
|V|
k_βa
0
1
2
3
4
6

Figure III.4

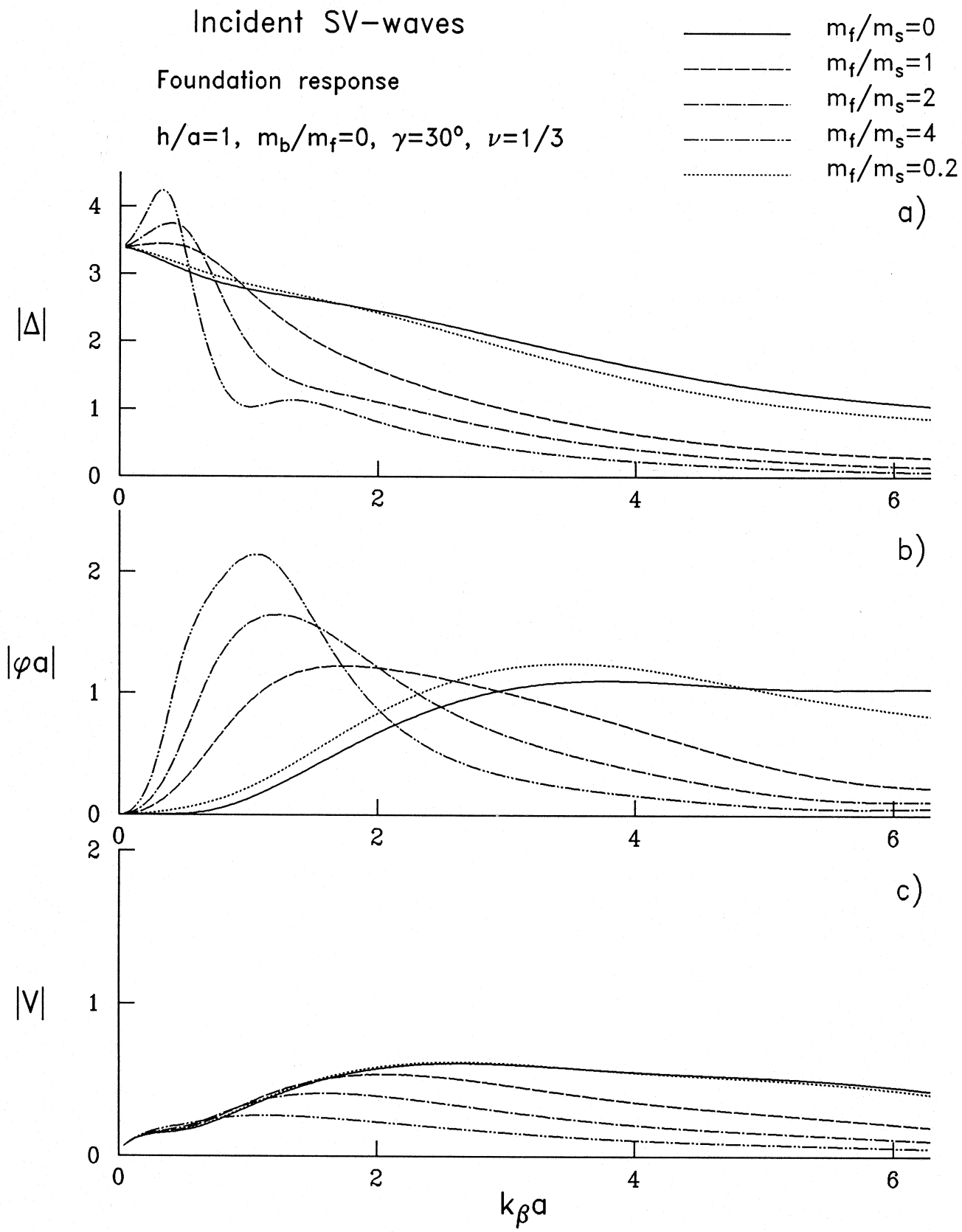
Incident SV−waves
Foundation response
h/a=1, m_b/m_f=0, γ=30°, ν=1/3
m_f/m_s=0
m_f/m_s=1
m_f/m_s=2
m_f/m_s=4
m_f/m_s=0.2
a)
b)
c)
|Δ|
|φa|
|V|
$k_\beta a$
0
1
2
3
4
6

Figure III.5

along the half-space surface and the canyon rim have been plotted, for the five values of the angle of incidence (as in Fig. III.1), and for frequencies at which the rotation is maximum.

III.2.2 Foundation-Soil Interaction

In Fig. III.4 a, b and c the responses $|\Delta|$, $|\varphi|$ and $|V|$ are plotted versus dimensionless frequency for a foundation with foundation-soil mass ratio $\frac{m_f}{m_f} = 1$ ($\frac{m_b}{m_s} = 0$) and for the same values of the incident angle as in Fig. III.1. Similar conclusions can be drawn about those responses, as in the case of incident P-waves, i.e. faster decrease of the response amplitudes for higher frequencies, and a slight increase of $|\Delta|$ and $|V|$ for very low frequencies, relative to the foundation input motion. The rotation amplitudes are significantly higher than for incident P-waves, by a factor of about 2, and have a maximum near $\Omega \approx 1 - 1.5$. Those maxima have higher or comparable values with the maxima of the foundation input rocking amplitudes.

In parts a, b and c of Fig. III.5, $|\Delta|$, $|\varphi_a|$ and $|V|$ are plotted versus dimensionless frequency for $\gamma = 30°$. Different types of lines in these plots correspond to different values of the foundation-soil mass ratio ($\frac{m_f}{m_s} = 0, 1, 2$ and 4). The dependance of the amplitude spectra in these figures on the value of $\frac{m_f}{m_s}$ is similar as in the case of incident P-waves. The peaks, at low frequencies, corresponding to the frequencies of the foundation-soil system can be seen. For higher values of $\frac{m_f}{m_s}$, those peaks are higher, sharper and shifted toward lower frequencies.

III.2.3 Building-Foundation-Soil Interaction

In this section, example cases of interaction of a building on a rigid foundation and the soil will be analyzed for incident SV-waves, as in the corresponding sections of Chapter II.

In the first part, Fig. III.6 through Fig. III.11, the foundation has a semi-cylindrical shape. In the second part, Fig. III.12 through Fig. III.16, similar cases are considered, but when the foundation is shallow ($\frac{h}{a} = 0.5$). In all the examples, $\frac{m_f}{m_s} = 0.2$, $W = 2a$ and the gravity forces are neglected.

In the examples in Fig. III.6, it can be seen how the responses of the foundation and the relative responses of a flexible building ($\varepsilon = 2$, $\frac{m_b}{m_f} = 2$ and $\frac{W}{H} = 1$) depend on the angle of incidence. It can be seen that $|\Delta|$, $|\varphi a|$ and $|u_b^{\text{rel}}|$ are, in general, higher for incident angles for which $|u^{ff}|$ is higher, while $|\Delta|$ and $|v_b^{\text{rel}}|$ are higher for angles of incidence for which $|v^{ff}|$ is higher. The base translation has highest amplitudes when $\gamma = 30°$ ($|u^{ff}| \simeq 3.4$) and lowest amplitudes when $\gamma = 45°$ ($|u^{ff}| = 0$). Since the building is relatively low, back bone curves for $|\Delta|$, $|\varphi|$ and $|V|$ are $|\Delta|$, $|\varphi|$ and $|V|$ of the foundation input motion. At the first three "natural" frequencies, the peaks of $|\varphi|$ are the highest for $\gamma = 30°$. This is the case even for the first peak which is at a frequency at which the rotation of the free-field motion is practically zero. The reason for this is the moment of

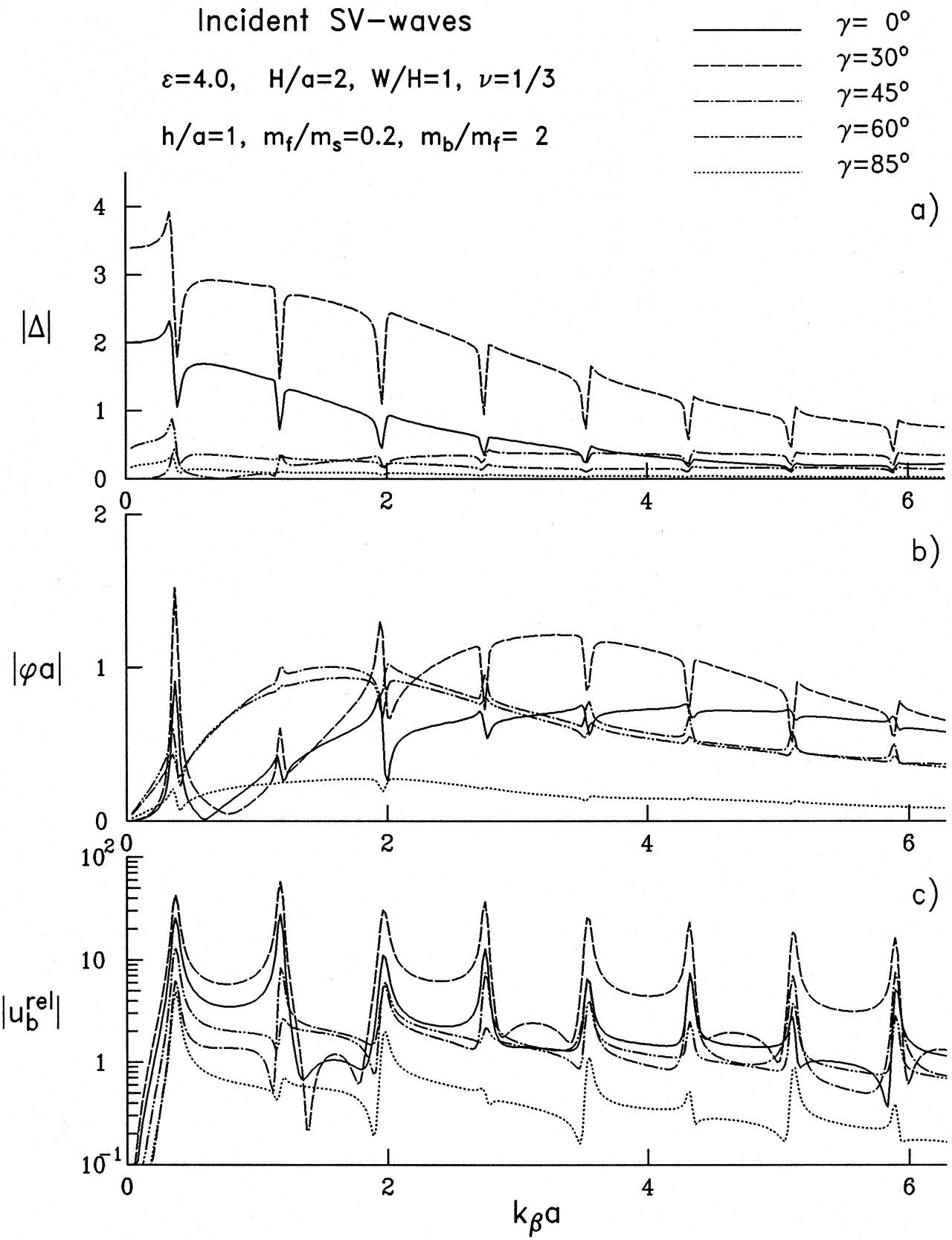

Figure III.6 a), b) and c)

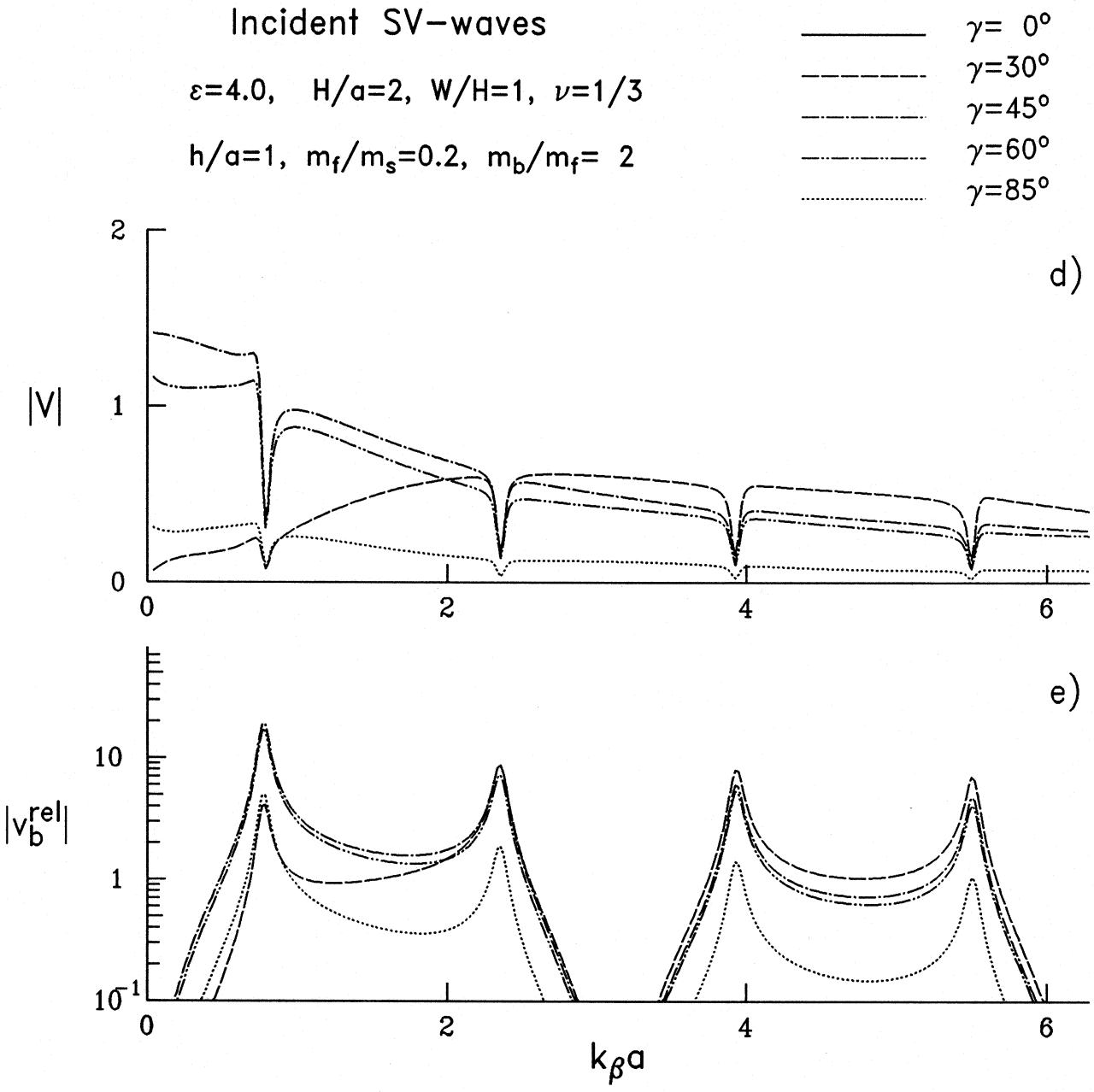

Figure III.6 d) and e)

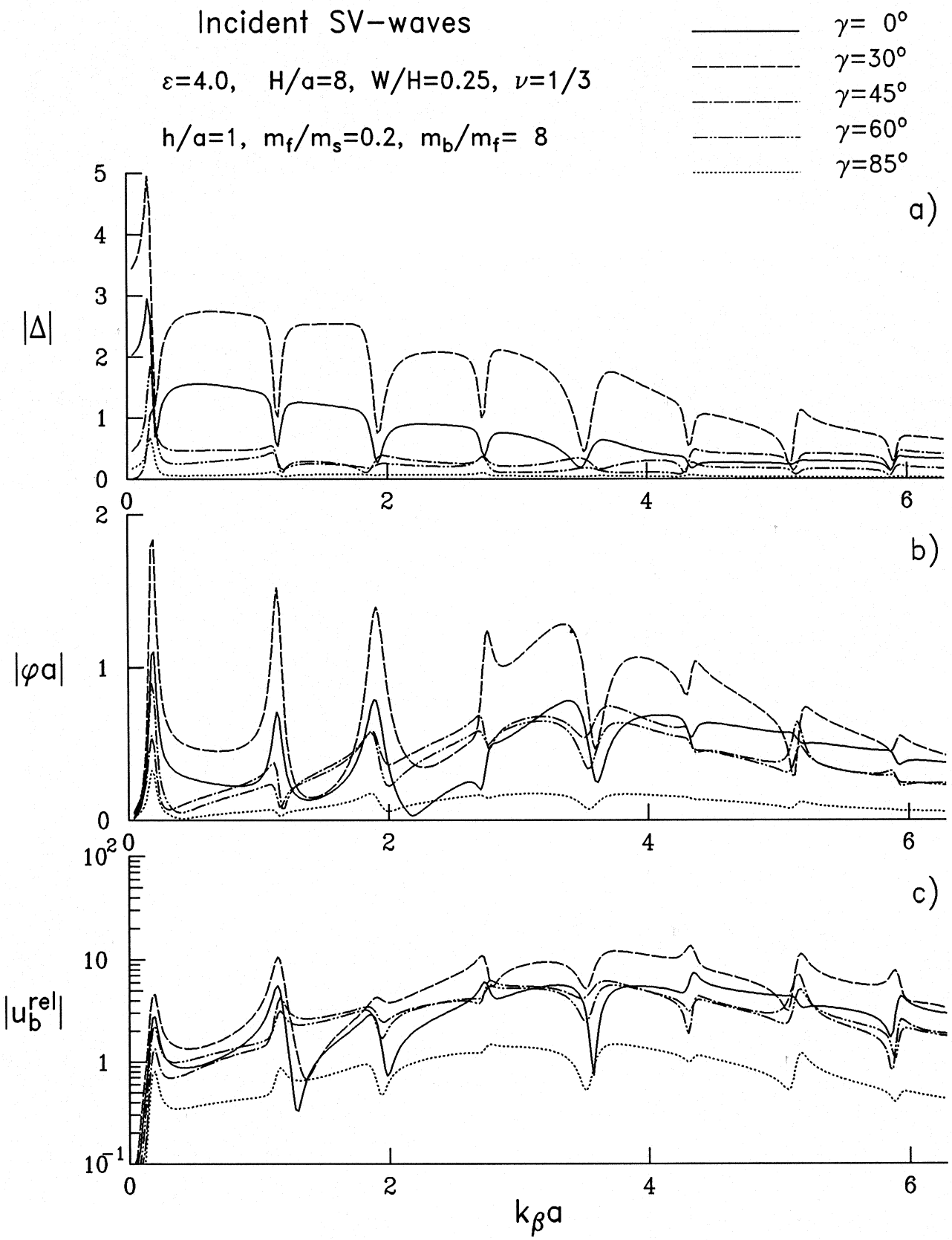

Figure III.7 a), b) and c)

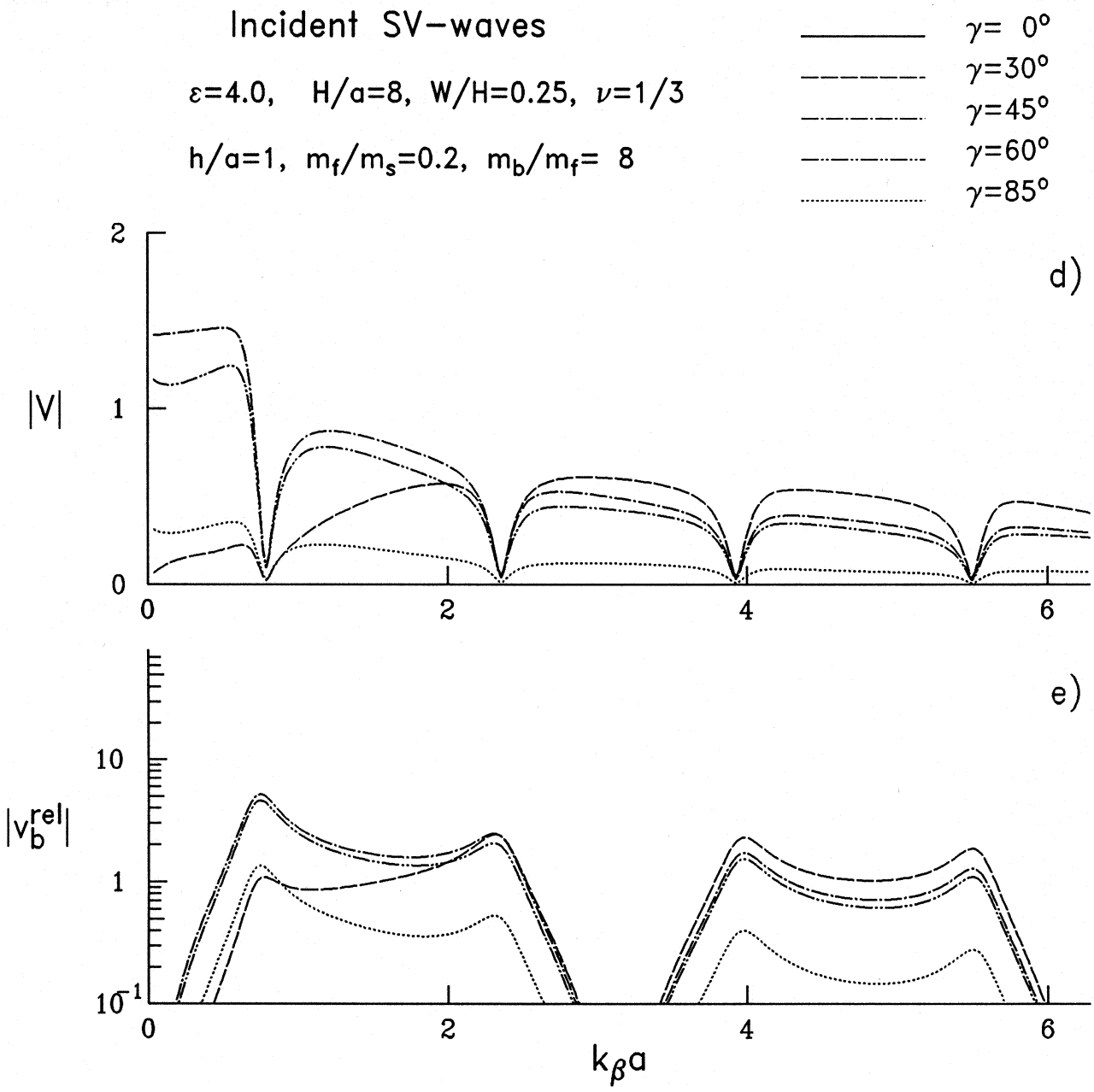

Figure III.7 d) and e)

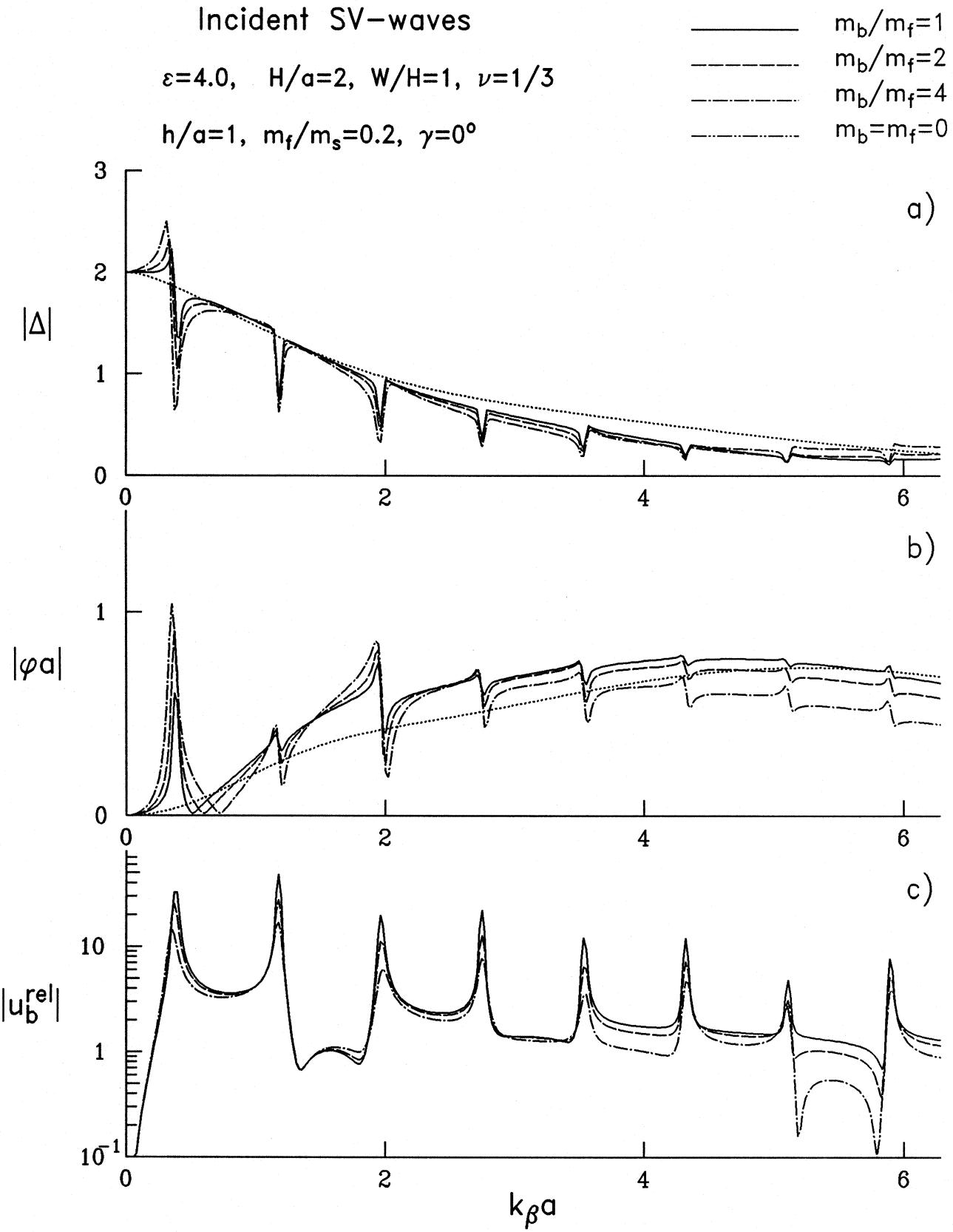
Incident SV−waves
ε=4.0, H/a=2, W/H=1, ν=1/3
h/a=1, m_f/m_s=0.2, γ=0°
m_b/m_f=1
m_b/m_f=2
m_b/m_f=4
m_b=m_f=0
a)
b)
c)
|Δ|
|φa|
|u_b^rel|
k_βa
0
2
4
6
1
3
10
10^-1

Figure III.8

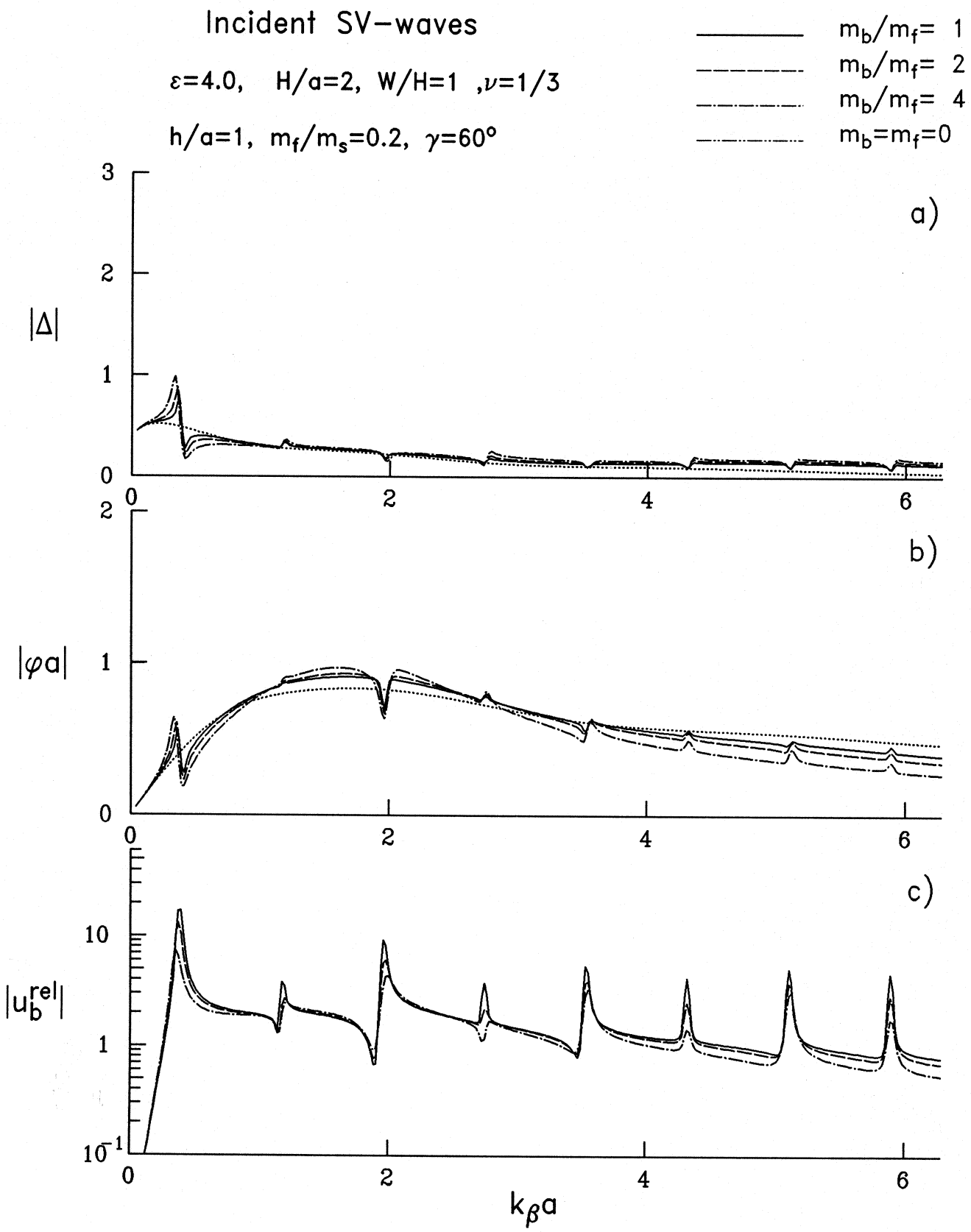

Figure III.9 a), b) and c)

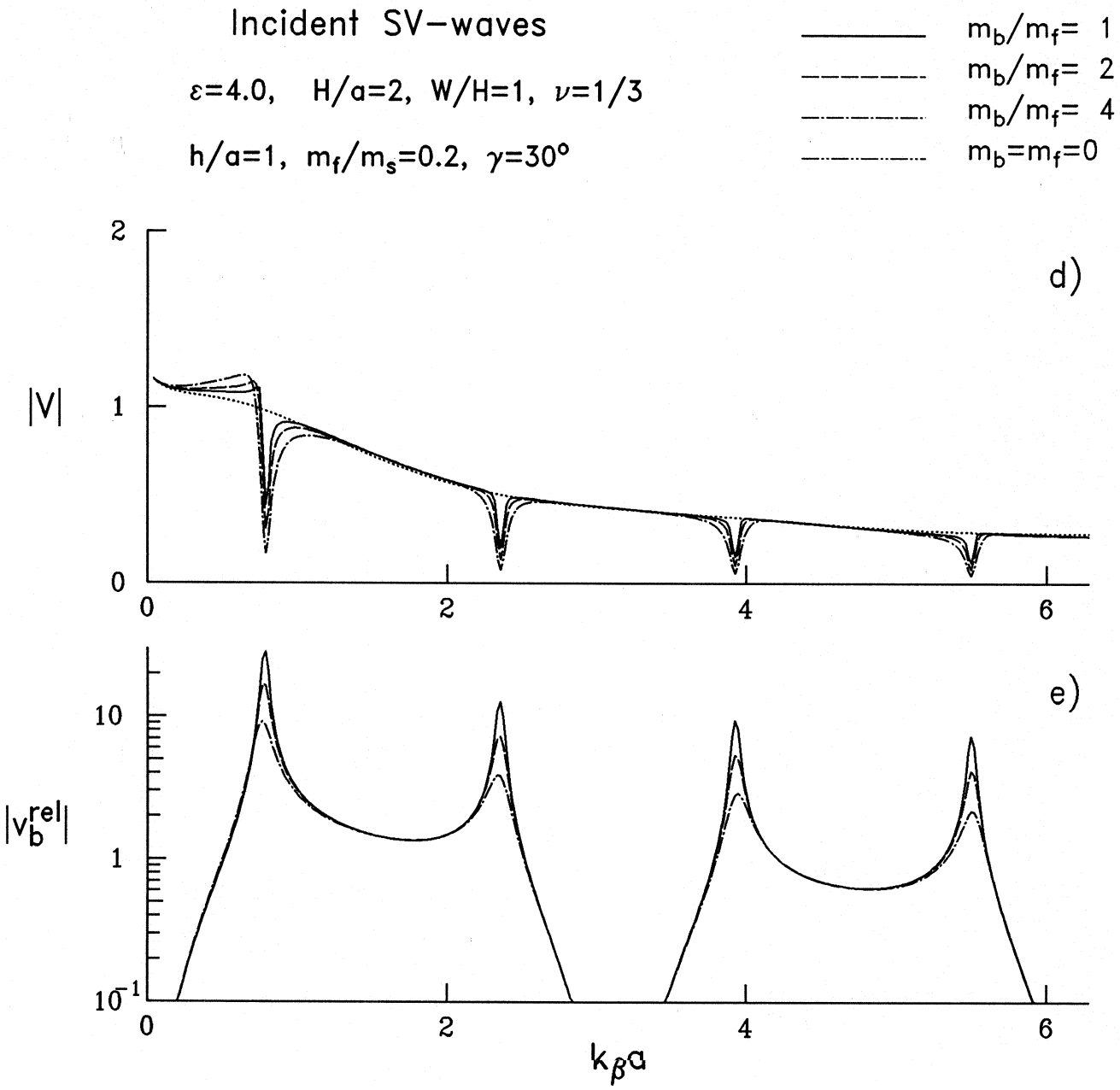

Figure III.9 d) and e)

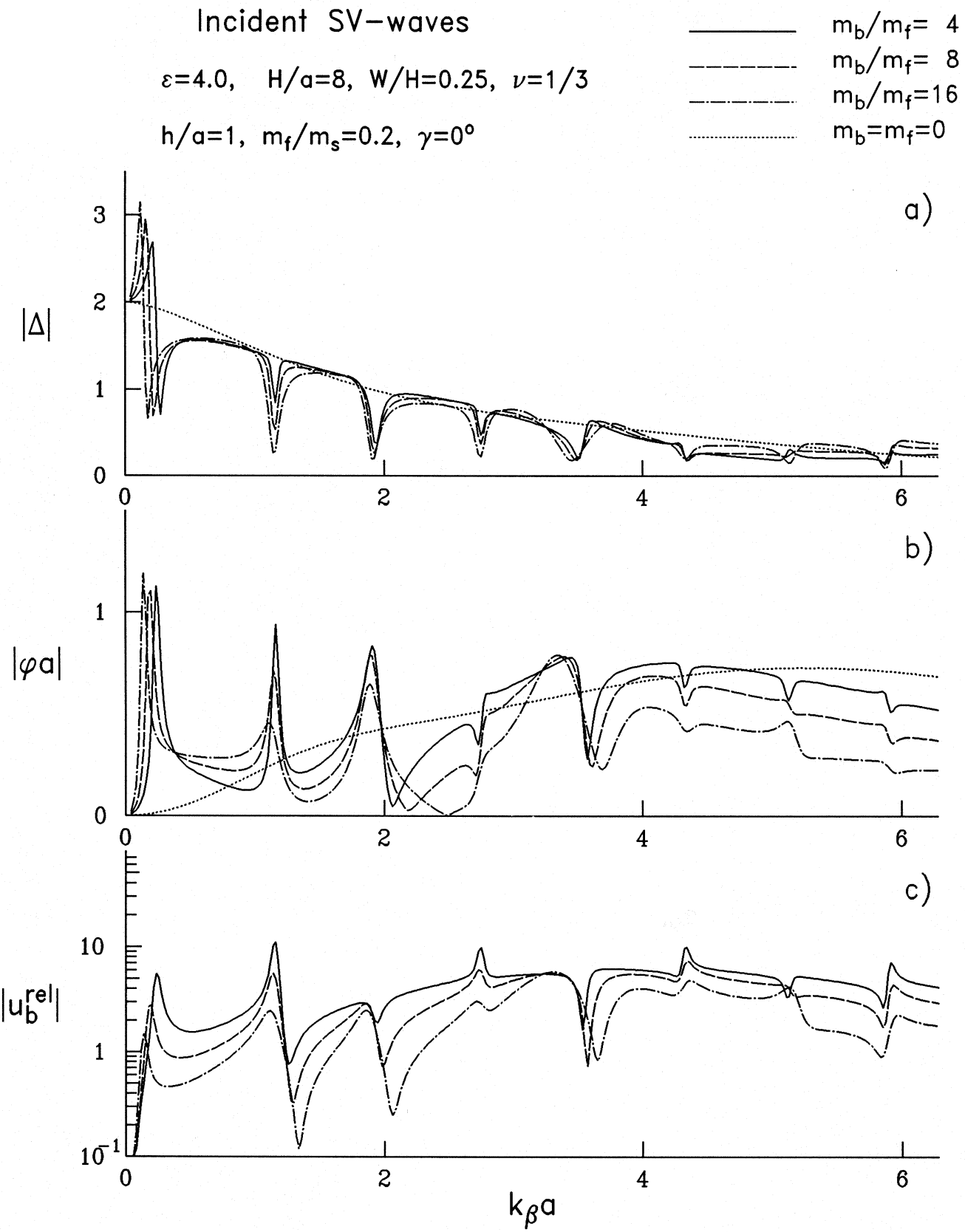

Figure III.10

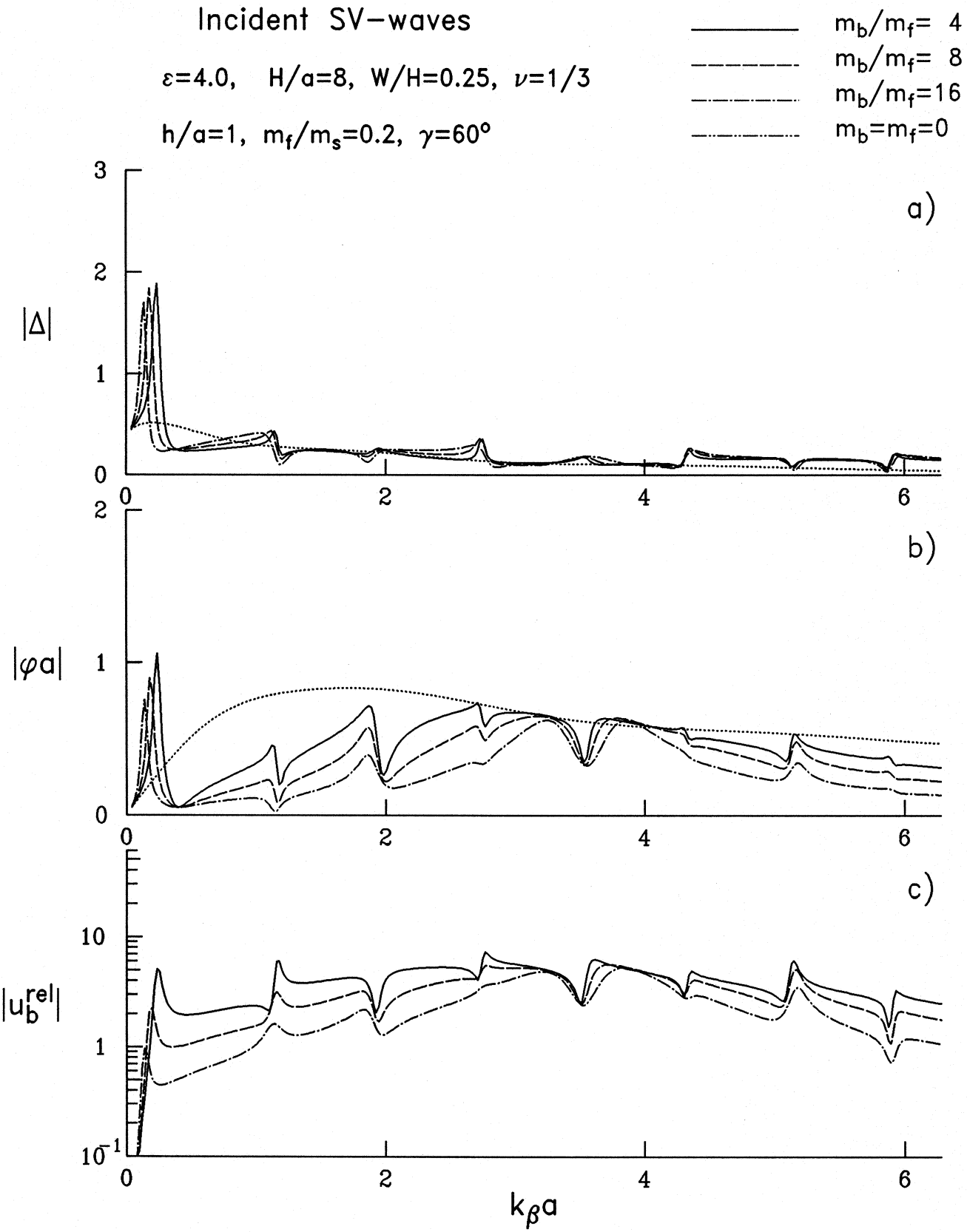

Figure III.11 a), b) and c)

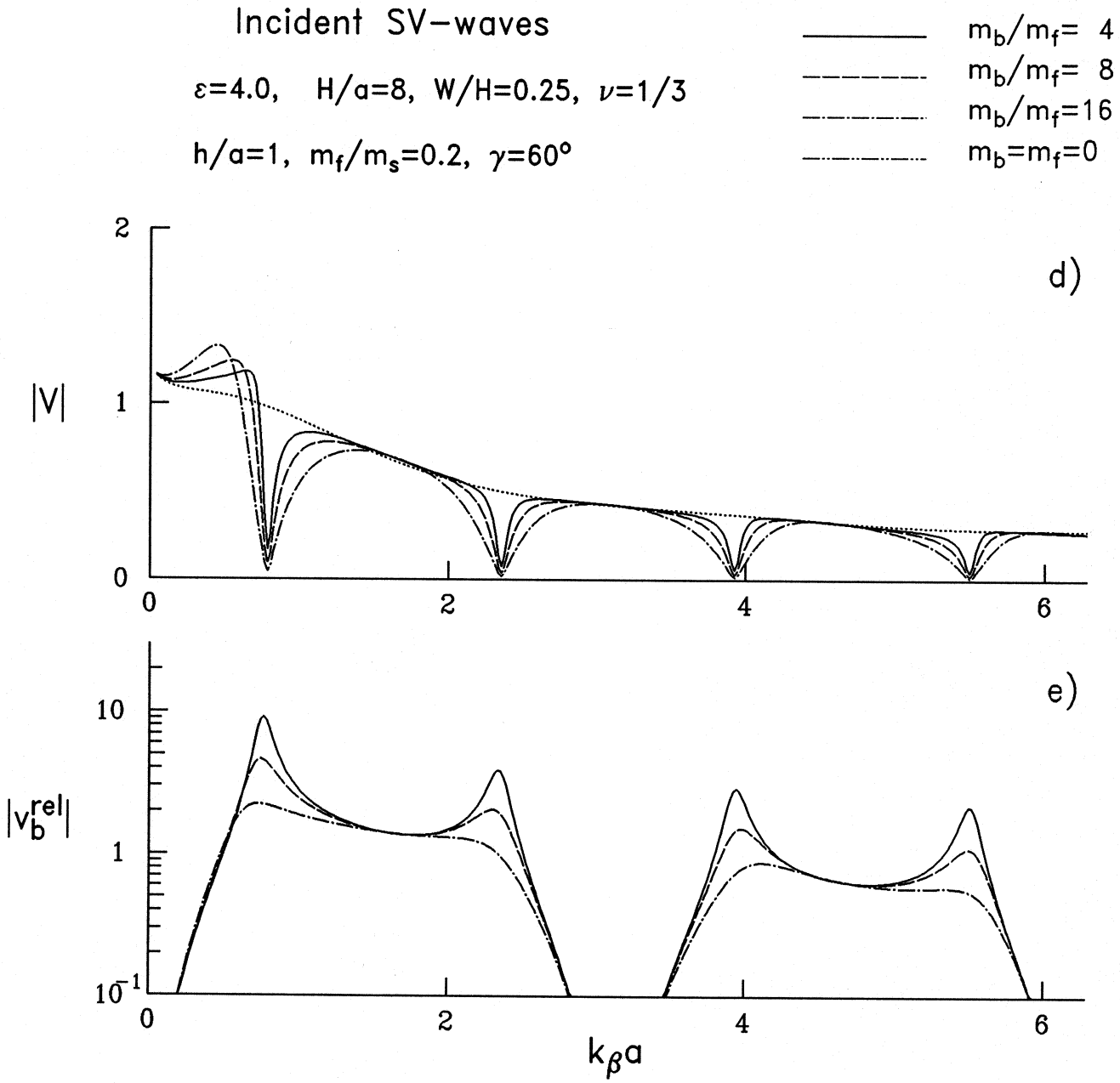

Figure III.11 d) and e)

the horizontal inertia forces of the building, caused by the large input base translation, which is much larger for $\gamma = 30°$ than for the other incident angles.

How important is the contribution of the rotation of the foundation input motion can be seen if the peak amplitudes of u_b^{rel} are compared with the amplitudes of u^{ff} or with the amplitudes of Δ of the foundation input motion. In Fig. III.6, the ratio $|u_b^{\text{rel}}|/|u^{ff}|$, where $|u_b^{\text{rel}}|$ is measured at the first peak, varies a lot depending on the incident angle. When $\gamma = 0°$ it is approximately equal to 6, when $\gamma = 30°$ to 4, when $\gamma = 60°$ to 20, and when $\gamma = 45°$ to infinity. Neglecting the rotation of the exciting motion can by far underestimate the forces in the building. If the ratio $|v_b^{\text{rel}}|/|v^{ff}|$ is calculated for the peak responses, it can be seen that the vertical forces in the building can also be underestimated if the embedment is neglected, and if v^{ff} is taken as the driving vertical motion of the building base. When $\gamma = 30°$ the second peak of $|v_b^{\text{rel}}|$ is higher than the peaks for $\gamma = 60°$, 45° and 85°, even though $|v^{ff}|$ is practically zero for $\gamma = 30°$.

In Fig. III.7, the same quantities are shown as in Fig. III.6 but for a higher and heavier building ($H/a = 8$, $W/H = 0.25$, $m_b/m_f = 8$, $m_f/m_s = 0.2$ and $\varepsilon = 4$). As mentioned in the previous chapter, this would correspond to a 50 story building, e.g. in Mexico City ($\beta \approx 100$m/s), while the previous example could correspond to a 10 story building in Los Angeles. It can be seen that, because of the interaction, the transfer function of u_b^{rel} for the taller building does not have higher first peak than the shorter building (recall that u_b^{rel} is the relative response on the top of the building), it is even lower. So, when the building is situated on softer soil, the "damping" due to radiation is larger. $|\varphi|$ of the foundation input motion is not the backbone curve for the base rotation of the higher building. It is important to notice that $|u_b^{\text{rel}}|$, at frequencies $k_\beta a \approx 4$, away from the natural frequencies, is even higher than the corresponding first peak, whose amplitude is sometimes taken as the only measure for the forces in the building. The reason for this is the high amplitude of the rotation of the foundation input motion at those frequencies.

For the purpose of completeness, as in Chapter II, in Figs. III.8, III.9, III.10 and III.11 the amplitudes of the transfer functions of the building base and top responses are shown versus $k_\beta a$, for two types of buildings ($H/a = 2$, $\varepsilon = 4$; and $H/a = 8$, $\varepsilon = 4$) for different values of the ratio m_b/m_s ($m_b/m_s = 1$, 2 and 4 for the lower building, and $m_b/m_f = 4$, 8 and 16 for the higher building). In Fig. III.8 and Fig. III.10 $\gamma = 0°$, and in Fig. III.9 and III.11 $\gamma = 60°$. The discussion of the similar examples in Chapter II would apply for those figures also. It can be added that, because of the large amplitude of the rotation of the foundation input motion that is superimposed on the rotation due to the dynamic interaction, when $\gamma = 60°$, in Fig. III.9, for the lower building, the backbone curve is higher and the height of the peaks of $|\varphi a|$ relative to the backbone curve is very small (e.g., the second peak can hardly be recognized).

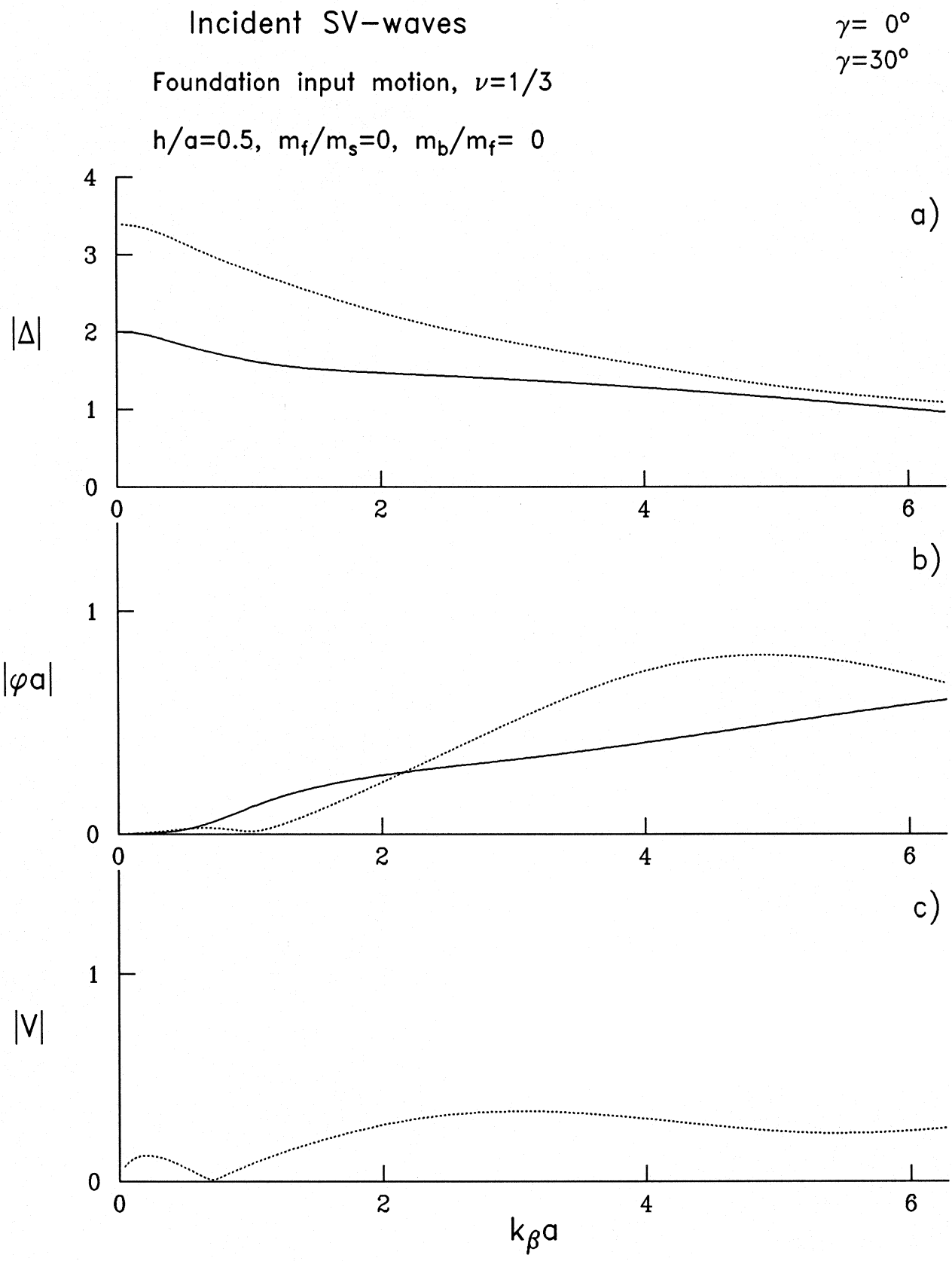

Figure III.12

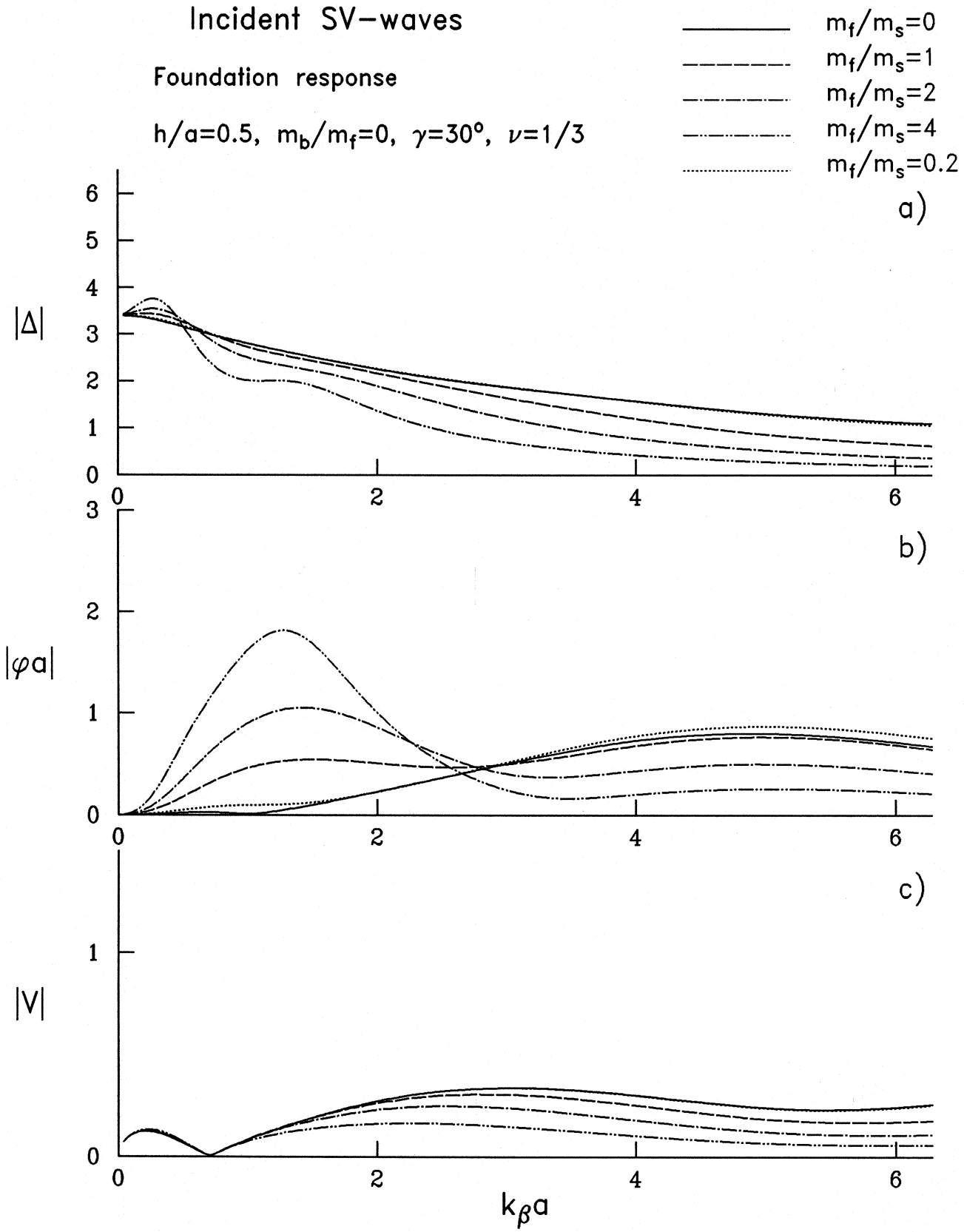

Figure III.13

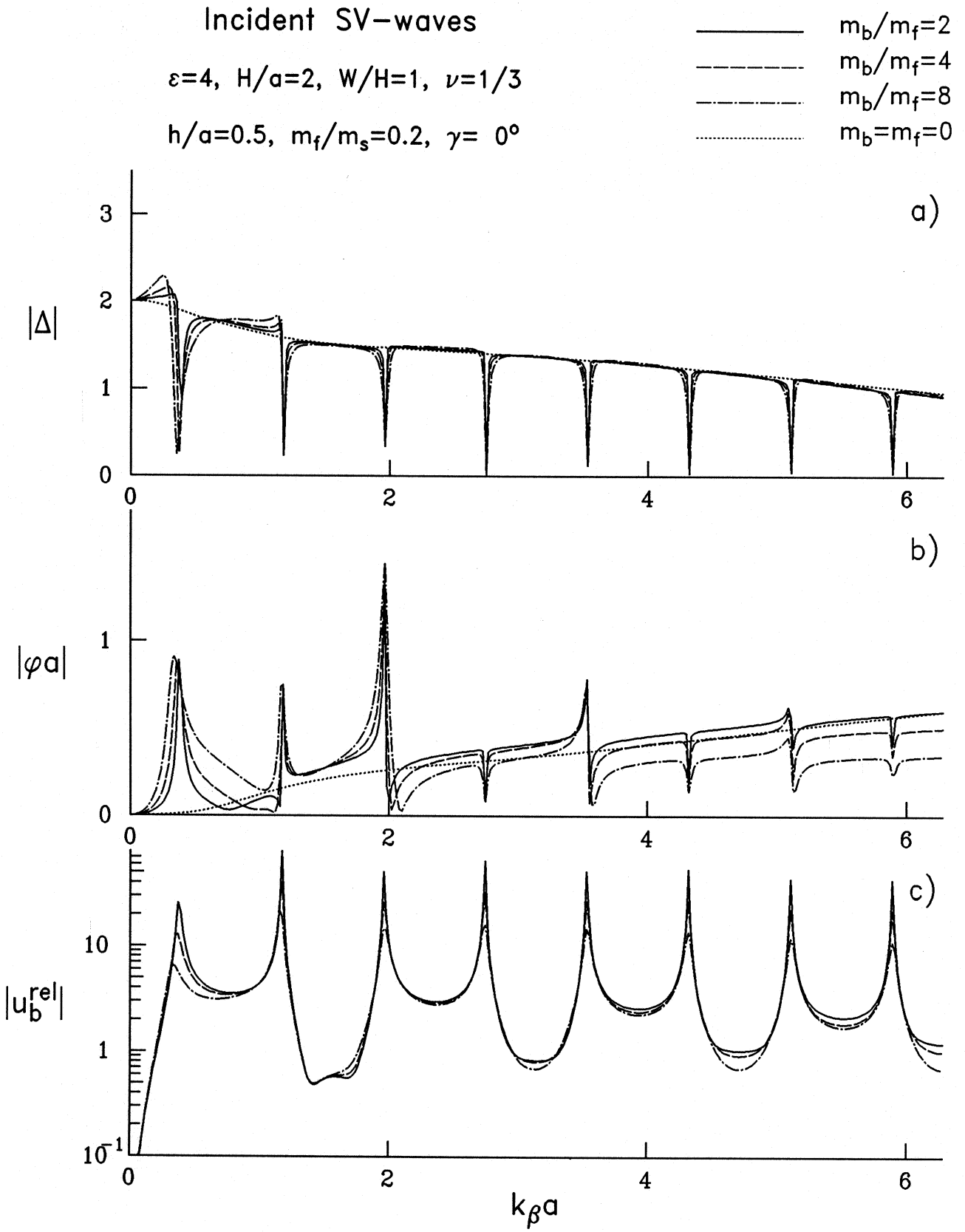

Figure III.14

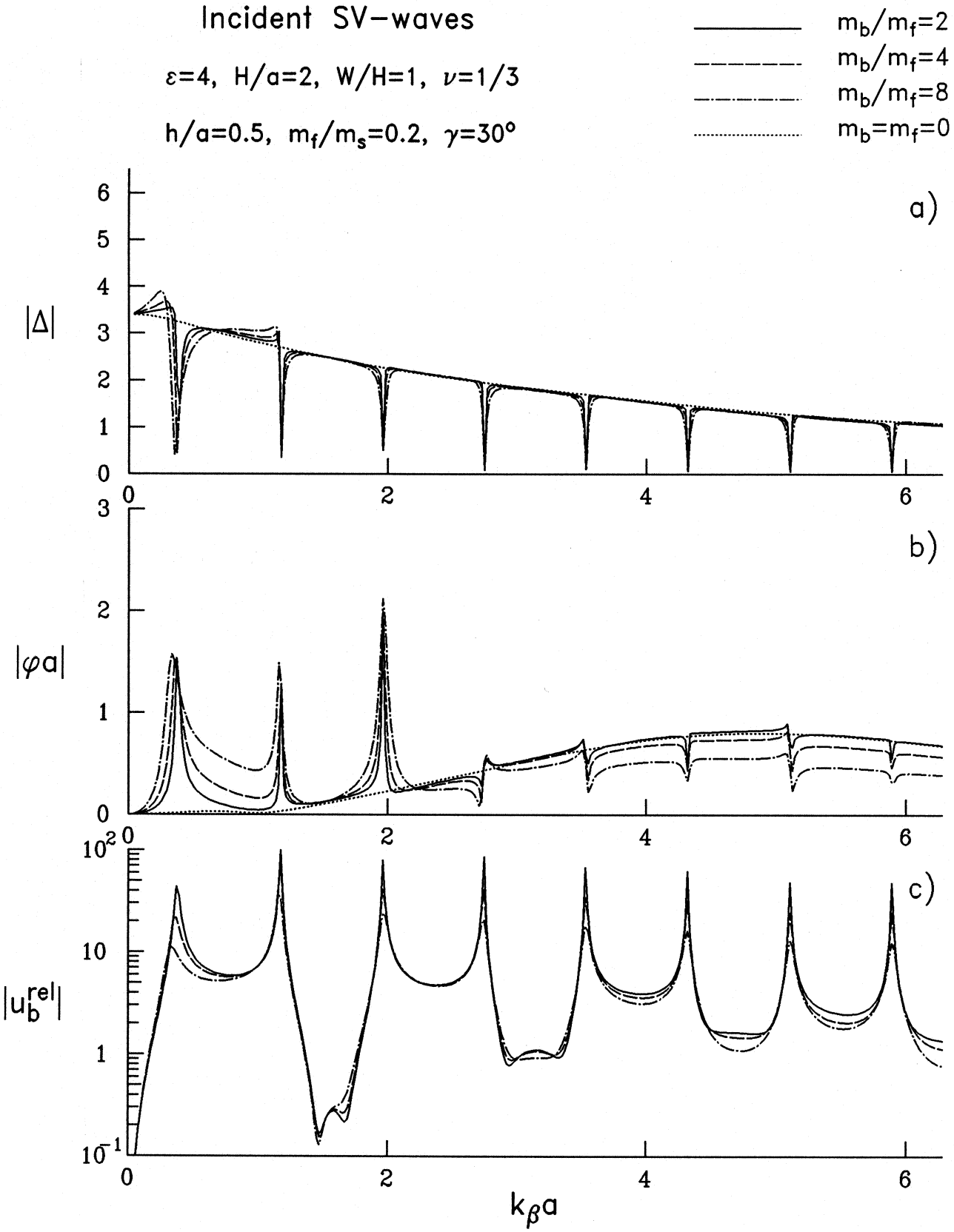

Figure III.15 a), b) and c)

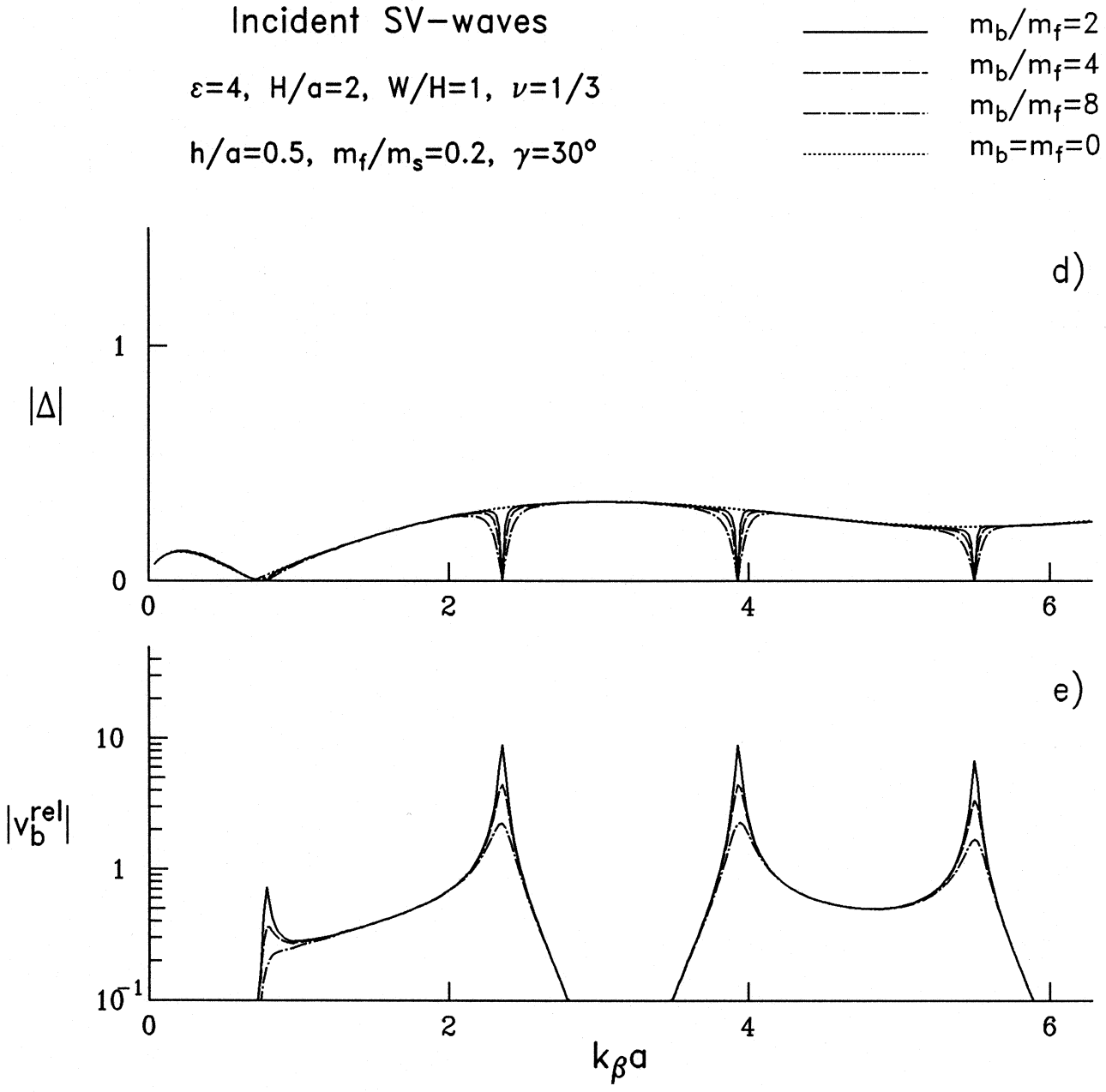

Figure III.15 d) and e)

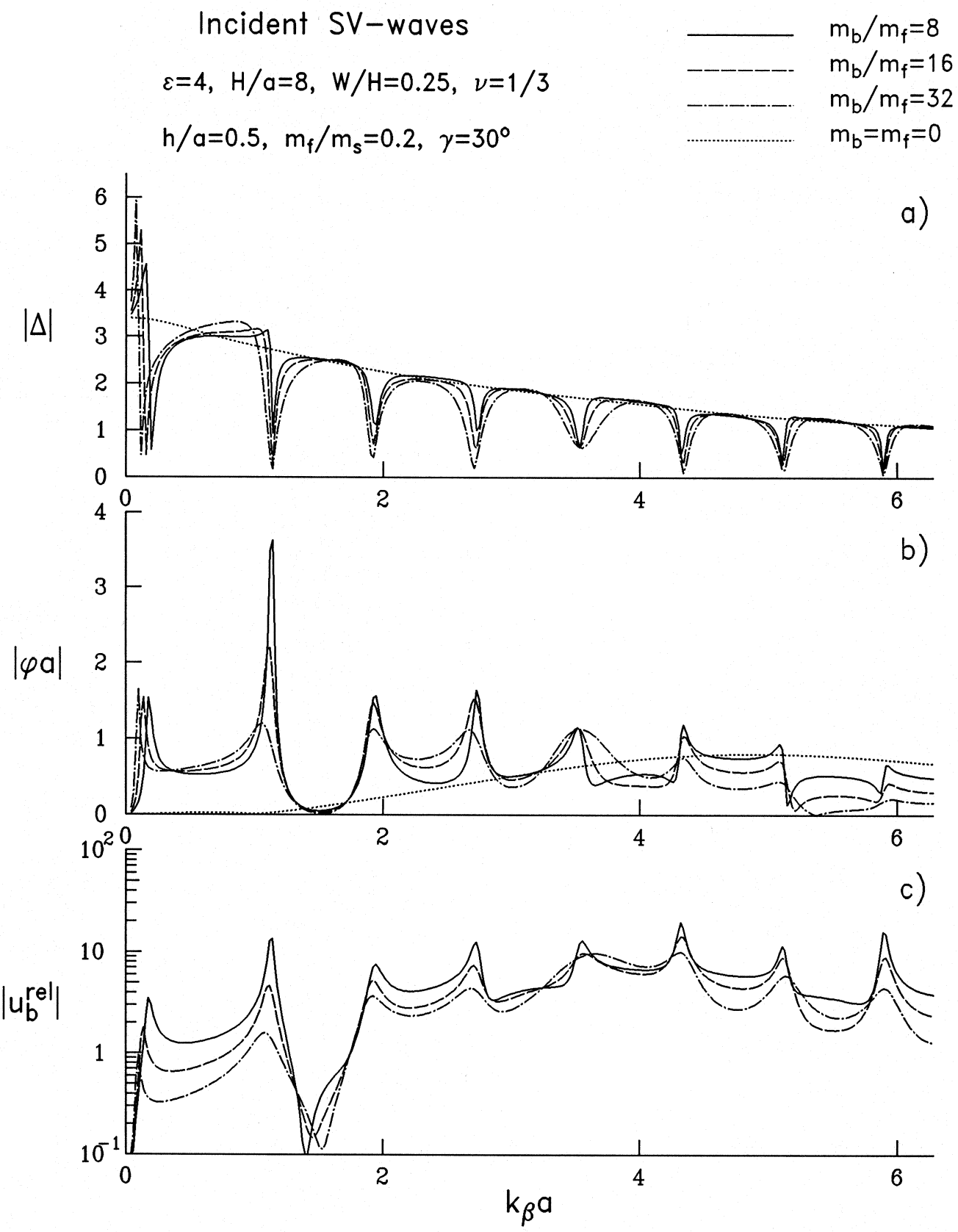

Figure III.16 a), b) and c)

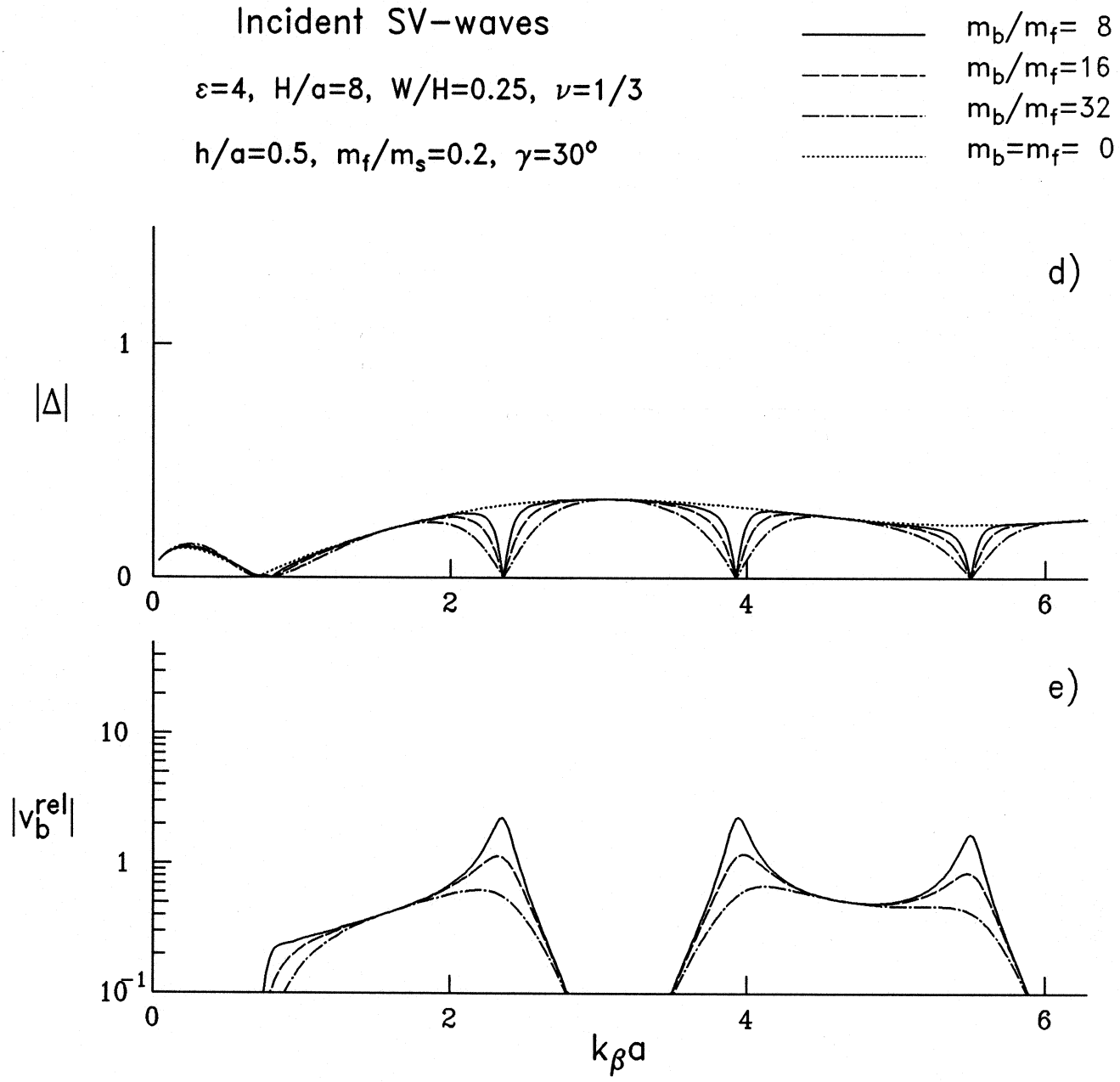

Figure III.16 d) and e)

III.2.4 Effect of the Depth of the Embedment

In the remaining examples in this chapter, in Fig. III.19 through Fig. III.25, the foundation is shallow and has depth-to-half-width ratio $\frac{h}{a} = 0.5$. The selection of the other parameters is similar as in the previous examples for semi-circular foundations.

In Fig. III.12 a, b and c, the components of the foundation input motion are shown versus Ω for $\gamma = 0°$ and 30°. Results for $\gamma > \gamma_{\text{crit}}$ will not be shown because of the lack of accuracy throughout the entire interval $\eta \in (0,2]$. Namely, lower value of h/a and the special expansion of the inhomogeneous wave require more terms in the series and, therefore, evaluation of Bessel functions of very high order, which have very small amplitudes and which, because of the finite arithmetics of the digital computer, cannot be evaluated with high degree of accuracy. For the purpose of this study, additional effort to improve the accuracy of the computer program for those cases was not considered to be of high priority. Comparing the foundation input motion for the semi-circular foundation with those for a shallow foundation, similar conclusions can be drawn as in Chapter I. For longer waves, the rotation of a deeper foundation is larger, and for shorter waves the rotation of a shallow foundation is larger. As $k_\beta a \to 0$, $|\varphi a| \to 0$ regardless of the size and the shape of the foundation. As $k_\beta a$ increases, $|\varphi a|$ grows at a higher rate for the deeper foundation, but it saturates and starts decreasing at lower frequencies than for the shallow foundation. For vertical incidence, at about $\eta = 2$, the rotation of the shallow foundation reaches approximately in amplitude the rotation of the deeper foundation. When $\gamma = 30°$, $|\varphi a|$ for the deeper foundation is higher than $|\varphi a|$ for the shallower foundation for all $k_\beta a \in (0,2]$. The horizontal translation Δ decreases with $k_\beta a$ at a much lower rate for the shallow foundation. When $\gamma = 0°$, the vertical translation is always zero, and when $\gamma = 45°$ it is significantly higher when the embedment is deeper.

In Fig. III.13, the foundation response is shown without the building at $\gamma = 30°$ and for $m_b/m_f = 1$,2, 4 and $m_b/m_f = 0.2$. The rotational amplitudes are largest at $k_\beta a \approx 1$, where the rocking frequencies are located.

In Fig. III.14 and III.15, the transfer functions of the building responses are shown for the lower building ($H/a = 2$, $\varepsilon = 4$, $m_f/m_s = 1$) for incident angles $\gamma = 0°$ and 30°, respectively, and for $m_b/m_f = 2$, 4 and 8. In Fig. III.16 the same is done for the higher example building ($H/a = 8$, $\varepsilon = 4$, $m_f/m_s = 0.2$, $m_b/m_f = 8, 16$ and 32). The first peaks of $|\Delta|$, $|\varphi|$ and $|u_b^{\text{rel}}|$ are lower for the building on shallow foundation, probably because of the smaller amplitudes of the foundation driving forces, as in the case of incident P-waves. In the relative horizontal building response, the higher order peaks have larger amplitudes than the first peak. The "damping" effect of the interaction is significant only for the first peak. In Fig. III.16, very high rotation can be seen in the rotation amplitudes at the second natural frequency.

CHAPTER IV

SOIL-STRUCTURE INTERACTION FOR INCIDENT RAYLEIGH-WAVES

IV.1 The Model

IV.1.1 The Free-Field Motion

A monochromatic Rayleigh wave can be represented by its potentials

$$\phi = Ce^{-b_1 z}e^{ik(x-ct)} \qquad (IV.1a)$$

$$\psi = De^{-b_2 z}e^{ik(x-ct)} \qquad (IV.1b)$$

where C and D are complex constants, b_1 and b_2 are real and positive constants and k and c, both real, are the wave number and the phase velocity of the surface waves propagating in the positive x-direction. These constants are related as follows

$$b_1 = k\sqrt{1-(c/\alpha)^2}$$

$$b_2 = k\sqrt{1-(c/\beta)^2}$$

and

$$D = \frac{1}{2b_2 ik}(k^2 + b_2^2)C$$

(Eringen and Suhubi, 1975). The eigenvalues of the phase velocity c satisfy the Rayleigh equation and have values $c = 0.9194\beta$ for $\nu = 1/4$ and $c = 0.9320$ for $\nu = 1/3$. The particle motion is elliptical retrograde up to certain depth, and then the direction of rotation changes.

The ratio of the coefficients C and D, as well as the eigenvalue of the phase velocity c, follow from the zero-stress condition $\tau_{zz} = \tau_{zx} = 0$ at $z = 0$, where the stresses are calculated from the potentials (through the displacements),

$$u_x = \frac{\partial\phi}{\partial x} - \frac{\partial\psi}{\partial z} \qquad (IV.2a)$$

$$u_z = \frac{\partial\phi}{\partial z} + \frac{\partial\psi}{\partial x} \qquad (IV2b)$$

$$\tau_{zz} = \lambda\left(\frac{\partial u_x}{\partial z} + \frac{\partial u_z}{\partial x}\right) + 2\mu\frac{\partial u_z}{\partial z} \qquad (IV3a)$$

and

$$\tau_{xz} = \mu\left(\frac{\partial u_z}{\partial x} + \frac{\partial u_x}{\partial z}\right). \qquad (IV3b)$$

IV.1.2 The Interaction Equations

It is convenient to introduce complex angles θ_α and θ_β, defined by

$$\theta_\alpha = \frac{\pi}{2} - i\phi_\alpha$$

$$\theta_\beta = \frac{\pi}{2} - i\phi_\beta \quad ,$$

where ϕ_α and ϕ_β are real quantities such that

$$\cosh\phi_\alpha = \alpha/c$$

$$\cosh\phi_\beta = \beta/c.$$

In terms of those angles

$$\phi = Ce^{b_1 d} e^{ik_\alpha r_1 \cos(\theta_1 - \theta_\alpha) - i\omega t} \qquad (IV.4a)$$

and

$$\psi = De^{b_2 d} e^{ik_\beta r_1 \cos(\theta_1 - \theta_\beta) - i\omega t}. \qquad (IV.4b)$$

Then, the displacement components u_r and u_θ and the stress components $\tau_{r_1 r_1}$ and $\tau_{r_1 \theta_1}$ can be calculated as follows:

$$u_{r_1} = \frac{\partial\phi}{\partial r_1} + \frac{1}{r_1}\frac{\partial\psi}{\partial\theta_1} \qquad (IV.5a)$$

and

$$u_{\theta_1} = \frac{1}{r}\frac{\partial\phi}{\partial\theta_1} - \frac{\partial\psi}{\partial r_1}. \qquad (IV.5b)$$

$$\tau_{r_1 r_1} = \lambda\left(\frac{\partial u_{r_1}}{\partial r_1} + \frac{u_{r_1}}{r_1} + \frac{1}{r}\frac{\partial u_{\theta_1}}{\partial\theta_1}\right) + 2\mu\frac{\partial u_{r_1}}{\partial r_1} \qquad (IV.6a)$$

and

$$\tau_{r_1\theta_1} = \mu\left(\frac{\partial u_{\theta_1}}{\partial r_1} - \frac{u_{\theta_1}}{r_1} + \frac{1}{r_1}\frac{\partial u_{r_1}}{\partial\theta_1}\right) \qquad (IV.6b)$$

where λ is the Lamé constant. The final expressions for the displacements and stresses evaluated along the canyon rim, at $r_1 = b$ and for $-\theta_0 \le \theta \le \theta_0$, are

$$u_{r_1}(b,\theta_1) = \frac{1}{b}\Big[Cik_\alpha b\cos(\theta_1 - \theta_\alpha)e^{b_1 d + ik_\alpha b\cos(\theta_1 - \theta_\alpha)}$$

$$- Dik_\beta b\sin(\theta_1 - \theta_\beta)e^{b_2 d + ik_\beta b\cos(\theta_1 - \theta_\beta)}\Big]e^{-i\omega t} \qquad (IV.7a)$$

$$u_{\theta_1}(b,r_1) = \frac{1}{b}\Big[-Cik_\alpha b\sin(\theta_1 - \theta_\alpha)e^{b_1 d + ik_\alpha b\cos(\theta_1 - \theta_\alpha)}$$

$$- Dik_\beta b\cos(\theta_1 - \theta_\beta)e^{b_2 d + ik_\beta b\cos(\theta_1 - \theta_\beta)}\Big]e^{-i\omega t} \qquad (IV.7b)$$

$$\tau_{r_1 r_1} = \frac{2\mu}{b^2}\Bigg[C(ik_\alpha b)^2\left(\frac{1}{2}\frac{\alpha^2}{\beta^2} - \sin^2(\theta_1-\theta_\alpha)\right)e^{b_1 d + ik_\alpha b\cos(\theta_1-\theta_\alpha)} - D(ik_\beta b)^2\sin(\theta_1-\theta_\beta)\cos(\theta_1-\theta_\beta)e^{b_2 d + ik_\beta b\cos(\theta_1-\theta_\beta)}\Bigg]e^{-i\omega t} \tag{IV.8a}$$

$$\tau_{r_1\theta_1} = \frac{2\mu}{b^2}\Bigg[-C(ik_\alpha b)^2\sin(\theta_1-\theta_\alpha)\cos(\theta_1-\theta_\alpha)e^{b_1 d + ik_\alpha b\cos(\theta_1-\theta_\alpha)} - D(ik_\beta b)^2\left(\frac{1}{2} - \sin^2(\theta_1-\theta_\beta)\right)e^{b_2 d + ik_\beta b\cos(\theta_1-\theta_\beta)}\Bigg]e^{-i\omega t}. \tag{IV.8b}$$

To match the displacements of the foundation with the displacements of the half-space at $r_1 = b$, and to expand the foundation driving forces in series of θ_1 (with period 2π), the same method is used as for the displacements and stresses induced by the inhomogeneous P-wave potential in the case of incident SV-waves. The finite Fourier series approximating those displacements and stresses are as follows

$$u_{r_1}^{ff}(b,\theta_1,t) \approx \frac{1}{b}\sum_{n=0}^{N}\left(A_{0,n}^{u_r}\cos n\theta_1 + B_{0,n}^{u_r}\sin n\theta_1\right)e^{-i\omega t} \tag{IV.9a}$$

$$u_{\theta_1}^{ff}(b,\theta_1,t) \approx \frac{1}{b}\sum_{n=0}^{N}\left(A_{0,n}^{u_\theta}\sin n\theta_1 + B_{0,n}^{u_\theta}\cos n\theta_1\right)e^{-i\omega t} \tag{IV.9b}$$

$$\tau_{r_1 r_1}^{ff}(b,\theta_1,t) \approx \frac{2\mu}{b^2}\sum_{n=0}^{N}\left(A_{0,n}^{\tau_r}\cos n\theta_1 + B_{0,n}^{\tau_r}\sin n\theta_1\right)e^{-i\omega t} \tag{IV.10a}$$

and

$$\tau_{r_1\theta_1}^{ff}(b,\theta_1,t) \approx \frac{2\mu}{b^2}\sum_{n=0}^{N}\left(A_{0,n}^{\tau_\theta}\cos n\theta_1 + B_{0,n}^{\tau_\theta}\sin n\theta_1\right)e^{-i\omega t}. \tag{IV.10b}$$

where the superscript "ff" stands for "free-field". The interaction equations and the related equations are same as the corresponding equations for incidents SV-waves beyond critical angle, (eqs. (III.20), and (III.25)), with the exception that for Rayleigh waves

$$\begin{Bmatrix} A_0^u \\ C_0^u \end{Bmatrix} = \begin{Bmatrix} A_0^{u_r} \\ A_0^{u_\theta} \end{Bmatrix} \tag{IV.11a}$$

$$\begin{Bmatrix} B_0^u \\ D_0^u \end{Bmatrix} = \begin{Bmatrix} B_0^{u_r} \\ B_0^{u_\theta} \end{Bmatrix} \tag{IV.11b}$$

$$\begin{Bmatrix} A_0^\tau \\ C_0^\tau \end{Bmatrix} = \begin{Bmatrix} A_0^{\tau_r} \\ A_0^{\tau_\theta} \end{Bmatrix} \tag{IV.11c}$$

$$\left\{ \begin{array}{c} B_0^r \\ D_0^r \end{array} \right\} = \left\{ \begin{array}{c} B_0^{rr} \\ B_0^{r\theta} \end{array} \right\} \qquad (IV.11d)$$

and that the normalizing factor for the displacement amplitudes is usually the amplitude of the horizontal component of the incident Rayleigh wave at the surface.

IV.2 Results and Analysis

In all of the following examples, $\nu = 1/3$, $W = 2a$, the foundation is semi-cylindrical and the gravity forces are neglected. The presented results will be for the same type of buildings as in Chapter II and Chapter III. The incident Rayleigh wave has unit horizontal displacement amplitude on the surface, which implies $|u^{ff}| = 1$ and $|v^{ff}| = 1.56$.

IV.2.1 Foundation Input Motion and Foundation-Soil Interaction

In Fig. IV.1 the response of the foundation (without the building) is shown for different values of the foundation-soil mass ratio ($\frac{m_f}{m_s}$ = 0, 1, 2, 4 and 0.2). The solid lines correspond to the foundation input motion. The amplitudes of Δ and V for very low frequency are smaller than the free-field surface amplitudes, because they are the average value of the free-field motion, that exponentially decreases with depth. On the other hand, the rocking amplitudes grow fast even for low frequencies, because of the large point rotation of the Rayleigh wave field. We recall that the motion of individual points of the elastic half-space, during the passage of the Rayleigh wave, is a retrograde ellipse on the surface. A periodic growth and decay with frequency (the period is $\eta \approx 1$) can be seen in the amplitudes of Δ, φ and V related to some particular values of the relative size of the foundation with respect of the wavelength of the incident wave. The rotation of the foundation input motion ($m_f = 0$) has local maxima at $\eta \approx 0.5$ and at $\eta \approx 1.5$ and has minima at $\eta \approx 1$ and 2. When $\eta \approx 0.5$ and 1.5, then the width of the foundation $2a \approx cT/2$ and $3cT/2$, respectively, i.e. the phase difference between the incident motion at the two corners is π and 3π. Then, the corners are pushed to move vertically in opposite directions. At the minima, when $\eta \approx 1$ and 2, the incident motion at the two corners is symmetric (phase difference of 2π and 4π). At the minima, φ rapidly changes in phase, as it can be seen from the phases versus $k_\beta a$ curves in Fig. IV.2, and the direction of rotation reverses. The trends of $|\Delta|$ and $|V|$ with increasing $\frac{m_f}{m_s}$ are similar to the trends we discussed for incident P- and SV-waves. The translational frequencies are lower and the peak response amplitudes are higher when $\frac{m_f}{m_s}$ is larger. However, the rocking peaks are not so obvious since the rotation due to the inertia forces competes with the rotation of the foundation input motion and those, in general, are not in phase. From the phase curves in Fig. IV.2, it can be seen that the frequencies at which the rotation reverses do not depend on the mass of the foundation, while Δ reverses at lower frequencies when the mass of the foundation is larger.

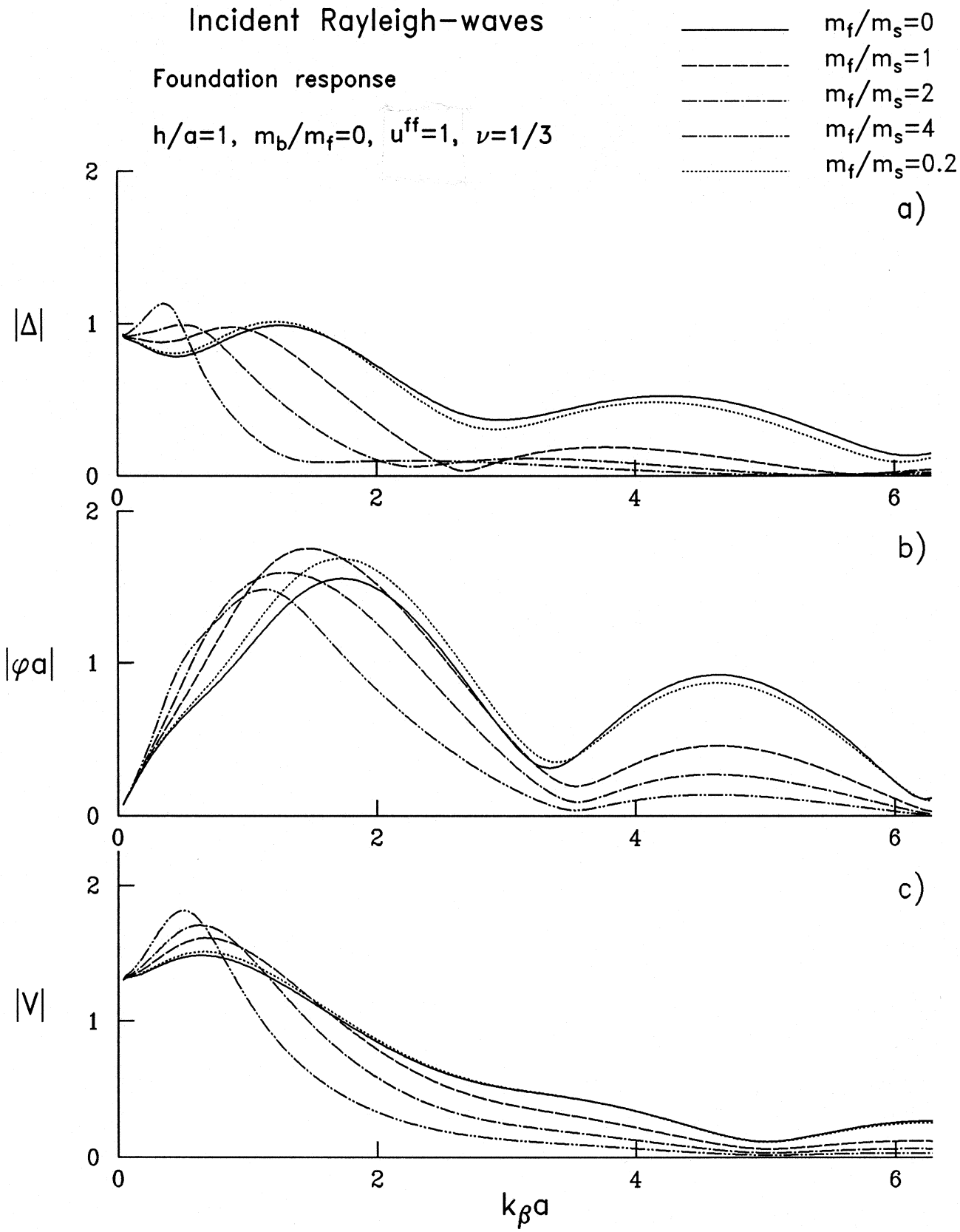
Incident Rayleigh–waves
Foundation response
h/a=1, m_b/m_f=0, u^{ff}=1, ν=1/3
m_f/m_s=0
m_f/m_s=1
m_f/m_s=2
m_f/m_s=4
m_f/m_s=0.2
a)
b)
c)
|Δ|
|φa|
|V|
$k_\beta a$
0
1
2
4
6

Figure IV.1

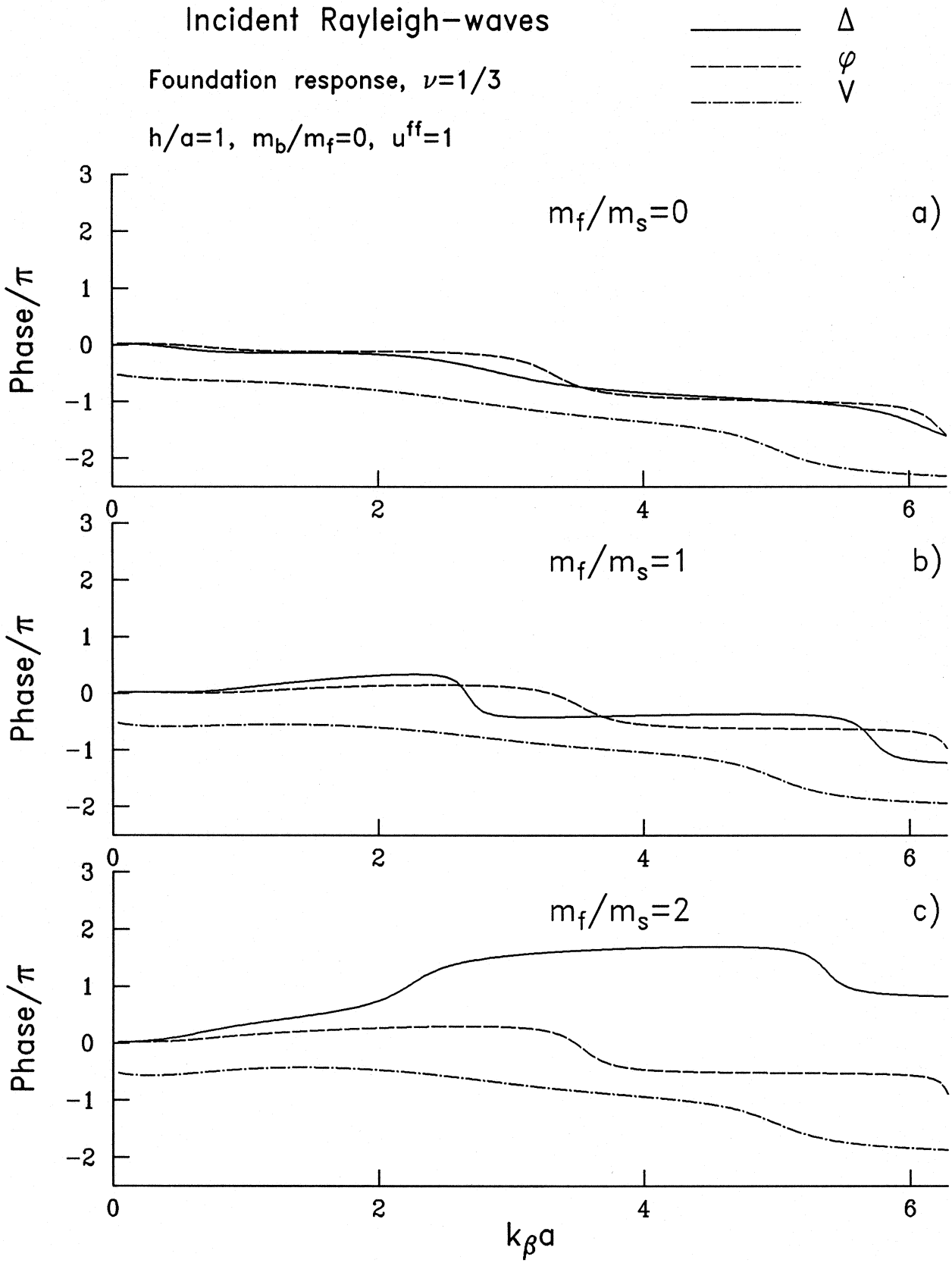
Incident Rayleigh-waves
Foundation response, ν=1/3
h/a=1, m_b/m_f=0, u^ff=1
Δ
φ
V
m_f/m_s=0
a)
m_f/m_s=1
b)
m_f/m_s=2
c)
Phase/π
3
2
1
0
−1
−2
0
2
4
6
k_βa

Figure IV.2

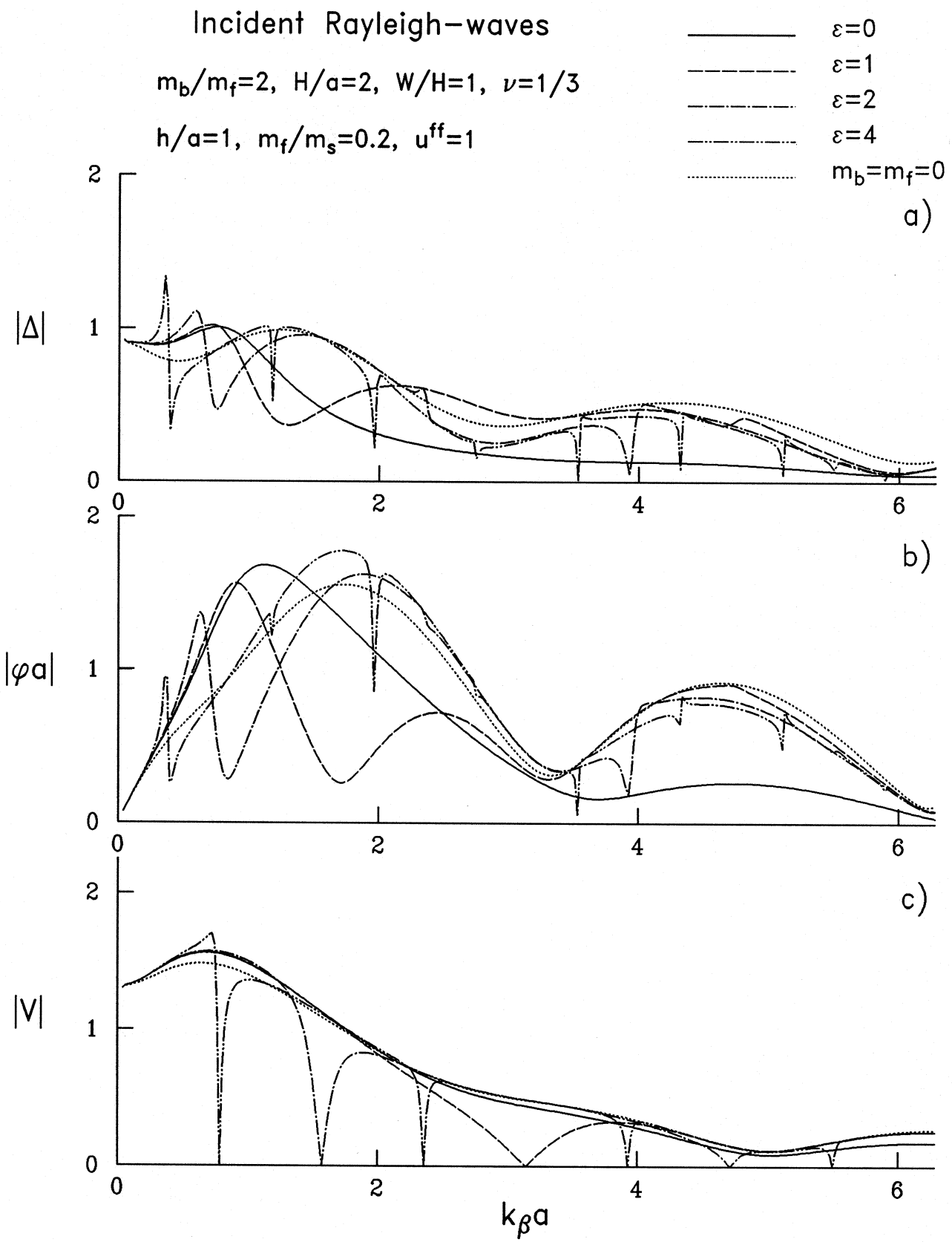
Incident Rayleigh−waves
m_b/m_f=2, H/a=2, W/H=1, ν=1/3
h/a=1, m_f/m_s=0.2, u^{ff}=1
ε=0
ε=1
ε=2
ε=4
m_b=m_f=0
a)
b)
c)
|Δ|
|φa|
|V|
$k_\beta a$
0
1
2
4
6

Figure IV.3

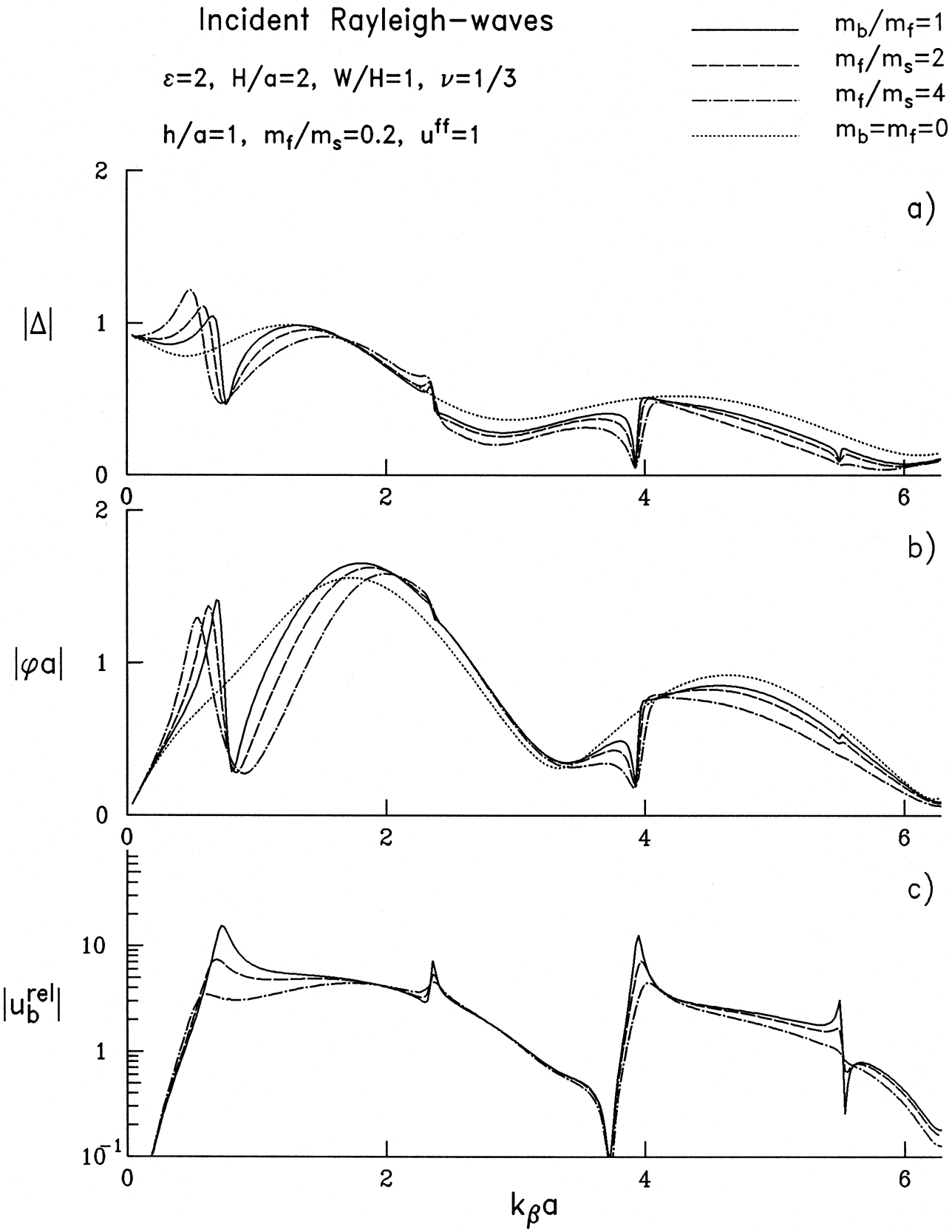

Figure IV.4 a), b) and c)

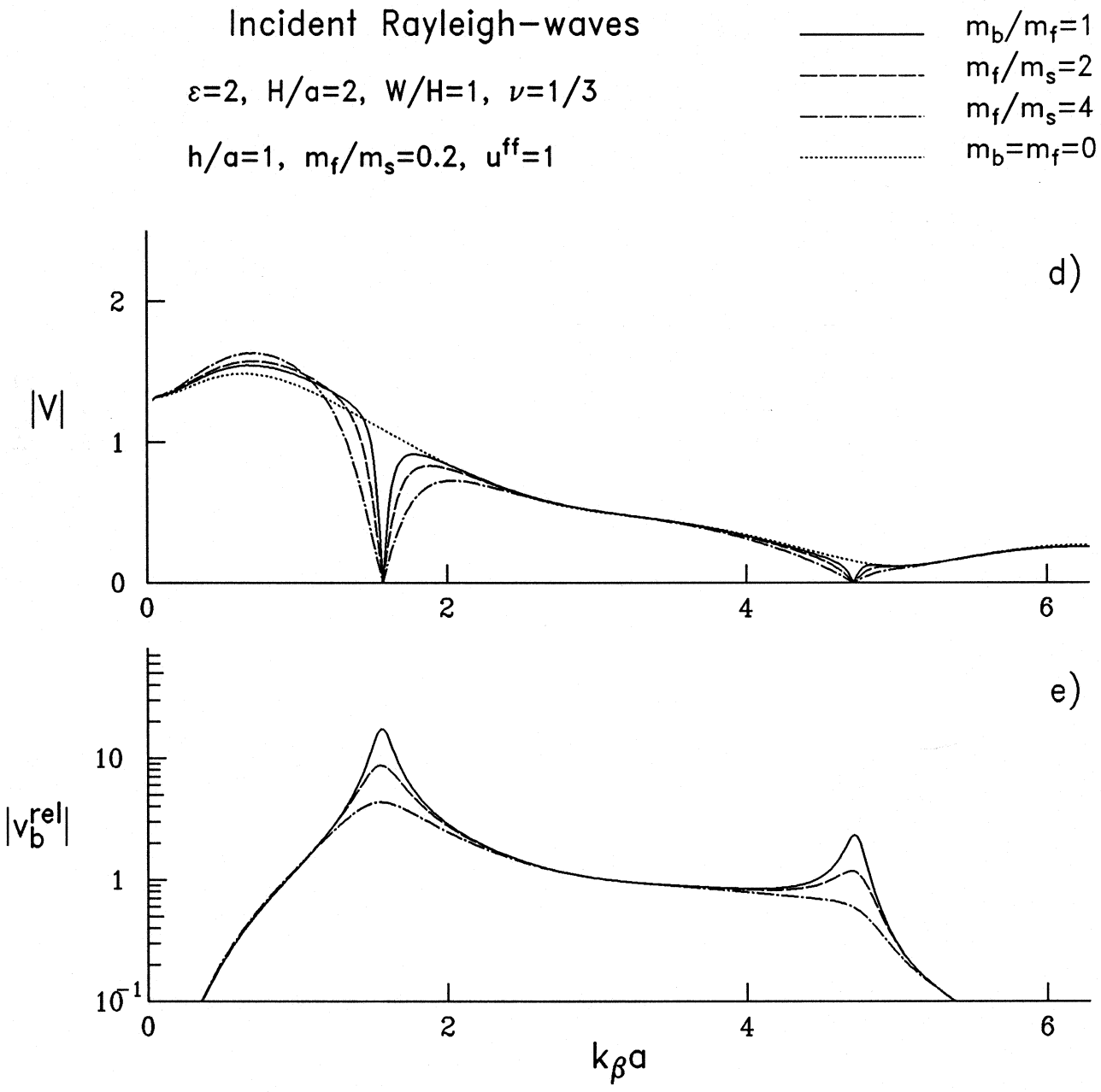

Figure IV.4 d) and e)

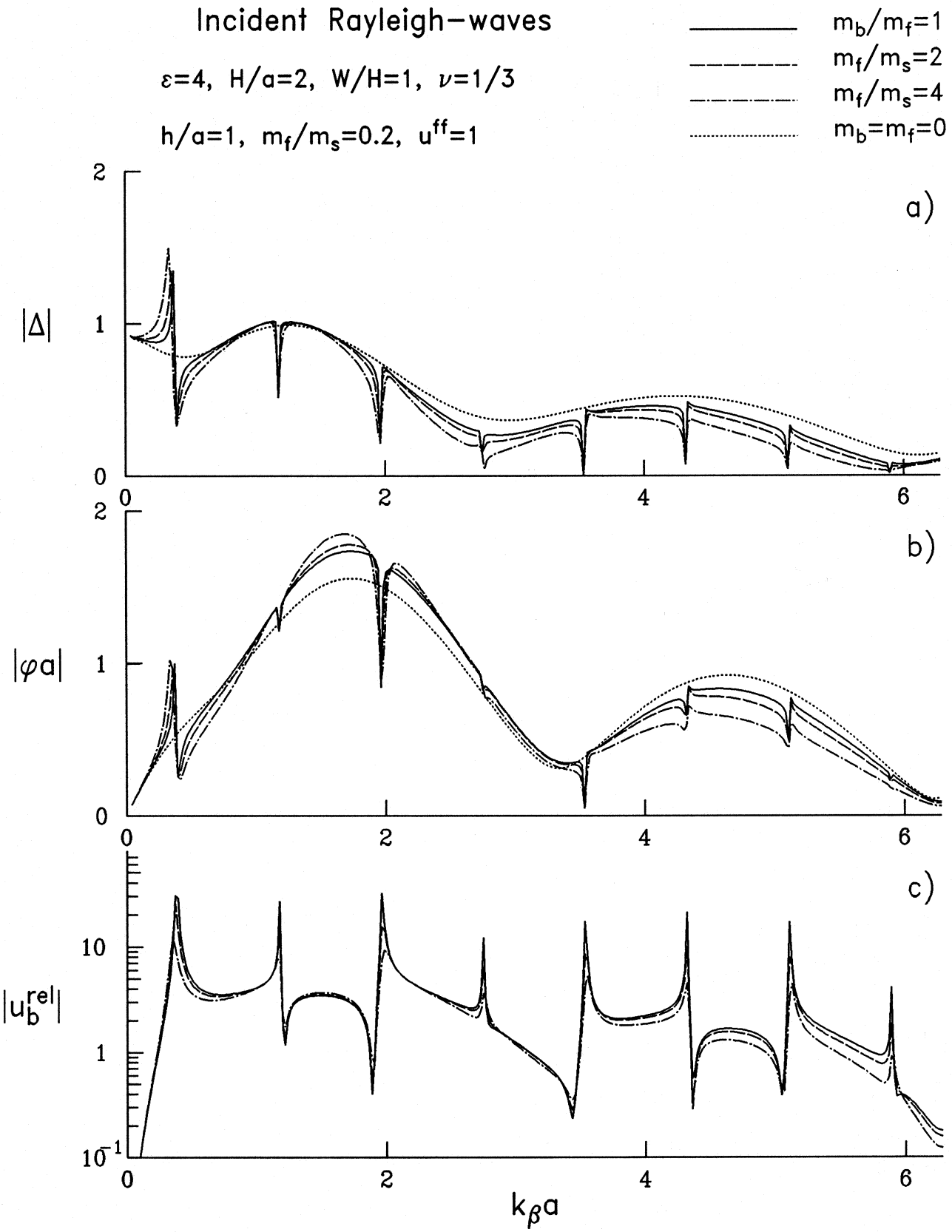

Figure IV.5 a), b) and c)

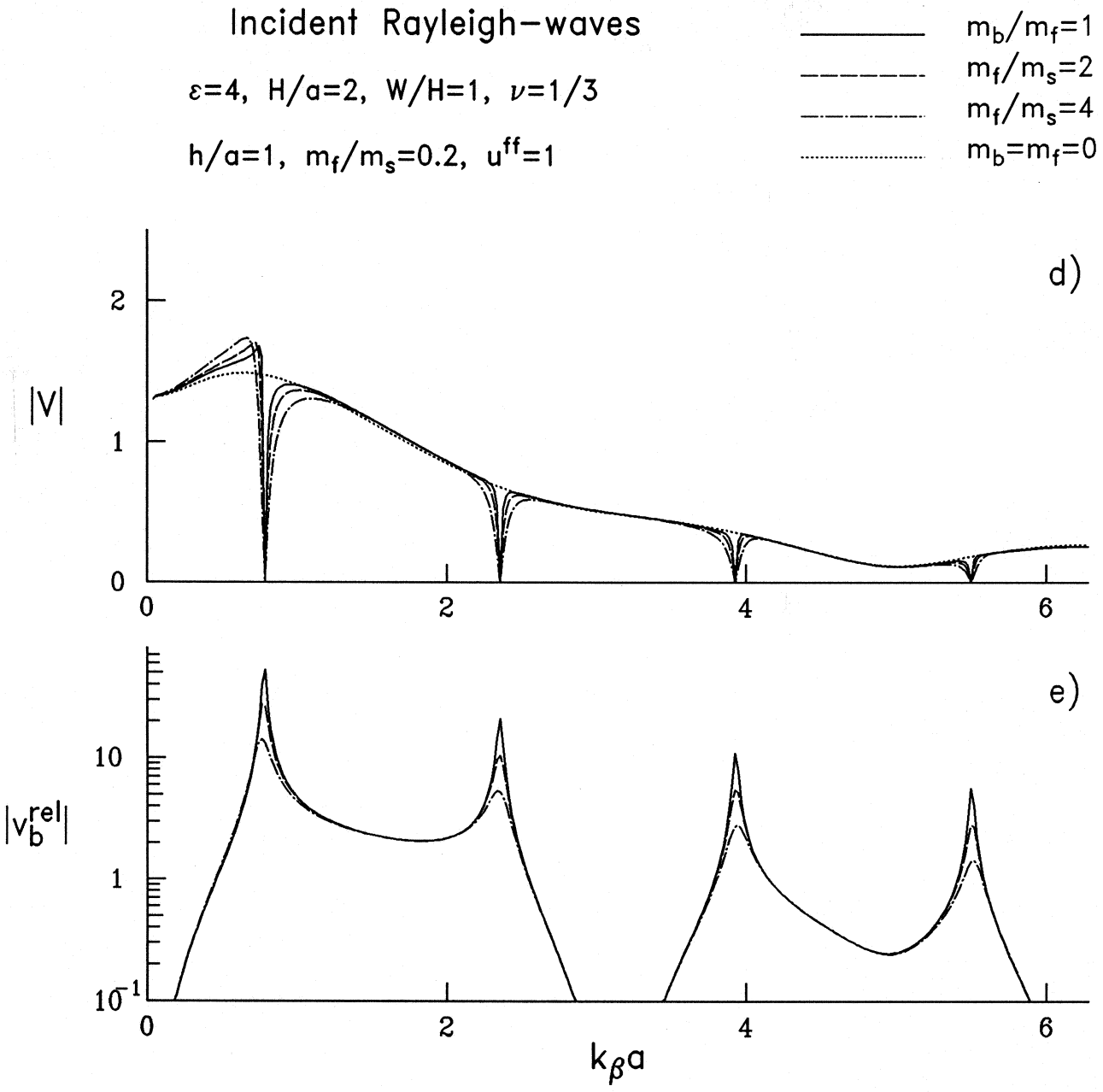

Figure IV.5 d) and e)

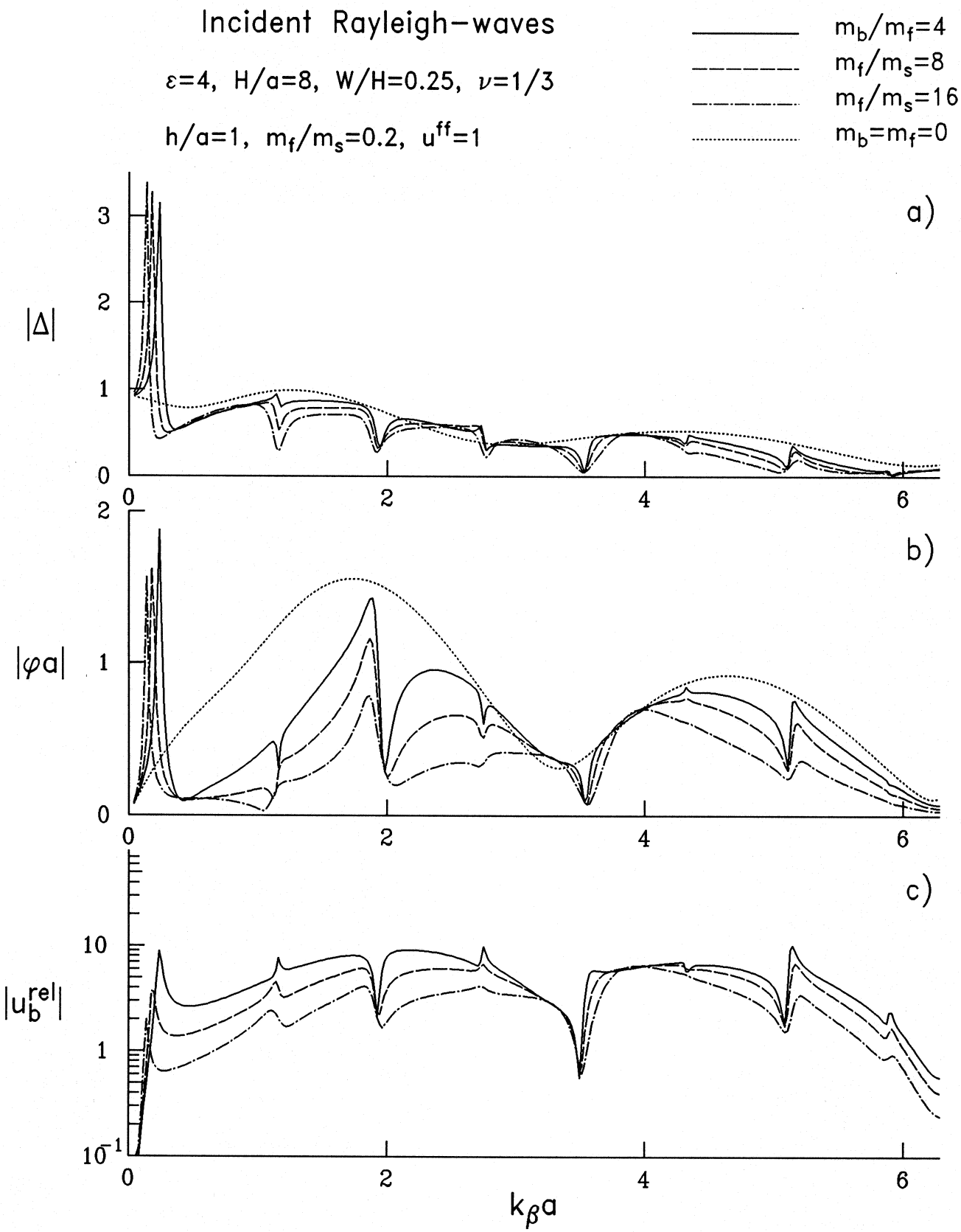

Figure IV.6 a), b) and c)

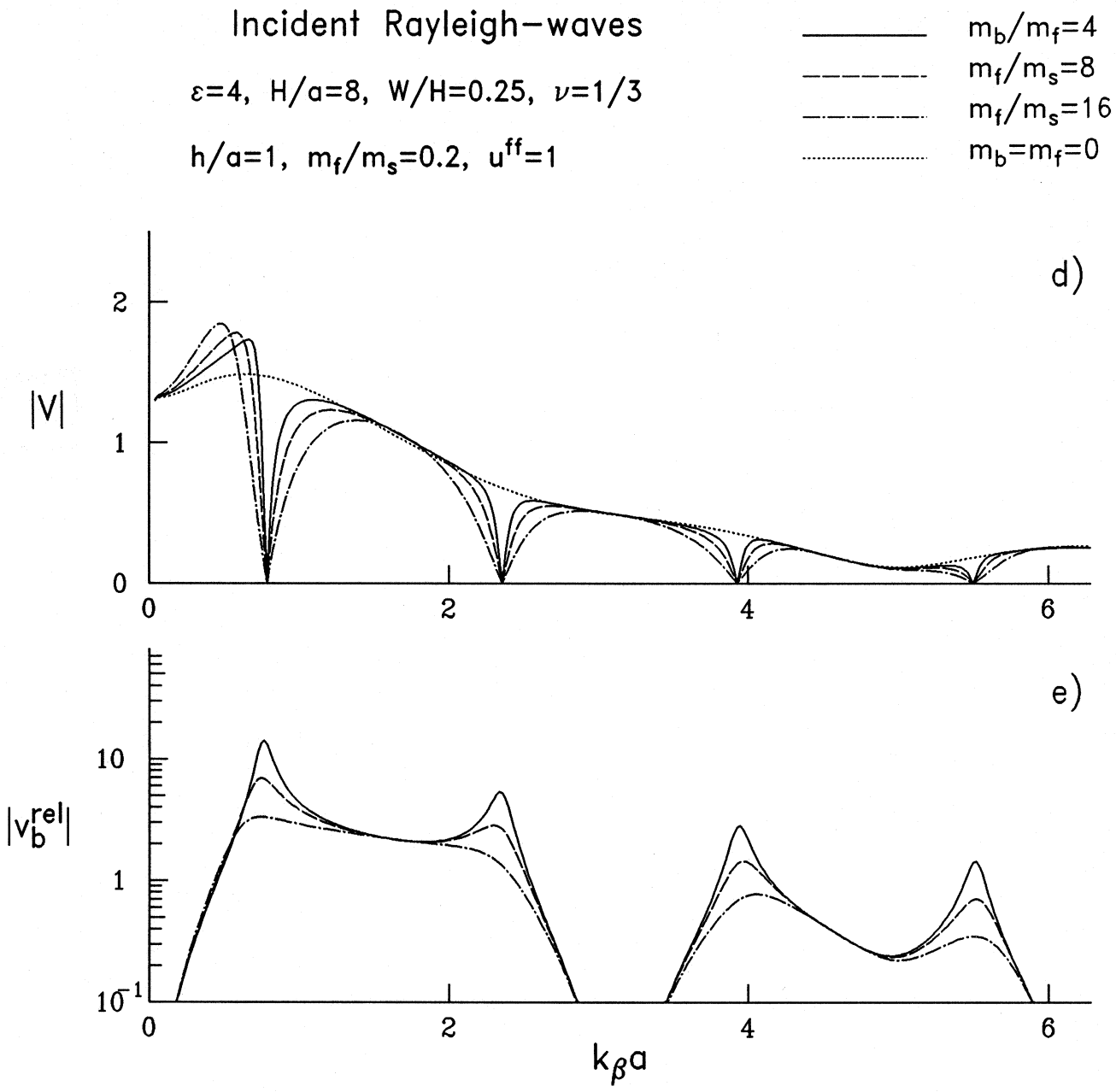

Figure IV.6 d) and e)

IV.2.2 Building-Foundation-Soil Interaction

In Fig. IV.3, the response of the lower building is shown ($H/a = 2$) when $m_f/m_s = 2$ and for four values of the relative stiffness parameter ($\varepsilon = 0$, 1, 2 and 4). In the case of incident P-waves, the smaller the value of ε, the larger is the rotation at the first "natural" frequency. For incident Rayleigh waves this is not the case (the first peak is highest when $\varepsilon = 1$), and the height of this peak depends on the rotation of the foundation input motion at the frequency of that peak. It is lowest when $\varepsilon = 4$, when the peak frequency is lower, and for which the rotation of the foundation input motion is smaller. It can be concluded that the rotation of the base has a very strong influence on the building base response.

In Fig. IV.4 and IV.5, the building base and relative responses are shown for different values of m_b/m_f ($m_b/m_f = 1$, 2 and 4) for the lower building ($H/a = 2$) for $\varepsilon = 2$ and $\varepsilon = 4$, respectively. The relative building horizontal response (on the top) is larger when the soil is stiffer ($\varepsilon = 4$). The influence of the value of m_b/m_f on the response is same as in the case of incident P and SV waves and, therefore, will not be commented on.

For completeness of the presentation, in Fig. IV.6, the response of the higher building ($H/a = 8$) is also included in this presentation.

CHAPTER V

SUMMARY AND CONCLUSIONS

Linear soil-structure interaction was studied using an analytical model, for a building on a cylindrical rigid foundation embedded in a homogeneous, isotopic semi-infinite medium, in the state of plane strain and for obliquely incident plane P-and SV- waves and surface Rayleigh waves. The motion in the half-space was represented as a superposition of cylindrical standing and waves propagating from the origin, at the center of curvature of the foundation. This representation is complete. The zero-stress condition on the half-space surface was applied approximately, while the conditions at the contact between the foundation and the soil were applied exactly for incident P- and SV-waves below critical angle. The free-field motion is expanded in series of those waves with the help of the expansion theorem for cylindrical Bessel functions. For incident Rayleigh waves, the displacements and stresses along the contact surface, produced by the inhomogeneous potential, were expanded in Finite Fourier series (with period 2π) of the angular coordinate. The building motion was represented by a one dimensional model, with its deformations being function only of the distance from the base. The horizontal deformations were assumed to be of pure shear and uncoupled from the longitudinal vibrations. Solution of the problem was obtained in an analytical closed-form. The response of the foundation and the relative response of the building were analyzed in the frequency domain. Such results can be used as transfer functions in calculation of the response in the time domain. The results by this method were physically sound and causal.

The objective of this work was to understand the interaction phenomenon and to see how different factors affect the transfer functions of the foundation response and the relative building response. The following factors were considered: type of incident waves and angle of incidence, mass per unit length of the foundation and of the building, stiffness of the building relative to the soil, height of the building, the effects of the wave passage and the depth of the embedment.

The results can be summarized as follows:

1. The foundation input motion depends significantly on the type of incident waves and the incident angle. In the limit when $\eta \to 0$, $\Delta \to u^{ff}$, $V \to v^{ff}$ and $\varphi \to 0$, i.e. for very long incident waves the translation of the foundation input motion approaches the translation of the free-field motion on the half-space surface. In the limit as $\eta \to \infty$, $\Delta \to 0$, $V \to 0$ and $\varphi \to 0$, i.e. for very short wavelengths of the incident waves both the translations and the rotation approach zero. The foundation acts as a low-pass filter because it averages the differential motions of the free-field motion along its boundary. For small η's (e.g. $\eta < 0.2$), $\varphi \approx \varphi^{ff}$ and the rotation of the foundation input motion can be approximated by the free-field point rotation. Then φ increases with η almost linearly. As η increases, $|\varphi| < |\varphi^{ff}|$, i.e. as the wavelength of the incident waves becomes shorter, the rotation of the foundation input motion has smaller amplitudes than the point rotation. For wavelengths comparable with the size of the foundation ($0.5 < \eta < 2$), the wave passage effects become important. The rotation seems to be the largest when the width of

the foundation is approximately equal to half of the horizontal apparent wavelength and the depth is approximately equal to half of the vertical apparent wavelength of the S-waves in the soil. Then the two corners of the foundation are forced to move vertically, and/or its top and bottom are forced to move horizontally with opposite phases. For incident Rayleigh waves, for which the free-field motion is an exponential function of the depth, in the interval $\eta \in (0,2]$, the rotation has maxima when $2a = cT/2$ and $3cT/2$. The comparison of the maximum rotational amplitudes in the interval $\eta \in (0,2\pi]$ for incident unit amplitude plane P- and SV-waves at incident angles $\gamma = 0°$, $30°$, $60°$ and $85°$, and a Rayleigh wave with unit surface horizontal displacement, for a semi-circular foundation, showed that the rotation is the largest for incident Rayleigh waves and smallest for incident P-waves. The maximum rotation for P-waves (at $\gamma = 30°$) is more than two times smaller than the maximum rotation for incident Rayleigh waves, and more than 1.5 times smaller than the maximum rotation for incident SV-waves (at $\gamma = 30°$). In the conventional analyses of the response of a building to seismic excitation, that include or exclude the interaction, the building models are excited only by horizontal and vertical translations. Our analysis showed that in some cases (e.g. incident SV-wave with $\gamma = 45°$ and $60°$) the rotational amplitudes can be larger and at the same time the horizontal translation can be small ($|u^{ff}| = 0$ and $|\varphi a|_{\max} \approx 1$) for $\gamma = 45°$, and $|u^{ff}| < 0.5$ and $|\varphi a|_{\max} \approx 0.9$ for $\gamma = 60°$). Therefore, in the conventional analyses a major component of the realistic foundation input motion is being neglected. Some authors include rocking motion to the base excitation, but approximated by the free-field point rotation. Our analysis showed that, as a result of the embedment, the foundation input motion may have significant rotational amplitudes even through the point rotation is equal to zero (e.g., incident SV-waves with $\gamma = 0°$ and $30°$). Therefore, those analyses may also underestimate the realistic building excitation. The realistic input base rotation can be represented by the free-field point rotation only for very long wavelengths of the incident waves.

2. A rigid cylindrical foundation, embedded into the half-space and excited by in-plane excitation, acts as a damped oscillator with three degrees-of-freedom (horizontal and vertical translations and a rotation) and system frequencies which are in the lower range of η. At those frequencies, the foundation response relative to the foundation input motion is the maximum. If the vertical motions are uncoupled from the horizontal and the rocking motions, there are two system frequencies: one for the coupled horizontal and rocking motion and one for the vertical motion. The system frequencies are lower and the corresponding peak response (relative to the foundation input motion) is larger when the foundation mass is larger. For shorter wavelengths of the excitation, the foundation response has smaller amplitudes than the foundation input motion. The response amplitudes decay with frequency at a faster rate when the foundation mass is larger and when the embedment is deeper. This behavior has been explained by the analogy with a single degree-of-freedom oscillator. As $\eta \to 0$, the foundation response approaches the free-field motion on the surface. For long wavelengths, the foundation driving forces are larger when the foundation is deeper, because the stresses of the free-field motion, which vary little along the contact area, are integrated over a larger area. For shorter wavelengths the situation reverses, because the deeper embedment averages more the driving forces. For

intermediate wavelengths, the rocking response depends on the amplitude of the rocking of the foundation input motion for the particular frequency and shape of the foundation.

3. The building-soil interaction modifies the amplitudes and the shape of the transfer function between the building relative response and the incident wave motion, relative to the transfer function of a fixed-base model subjected to base translations only. Changed are the characteristic frequencies and the peak relative responses. Even when there is no damping in the building, the peak responses are finite, because of radiation of the building vibrational energy into the half-space. However, the reduction of the relative response is accompanied by large rotations of the base. The modification of the transfer-function is a result of the dynamic and of the kinematic interaction (the wave passage effects). The dynamic interaction depends on the mass of the building, on its height relative to the base and on its stiffness relative to the stiffness of the half-space. It also depends on the foundation mass and on the depth of the embedment. The kinematic interaction depends on the shape of the foundation and on the type of waves and incident angle. It affects the building relative response through the modification of the foundation input motion relative to the free-field motion. Our analysis showed the following:

a) The dynamic interaction changes the system frequencies of the building relative response. The first peak is most affected. It is shifted towards lower frequencies and the amount of the shift is larger when the building mass is larger and when the half-space is "softer" relative to the building. Then, the reduction of its amplitude is the largest. The higher-order peaks are affected less by the interaction. The damping effect is smaller for those peaks, but the peak amplitudes are always finite.

b) The shape and size of the embedment affects the apparent flexibility of the half-space. When the foundation is deeper, the half-space acts as a "stiffer" medium. This was concluded from the larger reduction of the fundamental system frequency, when the same building model was placed on a shallower foundation ($h/a = 0.5$). The amplitude of the first peak of the relative response is smaller when the depth of the foundation is smaller. Our results showed that the first rocking peak may be lower when the foundation depth is smaller. This might be because of the smaller foundation driving forces for the shallower foundation, because the stresses of the foundation input motion (which do not vary much in the neighborhood of the first system frequency) are integrated over a smaller area.

The height of the relative response peaks and of the rocking response peaks depends also on the amplitudes of the foundation input motion in the particular frequency range. For deeper foundations, those are higher for η's between 0.5 and 1.5, where the input rotation is the highest. For a shallow foundation, those are higher for η's higher than 1.5, where also the input rotation is the largest. It may happen (for very soft soil and a high building), as a result of the large input rocking, the relative response to be larger away from the system frequencies.

From the above analysis the following conclusions can be made:

(1) The dynamic soil-structure interaction can significantly affect the building relative response and therefore has to be included in the analysis of buildings, especially when founded on soft foundation medium.

(2) The kinematic interaction due to the embedment can significantly modify the building input base motion. Neglecting it may lead to nonconservative estimates of the building design forces. It has to be included even when the soil is "harder", especially for analysis of taller buildings for which the "additional" rocking excitation, due to the embedment, may induce large forces in their components.

APPENDIX A

LIST OF SYMBOLS

$\eta = \frac{\omega a}{\pi \beta} = \frac{2a}{\beta T}$ = dimensionless wave length, frequency

$\Omega = k_\beta a$ = dimensionless wave number

$\varepsilon = \frac{\beta H}{\beta_b a}$ = measure of the flexibility of the building relative to the soil

β, μ, α, ν = shear wave velocity, shear modulus, longitudinal wave velocity and Poisson's ratio for the soil

$\beta_b, \mu_b, \alpha_b, \gamma_b$ = shear wave velocity, shear modulus, longitudinal wave velocity and Poisson's ratio for the building.

h, a, b = depth, half-with and radius of curvature of the foundation

W, H = width and height of the building.

ω, T = circular frequency and period of the incident wave

Δ, V, φ = horizontal and vertical displacements and rocking angle of point O on the foundation

$u_b^{\text{rel}}, v_b^{\text{rel}}$ = relative horizontal and vertical displacements of the building

u^{ff}, v^{ff}, φ^{ff} = horizontal and vertical components of the free-field motion and a point rotation

APPENDIX B

VALUES OF ε FOR THE FORMER IMPERIAL COUNTY SERVICES BUILDING IN EL CENTRO, CALIFORNIA

The former Imperial County Services Building in El Centro was a four story reinforced concrete building (height H = 22.5m, length L = 38.10m in the East - West (EW) direction and L = 22.86m in the North - South (N-S) direction), Kojić et al., 1984. Its fundamental fixed base natural frequency was estimated to be $T_1^{E-W} \approx$ 1sec, for horizontal vibration in the E-W direction, and $T_1^{N-S} \approx 0.28$ sec, for horizontal vibration in the N-S direction. Then the equivalent shear wave velocity of the shear beam building model would have been $\beta_b \simeq 100$ m/s for horizontal vibration in the E-W direction, and $B_b \approx$ 360m/s for horizontal vibration in the N-S direction $\left(\beta_b = \frac{4H}{T_1}\right)$.

The shear wave velocity of the soil can have values as low as e.g. $\beta = 40$ m/s (in the soft basin of Mexico City) or $\beta = 250$ m/s (in Los Angeles basin). The high values would be $\beta \approx 2000$ m/s (e.g. for basement rock). Then the range of the representative values of the parameter $\varepsilon = \beta H/\beta_b a$ for this building would be

$\beta[m/s]$	ε in E-W dir.	ε in N-S dir.
40	0.25	0.52
250	1.55	3.25
800	4.96	10.4
2000	12.39	26.